THOMPSON RIVERS UNIVERSITY

Controlling surface flux in landfill-well coupled flow in perforated horizontal wells

by

Mehrdad Sepehri

A THESIS SUBMITTED IN PARTIAL FULFILLMENT OF THE
REQUIREMENTS FOR THE DEGREE OF

MASTER OF SCIENCE

IN

ENVIRONMENTAL SCIENCE

THOMPSON RIVERS UNIVERSITY

(Kamloops, British Columbia, Canada)

April, 2023

Supervisor:
Dr. Yana Nec, Thompson Rivers University, Kamloops, BC

Supervisory committee:
Dr. Richard Brewster, Thompson Rivers University, Kamloops, BC

Dr. Robin Kleiv, Thompson Rivers University, Kamloops, BC

External examiner:
Dr. Ian Frigaard, University of British Columbia, Vancouver, BC

Acknowledgement

I would first like to express my sincere gratitude to my supervisor Dr. Yana Nec for being incredibly patient with me over the years. Your support and guidance throughout this project helped me complete the work. Thank you for the regular meetings and your continuous drive to help me make progress in a timely manner. Thank you for providing me with good exposure opportunities by guiding me through various conferences and seminars. I am extremely grateful for the graduate scholarship you allotted me from your research grants. It has been a true honor working as a student of yours.

I would also like to acknowledge the rest of my thesis supervising committee: Dr. Richard Brewster and Dr. Robin Kleiv for their expertise and guidance. Thank you all for your amazing insights, ideas, comments and suggestions.

Finally, a very special thanks to my family and friends for their continuous support.

Abstract

Throughout the existence of human settlements disposing of waste materials historically caused numerous environmental problems. Sanitary landfills are now known as one of the most efficient ways to treat waste with minimal environmental impact. When operated correctly, the landfill can be regarded as a potential source of renewable energy.

Past research addressed different aspects of sanitary landfill sites. This study focuses on the simulation of a flow of landfill gas through the porous medium of the waste matrix and in a collection well, with a special emphasis on the influence of the well geometry on the surface mass flux. For this purpose a model containing three layers, namely cover, waste, and gravel is constructed. Two fluid flow types govern the coupled system: porous medium flow and unobstructed flow obeying Darcy's law and Navier-Stokes equations respectively. The COMSOL solver is utilized to perform the numerical simulations. The GNU Octave software is used for post-processing and visualization of both solutions.

Different well geometries in terms of perforation size and position along the well are evaluated. In the beginning, gravity is excluded in order to focus on the sole impact of well geometry. A two-step assessment is conducted: in the first stage a 1D analytical solution of a simplified problem is utilized to validate the 2D numerical model setting. Then for different well geometry modifications pressure profiles in the well, velocity profiles at the surface and surface mass flux are investigated. Studied modifications and their potential combinations are prioritized based on the observed impact of each modification on the surface mass flux and pressure values throughout the landfill. Prior to stage two, there is a validation process for the utilized computational meshes to guarantee the accuracy of all simulations. In stage two for prioritized modifications and their combinations several sensitivity analyses are conducted on cover permeability, waste permeability, and pump pressure to understand the behavior of the landfill-well system. In the end, the effect of gravity on the system is investigated.

The results suggest that well geometry modification–in terms of changing well perforation size and longitudinal distribution–influences the pressure field in the landfill as well as the surface flux. Changing perforation size and position are the first and second priorities, respectively. Moreover, a synergistic effect can be derived from the combination of these modifications. The surface flux increases with larger perforations or a higher number thereof unless the cover permeability is extremely tight. Well production capability decreases as a result of decreasing the number of perforation sets. In terms of landfill-well system properties, cover permeability and suction strength are the main means of control of landfill pressure and surface flux, while waste permeability is not. The gravity effect is shown to be of considerable importance.

Keywords: landfill gas, horizontal well, surface flux, porous media flows, 2D simulation, COMSOL, finite elements.

Contents

List of Figures

List of Tables

Chapter 1

Background

1.1 Introduction

During the recent decades sanitary landfill sites have been considered as a safe solution for the waste disposal problem. Generating energy from these ostensibly useless disposal sites has become a promising alternative fuel resource. Nowadays this process is highly recommended due to its economic and environmental positive effects. Regardless of the desired results, if a landfill is not properly sited and constructed, maintained, and operated, it morphs into a dumpsite and has extreme side effects on the environment (Kaza and Bhada-Tata, 2018).

Historically, researchers working on sanitary landfill sites have evaluated various aspects of construction, maintenance, and operation aspects (Clayton and Huie, 1900). Evaluating gas migration and production had become an interesting subject for studying when researchers fathomed that gas generated in a landfill might be not as devastating if its migration is controlled: gas production can help to make profit, preventing gas emissions into the atmosphere and surrounding soil layers, and preserving the environment.

Landfill gas is mainly composed of methane, carbon dioxide, water vapour, and a minor portion of other gases (Sabour et al., 2007). The presence of the two main greenhouse gases, methane and carbon dioxide, indicates that research on landfill gas generation and migration is necessary due to their harmful effects on global climate change. Gas extraction from sanitary landfills is one of the methods whereby the gas emissions into air and adjacent layers can be reduced, and the extracted gas can be used as a source of energy, possibly with the addition of natural gas. Landfill gas flow should be analyzed to estimate the gas flow rate. Another aim of the gas flow assessment is to predict the interchange of the landfill gas with the atmosphere. Statistical and deterministic techniques are the main methods of such investigation. Flow models of the latter type provide a means to evaluate temporal and spatial variation of gas emission rates, assess the factors influencing these rates, and design control measures to eliminate or minimize gas emissions (El-Fadel et al., 1995). The models stem from theoretical fluid mechanics and might augment direct field measurements.

In reality, a multiphase flow of gas and liquid leachate takes place with both phases interacting with the solid waste matrix. Numerous models have been devel-

oped based on stochastic (Zacharof and Butler, 2004; Copty et al., 2004; Ptak et al., 2004; Chaudhuri and Sekhar, 2005; Sudicky et al., 2010) and deterministic analyses (Poulsen et al., 2003; Kindlein et al., 2006; Yu et al., 2009; Xie et al., 2018, 2019; Lu et al., 2019; Feng et al., 2020; Lu and Feng, 2020). Concerning the deterministic approach, both analytical and numerical methods are applied, developing models to predict and simulate the gas generation, migration, and production in order to optimize the design of landfill systems.

Generation of gas within sanitary landfills has been investigated in a large number of studies (Scharff and Jacobs, 2006; Donovan et al., 2010; Ishii and Furuichi, 2013; Krause et al., 2016; Kumar et al., 2016; Kamalan, 2016). Many of these works are based on models developed utilizing Monod equation and first order decay, such as GasSim (Gregory, 2003), TNO (Oonk and Boom, 1995), Afvalzorg (Jacobs and Scharff, 2001), LandGEM (US-EPA, 2001), and IPCC (Eggleston et al., 2006), as well as models based on Monod equation and zero order decay, such as the French EPER model (Budka, 2003) and German EPER model (Hermann, 2005). Furthermore, some researchers developed numerical models based on neural networks and weighted residual methods (Ozkaya et al., 2007; Shariatmadari et al., 2007). The aforementioned models incorporate various mechanisms of contaminant migration.

In the past, models primarily regarded the landfill as a constant linear source and simulated gas migration beyond the landfill boundaries. Some models proposed the finite elements methods to solve a coupled system of convection-diffusion and mass conservation equations (Mohsen et al., 1980; Metcalfe and Farquhar, 1987). A second group of models was proposed to model gas migration through the landfill itself as well as emission to the atmosphere. The simplest one-dimensional model simulated gas migration with respect to different degrees of complexity in gas generation (Findikakis and Leckie, 1979; El-Fadel et al., 1989).

With the passage of time, proposed models have become more complex, studied different detailed aspects of gas and leachate migration, and analyzed various parameters that affect fluid flow through the landfill and beyond its boundaries. These models were based on analytical and/or numerical solutions. In some cases, researchers used the TOUGH[1] simulator and its derivatives (Pruess, 1987, 1991; Pruess et al., 1999) by which gas production and migration within and beyond the landfill could be estimated (Nastev et al., 2001; Vigneault et al., 2004). Others simulate the process using custom-developed models (Arigala et al., 1995; Poulsen et al., 2001; Perera et al., 2002a,b; Chen et al., 2003; Copty et al., 2004; Townsend et al., 2005; Xi and Xiong, 2013; Xie and Chen, 2014; Feng et al., 2015; Zheng et al., 2019; Halvorsen et al., 2019; Nec and Huculak, 2019; Zeng, 2020).

One of the most important parameters in the landfill fluid flow studies is the gas flux near the surface, which can be used as the indicator of gas emissions into the atmosphere. Landfill gas contains mainly methane and carbon dioxide, 45-60% and 40-55% by volume, respectively (Oonk, 2010; Jeong et al., 2015), and the methane's global warming potential is about 21 times higher than that of carbon dioxide (Lelieveld et al., 1998). A fraction of about 10% of the total anthropogenic

---

[1]The TOUGH (Transport Of Unsaturated Groundwater and Heat) suite of software comprises multi-dimensional numerical models for simulating the coupled transport of water, vapor, non-condensible gas, and heat in porous and fractured media (`https://tough.lbl.gov/`).

emissions is related to methane from landfills (Adler, 1994). Hence, estimating the amount of gas flux using simulation and mathematical modeling is a vital step in an effort to control emissions from the landfill and to optimize the gas extraction process.

Landfill gas emissions can be lateral through the surrounding layers or vertical through the cover (Perera, 2001). Lateral gas migration was investigated in previous literature (Esmaili, 1975; Alzaydi et al., 1978; Moore et al., 1979; Mohsen et al., 1978; Poulsen et al., 2001). These simulations were based on finite differences or finite elements methods considering a constant molar concentration within the landfill. These models were developed based on just two or three gas components and in some cases neglecting nitrogen as a neutral component.

Findikakis and Leckie (1979) developed a 1D model for vertical gas migration through the landfill and its cover combined with gas generation within the landfill. Transport equations were solved numerically for a three-component gas system comprising methane, carbon dioxide and nitrogen to estimate methane and carbon dioxide flux into the atmosphere and nitrogen influx into the landfill. Spokas and Bogner (1996); Bogner et al. (1997) developed a three-dimensional model based on vertical concentration gradients using finite differences to estimate the amounts of methane oxidized during the traversal of a layered cover soil and emitted therefrom. This model utilized modified mass transfer coefficients obtained from field concentration profiles and physical properties of the landfill-atmosphere system; the model could simulate negative flux[2].

Gas flux in terms of air intrusion or landfill gas emission has become a part of the landfill research (Arigala et al., 1995; Nastev et al., 2001; Poulsen et al., 2001; Perera et al., 2002b; Vigneault et al., 2004; Feng et al., 2015). These 1D and/or 2D models were mainly constructed to simulate gas migration through and/or beyond the landfill. The transport equations were based on different mechanisms such as diffusion, advection, and even conduction. In some cases methane oxidation was incorporated. In certain cases flux measurements were used to calibrate the proposed models.

Zheng et al. (2019) proposed a two-dimensional analytical model (using eigenfunction expansion and Fourier expansion) considering an exponential decrease in gas permeability and generation rate with depth. Horizontal wells were investigated from the aspects of burial depth and horizontal spacing. An upper limit for well spacing (for an 85% recovery rate) and a simple formula to estimate the air intrusion into horizontal gas collection wells were introduced. The effects of waste properties, cover characteristics, vacuum pressure, and well burial depth on air influx, landfill gas recovery, and horizontal well spacing were studied.

Nec and Huculak (2019) developed a model to study landfill gas collection by horizontal perforated wells. A semi-analytical solution was implemented with a minimal number of parameters for the axisymmetric coupled porous media-well system. That work clarified three control-related phenomena encountered in the landfill: (1) no perceptible variation in collected mass with a change in induced

---

[2]The negative flux can be caused by negative induced pressure in the soil pore spaces and/or an increase in methanotrophic population, which leads to higher methane consumption (Klusman and Dick, 2000).

sub-atmospheric extraction pressure, (2) a lower than expected collected mass as a result of adequate extraction strength, and (3) air intrusion and over-extraction. The flux in terms of gas escape and air intrusion across the horizontal surface above the landfill was estimated for the cases of adequate, threshold, and insufficient extraction pressure, allowing to define the well radius of influence.

A 2D horizontal well model was proposed in 2019 (Halvorsen et al.) with a focus on elliptic and rectangular cross-sectional domains. It was illustrated that precise modeling of medium resistance and geometry is vital in determining pressure distribution that can be used to optimize gas collection. Furthermore, it was shown that gravity might not be negligible, whereas the impact of temperature was about an order of magnitude less than that of gravity. The gas flux was analyzed and then the radius of influence was estimated for a rectangular cross-section of a perforated well for different scenarios–landfill with no cover, sealed surface and partly permeable cover–with and without gravity. An attainable landfill design tool was proposed based on a numerical solution. Using this analytical formulation, the pressure profile within the landfill could be estimated, and thereby the surface flux and radius of influence could be assessed.

In the two aforementioned papers the variation of surface flux along the well was estimated numerically, then it was validated by an analytical solution. This approach could only offer an approximate prediction of the gas flux and the radius of influence. The reason was that the gas flux as a function of horizontal distance from the well's center did not have any root and it decayed to zero asymptotically, requiring the definition of an arbitrary cut-off threshold. As a standard approach, a cut-off point of a minimal normal velocity was introduced, by which the radius of influence could be obtained. By using a mixed 2D rectangular domain, Halvorsen et al. (2019) rectified the mentioned drawback, so that the flux surface coincided with the uppermost boundary. Consequently, the flux function did possess a root, attaining a definitive estimation of the radius of influence.

In summary, it is essential to control the gas flux through the landfill surface or cover. It is important to distinguish between two cases: (1) when an inadequate suction strength is imposed, landfill gas can be emitted into the atmosphere, and (2) if the vacuum is too strong, air intrusion is likely to happen, decimating the population of anaerobic bacteria responsible for waste decomposition. In reality the suction might be strong near the outlet, but become insufficient at the blocked end of the well, so that both of these detrimental phenomena take place. Therefore adequate control and reduction of surface flux contribute to a more efficient operation of landfills, reduce emissions into the environment and improve the prospects of energy recovery.

1.2   Objectives

In a landfill, cylindrical pipes are used, which they can be embedded in the landfill vertically or horizontally. During the current research a horizontal well is modeled. The common design of a landfill well is a cylindrical pipe with a blocked end and perforated wall to allow gas collection along its entire length. Due to pressure continuity throughout the landfill-well system, changes in any component

of this system might change the pressure distribution, leading to a surface mass flux variation. It is expected that modifying the hole size and position along the well affects the surface flux. To clarify, the perforations act virtually like point mass sinks, whilst in between the well wall is impermeable. Each perforation has a certain radius of influence, so that a certain balance is created. By shifting the perforations or varying their size, the local resistance to flow is changed, which should influence the surface flux.

The existing literature addressed surface gas flux to some extent, however no attempt was made to test variation in the geometry of the collection well (Esmaili, 1975; Lelieveld et al., 1998; Perera, 2001; Poulsen et al., 2001; Nastev et al., 2001; Perera et al., 2002b; Feng et al., 2015; Zheng et al., 2019; Halvorsen et al., 2019; Nec and Huculak, 2019; Feng et al., 2020). The cornerstone intent of the current research project is to understand how the pressure distribution throughout the system can be modified via well geometry with the intent to control the surface flux. The fact that with every geometry variation the pressure distribution changes throughout the landfill, including below the well, makes the surface flux control problem an interesting challenge.

There are two purposes for extracting landfill gas: one, to reduce gas emissions into the atmosphere and two, to make a profit from the collected methane. When pressure below the surface is higher than atmospheric, gas escaping occurs. On the other hand when the atmospheric pressure is dominant, air intrusion into the landfill happens, resulting in methane oxidation. Consequently both cases are environmentally and economically detrimental. In a real landfill both phenomena are expected for a given pump pressure: a part closer to the sink source experiences air intrusion and the farther part encounters gas escaping. The main criterion is to find balanced minimal amounts of surface efflux and influx.

To begin, a basic configuration containing some perforations of a uniform size and interval along the well is considered. Then several modifications of the basic geometry are created: varying the number of perforations at each section, allowing a non-uniform longitudinal perforation distribution and/or perforation radius. For each modification the efflux of gas and influx of air at the surface along the well are computed for a range of viable operational parameters. The longitudinal dependence of the flux is assessed and correlated with the type of modification. Modifications that allow a straightforward control of the flux at desired locations along the well are identified and discussed. These prioritized modifications are examined in combinations to test for a possible synergy. In all these simulations gravity is excluded in order to focus on the sole effect of geometry. This exclusion is crucial, since gravity in this application is known to be non-negligible in some circumstances (Halvorsen et al., 2019). As the last step, the influence of gravity on pressure distribution within the landfill and flux at the surface is evaluated. It is understood that reducing the flux to zero identically along the entire well is impossible. The practical goal is to provide recommendations as to ways landfill engineers or operators can diminish landfill gas escape or air influx along the well.

Chapter 2

Methodology

2.1 Geometry and governing equations

The impact of well geometry on the gas migration in a landfill is studied and several geometry modifications for a well are assessed to diminish the expected surface flux along the well. To do so, first, the transport equations are solved numerically utilizing the finite element solver COMSOL Multiphysics® (2021). Then analytical modeling is conducted to help engineers create a practical tool to facilitate the process of landfill design in terms of flux control. Fluid flow in a landfill generally occurs in three dimensions. It should be evaluated vertically, horizontally and laterally to understand the flow behavior in a landfill collection system. A 1D model can simulate fluid flow in one direction, nonetheless in a landfill-well coupled system, there are dominant vertical and horizontal flow directions in a porous matrix and well, respectively. A 3D model is not feasible since it is computationally prohibitive. A 2D model renders the computational cost reasonable while permitting the coupling of two principal flow directions, namely vertically through the porous matrix and horizontally along the collection well. Hence a longitudinal cross-section of the landfill is considered for the 2D model. The main quantity of interest is surface flux along the well.

Figure 2.1 shows a simplified 3D sketch of a landfill consisting of a well (blue), supporting gravel pack (orange), waste layer (yellow) and cover (green). When viewed from the side, the 2D projection would look as shown in figure 2.2. The cover is the top layer and acts as the first barrier to reduce the surface flux. However, the mismatch between the cylindrical geometry of the well and rectangular shape of the landfill must be reconciled. Thus the well is converted into a 2D well that collects an equivalent amount of fluid. Below this will be referred to as an equivalent well. The reason for this conversion is that, in practice, the landfill cavity is rectangular, and this is the dominant geometry near the surface, although the well and gravel pack are of a cylindrical shape. To reconcile the two types of geometry, the well and gravel domains are replaced by rectangular channels of unit depth. The new well is equivalent to two parallel plates. The perforations then morph into penetrating narrow slits that go through the entire unit width of the equivalent well, so that all 2D simulations correspond to unit depth geometry in 3D. The Cartesian coordinates are selected for the 2D longitudinal cross-section. The

dimensions of the equivalent well and its perforations must be calculated based on the cross-section area of the corresponding real well and its perforations. In figure 2.3 an interactive 3D visualization is presented for both the well and its equivalent.

(a) landfill with real well

(b) landfill with equivalent well
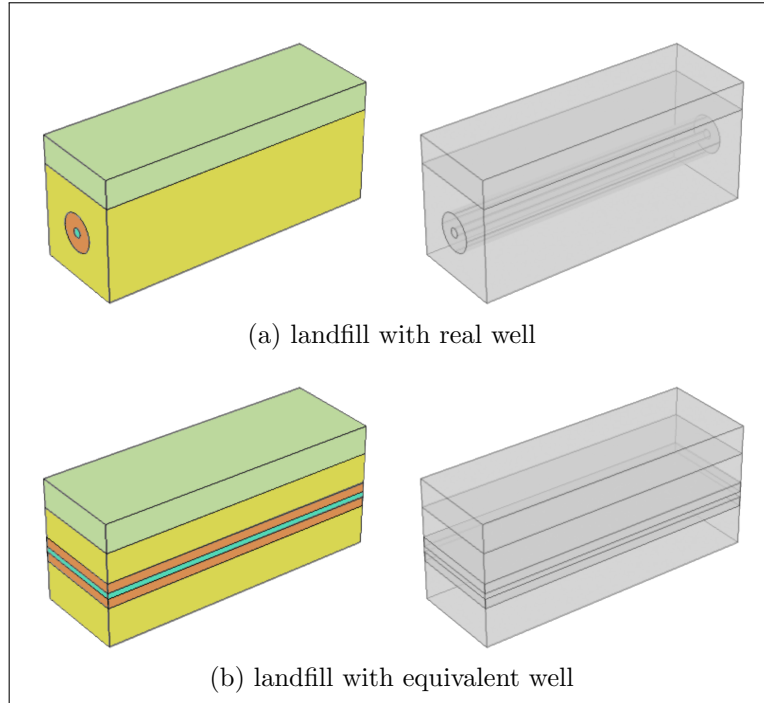
Figure 2.1: 3D Conceptual sketch of the landfill with real (a) and equivalent (b) wells. The corresponding transparent version of each sketch is presented on the right hand side. Cover, waste and gravel layers are in green, yellow and red, respectively. The well is coloured in blue. Dimensions not to scale.
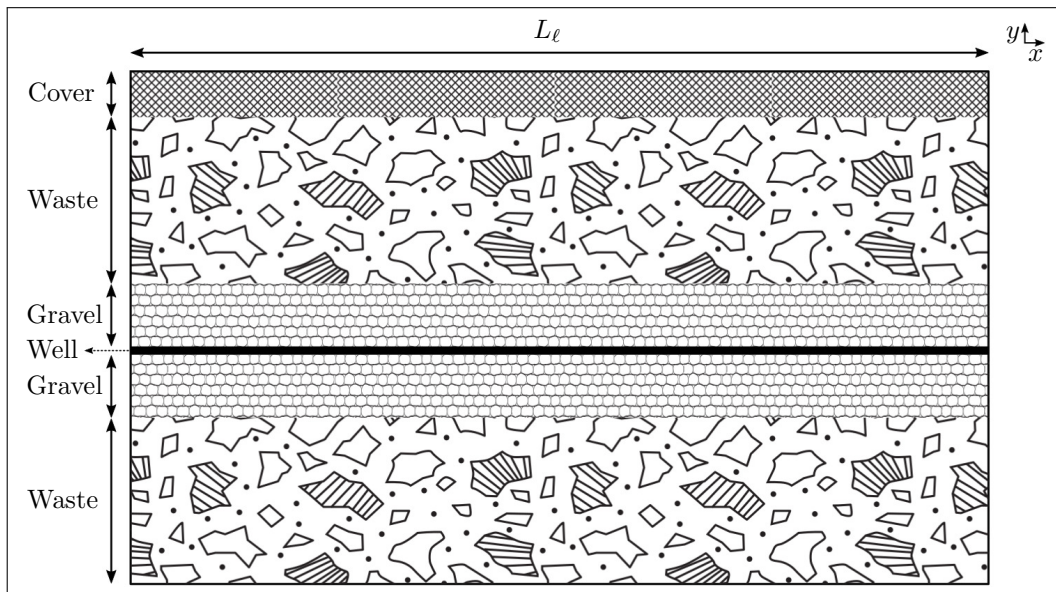
Figure 2.2: Schematic view of the landfill. L_ℓ is the length of the landfill. Dimensions not to scale.
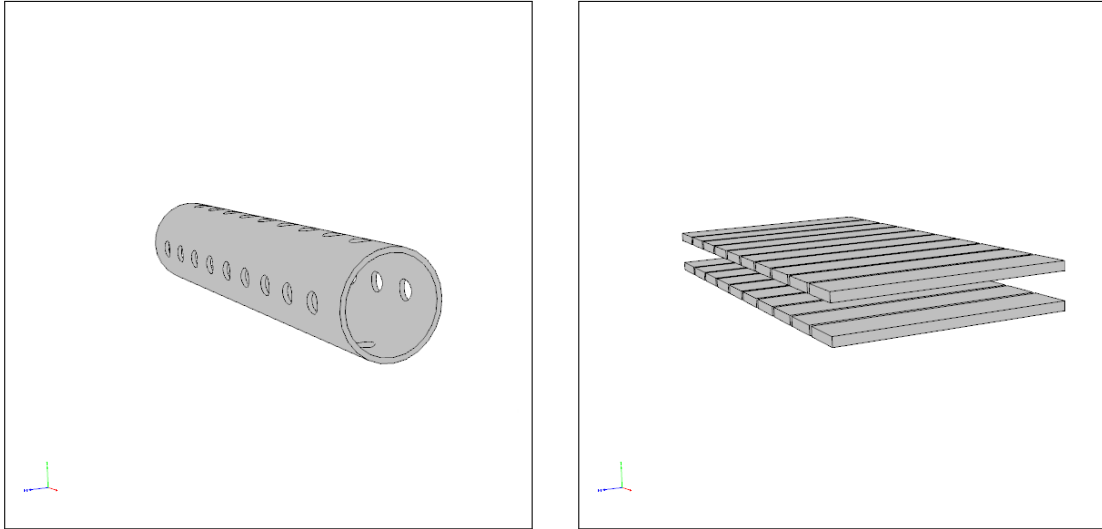
Figure 2.3: 3D visualization of the real well (left) and equivalent well (right). Dimensions not to scale. This figure contains interactive features. The instructions to enable 3D content can be found on Adobe website[3].

Figure 2.4 depicts the 2D views of the real and equivalent wells, and the parameters used for the equivalence calculation. First the height of the equivalent well is calculated based on the equality of cross-section area of a circle of radius R_{w}, and a rectangle of height H_{ew} and width W_{ew}: $H_{\text{ew}} = \pi R_{\text{w}}^2 / W_{\text{ew}}$. Then the width of each equivalent perforation W_{ep} is calculated by: $W_{\text{ep}} = (n\pi R_{\text{h}}^2)/(2W_{\text{ew}})$; where n and R_{h} are the number of real perforations and hole radius, respectively. Since all simulations conducted in this study are per unit depth, for the equivalent well $W_{\text{ew}} = 1$. The factor of 2 in the denominator refers to the number of equivalent perforations for each extraction segment: two equivalent perforations must correspond to the top and bottom matching slits.

The simulation couples fluid flow through porous media and unobstructed flow in the well. The fluid flow through porous media and in the well, respectively governed by Darcy's law and Navier-Stokes equation. In the porous part of the domain the following equations are solved: conservation of mass,

$$\nabla \cdot (\rho \mathbf{u}) = Q, \tag{2.1a}$$

and Darcy's law (conservation of momentum),

$$\mathbf{u} = -\frac{K}{\mu} \left(\nabla P - \rho \mathbf{g} \right), \tag{2.1b}$$

where $\mathbf{u}$ is the fluid velocity. P, ρ, and μ are fluid pressure, density, and dynamic viscosity, respectively. K stands for the permeability, $\mathbf{g}$–gravity vector, and Q– source term. Moreover within the well the following steady-state, compressible form of the Navier-Stokes equation is used:

$$\nabla \cdot (\rho \mathbf{u}) = 0, \tag{2.2a}$$

---

[3]`https://helpx.adobe.com/ca/acrobat/using/enable-3d-content-pdf.html`
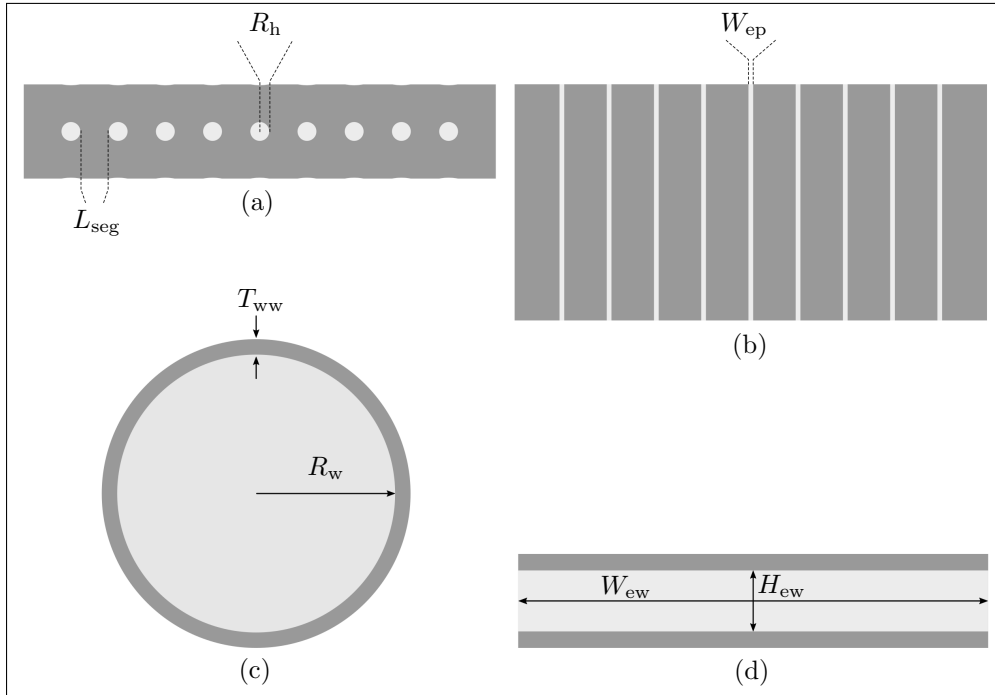
Figure 2.4: 2D visualization of the real well (left) and equivalent well (right). Panels (a) and (b): top view. Panels (c) and (d): cross-sectional view. R_{h}: hole radius; R_{w}: well radius; W_{ep}: equivalent perforation width; H_{ew}: equivalent well height; W_{ew}: equivalent well depth; T_{ww}: thickness of the well's wall; L_{seg}: length of extraction segment. Dimensions not to scale.

$$\rho(\mathbf{u} \cdot \nabla)\mathbf{u} = -\nabla P + \nabla \cdot \left(\mu \left(\nabla \mathbf{u} + (\nabla \mathbf{u})^{T} \right) - \frac{2}{3}\mu \left(\nabla \cdot \mathbf{u} \right) I \right) + \rho \mathbf{g}, \qquad (2.2b)$$

where I is identity tensor. The left-hand side contains the terms representing inertial forces. On the right-hand side, from left to right the terms correspond to the pressure, viscous and gravity forces, respectively. Although gravity is excluded at the beginning of the assessment, its impact on the pressure distribution and surface flux is investigated in the end.

Because the fluid flow equation is solved for a gaseous phase, the dependence of the pressure on density has to be specified. Temperature is taken constant because: one, it is known that the landfill wells are working in thermal equilibrium (Young, 1989); two, past numerical investigations showed that the effect of varying temperature is small (Halvorsen et al., 2019). The equation of state of gases is needed to obtain a closed mathematical system. For an ideal gas the equation of state is:

$$P M_{\mathrm{w}} = \rho R T, \qquad (2.3)$$

where M_{w}, R, and T are molecular weight of gas mixture, universal gas constant, and temperature, respectively.

The COMSOL solver is utilized to perform the numerical simulations. The GNU Octave (2022) software is used for post-processing and visualization of both analytical and numerical solutions. In order to confirm a correct handling of fluid properties and flow equations by COMSOL, a simplified 2D numerical solution is

obtained and validated against a known 1D analytical solution first. The simplified 2D model is to be as close to the final model as possible. To achieve this, a sub-unit containing a segment of the full geometry is selected, as represented in figure 2.5. A 2D geometry comprising three domains above the well (cover, waste, and gravel) and two domains below the well (gravel and waste) is used. Flow in the well is excluded, and suction is applied to the entire boundary between gravel and well. A no flux boundary condition is imposed on all vertical boundaries.
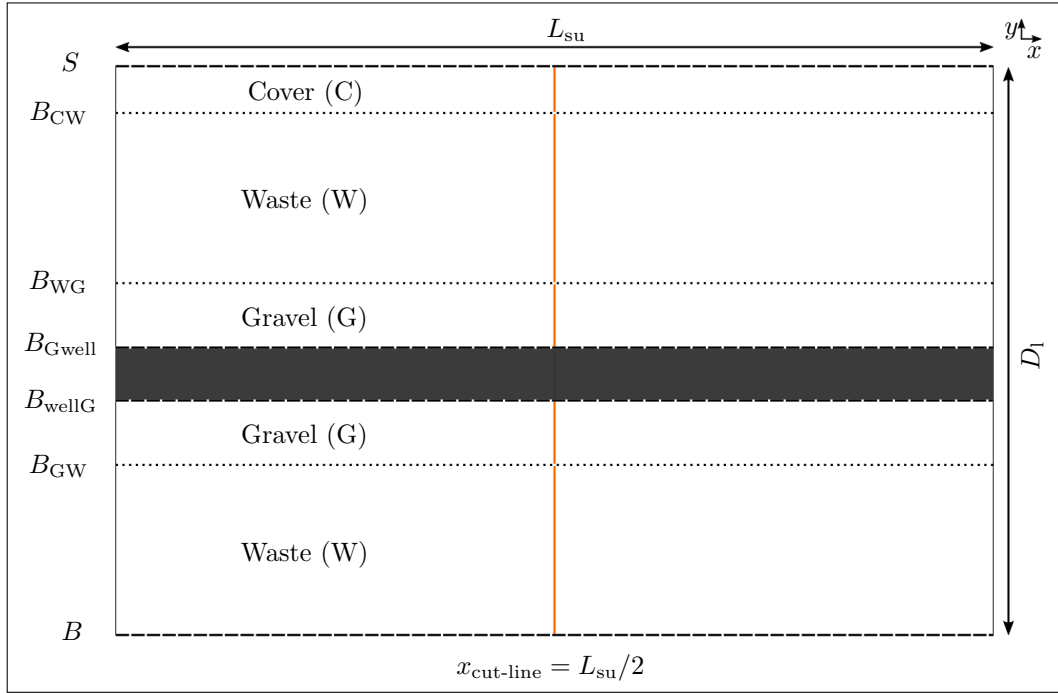
Figure 2.5: Schematic view of the sub-unit geometry. S: Surface; B_{CW}: boundary between cover and upper waste; B_{WG}: boundary between upper waste and upper gravel; B_{Gwell}: boundary between upper gravel and well; B_{wellG}: boundary between well and lower gravel; B_{GW}: boundary between lower gravel and lower waste; B: bottom. L_{su} and D_l are sub-unit's length and depth, respectively. Vertical orange line represents the cut-line position. Shaded part marks the excluded fluid flow in the well. Dimensions not to scale.

Since the flow in the well is excluded, only equations (2.1) are solved. The 1D analytical solution should hold along any arbitrary vertical cut-line (profile) sufficiently far away from vertical boundaries, an example of which is the orange vertical line shown in figure 2.5. In this simplified setting, four boundary conditions on S, B_{Gwell}, B_{wellG}, and B boundaries (dashed lines in figure 2.5) are applied and presented in table 2.1. Since landfills customarily have an impermeable liner on the bottom, the relevant boundary condition is a no-flow boundary, i.e. normal velocity equals zero. Hence based on Darcy's law in the case of excluded gravity, pressure gradient in y direction should be zero.

Substituting equation (2.3) into equation (2.1) gives the steady-state gas flow equation through porous media:

$$\Delta P^2 + \frac{2\mu RT}{K M_w} Q = 0, \tag{2.4a}$$

10

Table 2.1: Boundary conditions used in solving fluid flow equations.

Boundary name	Boundary condition type	Value
S	Dirichlet	$P = P_{\text{atm}}$
B_{Gwell}	Dirichlet	$P = P_{\text{pump}}$
B_{wellG}	Dirichlet	$P = P_{\text{pump}}$
B	Neumann	$\mathrm{d}P/\mathrm{d}y = 0$

with ΔP^2 in the 2D Cartesian system defined as:

$$\Delta P^2 = \frac{\partial^2 P^2}{\partial x^2} + \frac{\partial^2 P^2}{\partial y^2}. \tag{2.4b}$$

The boundary conditions are the same for most of the length of the common boundaries between gravel pack and well, except for the area very close to the vertical side boundaries. Therefore the flow direction is predominantly vertical in the interior part of the landfill. As the flow is predominantly in the y direction, the variation in the x direction can be neglected:

$$\frac{\mathrm{d}^2 P^2}{\mathrm{d}y^2} = -\frac{2\mu RT}{K M_{\text{w}}} Q. \tag{2.5}$$

After integrating and applying boundary conditions, the pressure is given by:

$$P(y) = \begin{cases} \sqrt{C_1 y + C_2}, & \{D_{\text{UB, i}} < y < D_{\text{LB, i}} \,|\, \text{i} = \text{C, G}\}, \\[2ex] \sqrt{-\dfrac{\gamma}{2} y2 + C_1 y + C_2}, & \{D_{\text{UB, i}} < y < D_{\text{LB, i}} \,|\, \text{i} = \text{W}\}, \end{cases} \tag{2.6a}$$

$$C_1 = \begin{cases} \dfrac{P^2{}_{\text{LB, i}} - P^2{}_{\text{UB, i}}}{D_{\text{LB, i}} - D_{\text{UB, i}}}, & \{D_{\text{UB, i}} < y < D_{\text{LB, i}} \,|\, \text{i} = \text{C, G}\}, \\[3ex] \dfrac{P^2{}_{\text{LB, i}} - P^2{}_{\text{UB, i}} + \dfrac{\gamma}{2}\left(D^2{}_{\text{LB, i}} - D^2{}_{\text{UB, i}}\right)}{D_{\text{LB, i}} - D_{\text{UB, i}}}, & \{D_{\text{UB, i}} < y < D_{\text{LB, i}} \,|\, \text{i} = \text{W}\}, \end{cases} \tag{2.6b}$$

$$C_2 = \begin{cases} P^2{}_{\text{UB, i}} - C_1 D_{\text{UB, i}}, & \{D_{\text{UB, i}} < y < D_{\text{LB, i}} \,|\, \text{i} = \text{C, G}\}, \\[2ex] P^2{}_{\text{UB, i}} + \dfrac{\gamma}{2} D^2{}_{\text{UB, i}} - C_1 D_{\text{UB, i}}, & \{D_{\text{UB, i}} < y < D_{\text{LB, i}} \,|\, \text{i} = \text{W}\}, \end{cases} \tag{2.6c}$$

$$\gamma = \frac{2\mu RTQ}{K_{\text{W}} M_{\text{w}}}, \tag{2.6d}$$

where K_{W} stands for waste permeability. For each domain, i, $P_{\text{LB, i}}$, $D_{\text{LB, i}}$, $P_{\text{UB, i}}$, and $D_{\text{UB, i}}$ are the pressure and depth values of the corresponding lower and upper boundaries, respectively.

Both pressure and velocity continuity must hold at common boundaries:

$$P\Big|_{\text{cb}+} = P\Big|_{\text{cb}-} \quad \text{and} \quad \left(K\frac{\mathrm{d}p}{\mathrm{d}y}\right)_{\text{cb}+} = \left(K\frac{\mathrm{d}p}{\mathrm{d}y}\right)_{\text{cb}-}, \tag{2.7}$$

where cb+ and cb− refer to the laminae above and below the common boundaries, respectively. The second equality is by Darcy's law. With the obtained pressure equation 2.6, pressure values for the three common boundaries between domains (dotted lines in figure 2.5) are thus calculated as:

$$P_{\text{CW}} = \sqrt{\frac{ad + b}{1 - ac}}, \tag{2.8a}$$

$$P_{\text{WG}} = \sqrt{\frac{bc + d}{1 - ac}}, \tag{2.8b}$$

$$P_{\text{GW}} = \sqrt{e}, \tag{2.8c}$$

$$a = \frac{K_{\text{W}} D_{\text{CW}}}{K_{\text{C}} \left(D_{\text{WG}} - D_{\text{CW}}\right) + K_{\text{W}} D_{\text{CW}}}, \tag{2.8d}$$

$$b = \frac{\frac{\gamma}{2} K_{\text{W}} D_{\text{CW}} (D_{\text{WG}} - D_{\text{CW}})^2 + P^2_{\text{atm}} K_{\text{C}} \left(D_{\text{WG}} - D_{\text{CW}}\right)}{K_{\text{C}} \left(D_{\text{WG}} - D_{\text{CW}}\right) + K_{\text{W}} D_{\text{CW}}}, \tag{2.8e}$$

$$c = -\frac{K_{\text{W}} \left(D_{\text{WG}} - D_{\text{Gwell}}\right)}{K_{\text{G}} \left(D_{\text{WG}} - D_{\text{CW}}\right) - K_{\text{W}} \left(D_{\text{WG}} - D_{\text{Gwell}}\right)}, \tag{2.8f}$$

$$d = \frac{\frac{\gamma}{2} K_{\text{W}} \left(D_{\text{Gwell}} - D_{\text{WG}}\right) \left(D_{\text{WG}} - D_{\text{CW}}\right)^2 + P^2_{\text{pump}} K_{\text{G}} \left(D_{\text{WG}} - D_{\text{CW}}\right)}{K_{\text{G}} \left(D_{\text{WG}} - D_{\text{CW}}\right) - K_{\text{W}} \left(D_{\text{WG}} - D_{\text{Gwell}}\right)}, \tag{2.8g}$$

$$e = \gamma \frac{K_{\text{W}}}{K_{\text{G}}} \left(D_B - D_{\text{GW}}\right) \left(D_{\text{GW}} - D_{\text{wellG}}\right) + P^2_{\text{pump}}, \tag{2.8h}$$

where K_{C} and K_{G} are permeabilities of cover and gravel layers, respectively. D_{CW}, D_{WG}, D_{Gwell}, D_{wellG}, D_{GW}, and D_B are the depths of corresponding boundaries represented in figure 2.5. P_{atm} and P_{pump} are atmospheric pressure and the given pump pressure, respectively.

Table 2.2 represents the minimal values of parameters used for the simulations. In stage one a comparison between the simplified 2D numerical and 1D analytical solutions is made. The verification is completed for multiples of a base generation rate Q up to 100. The results are reported in section 3.1. In stage two some validations and sensitivity analyses are conducted and obtained results are given in sections 3.2 and 3.3.

Table 2.2: Values used for simulations.

Parameter	Value	Description
n	2	Number of real perforations at each slit
L_ℓ	210 m	Length of landfill for stage one
	420 m	Length of landfill for stage two
T_{C}	3 m	Thickness of cover domain
T_{W}	8 m	Thickness of waste domain
T_{G}	1 m	Thickness of gravel domain
H_{ew}	0.018241 m	Height of equivalent well
T_{eww}	0.001 m	Thickness of equivalent well wall
K_{C}	$1\mathrm{E}-11$ m^2	Cover permeability for stage one
	$1\mathrm{E}-15 \rightarrow 1\mathrm{E}-11$ m^2	Cover permeability range for stage two
K_{W}	$1\mathrm{E}-9$ m^2	Waste permeability for stage one
	$1\mathrm{E}-10 \rightarrow 1\mathrm{E}-6$ m^2	Waste permeability range for stage two
K_{G}	$1\mathrm{E}-6$ m^2	Gravel permeability for stage one
	$1\mathrm{E}-5$ m^2	Gravel permeability for stage two
μ	$1.074\mathrm{E}-5$ Pa·s	Dynamic viscosity
M_{w}	0.028508 kg/mol	Molecular weight of gas mixture
T	288.15 K	Temperature
R	8.3145 J/(mol·K)	Universal gas constant
Q	$1\mathrm{E}-6$ kg/(m^3·s)	Gas generation rate
$P_{\mathrm{pump}} - P_{\mathrm{atm}}$	-1250 Pa	Pump gauge pressure for stage one
	$-1250 \rightarrow -12500$ Pa	Pump gauge pressure range for stage two

2.2 Modifying well geometry

Different geometric modifications of the well perforations and their combinations are assessed, as shown in figure 2.6. In this figure: (a) at each perforation section, the number of perforations are changed from 2 to 6; (b) all sets of perforations, as a group, are shifted to the left or right by the same value; as a result the number of perforated sections is reduced, depending on the shift length; (c) intervals between sets of perforation are decreased or increased linearly, so that a non-uniform distribution ensues; (d) radius of all perforations is changed, while the spacing is maintained the same; (e) the radius of perforations is decreased or increased linearly, while the spacing is maintained the same. To have a better insight into each type of modification, several derivatives of single modifications are assessed (table 2.3). Relying on the insight obtained with these basal modifications, prioritized well geometries are investigated with the purpose to diminish the landfill gas efflux and the air influx. In the base configuration each perforation set contains two holes ($n = 2$), and the spacing is at every 15 m from the well outlet to its end. The well pressure, surface velocity and mass flux profiles are constructed for this configuration and used as the reference for the counterparts obtained for modified geometries.
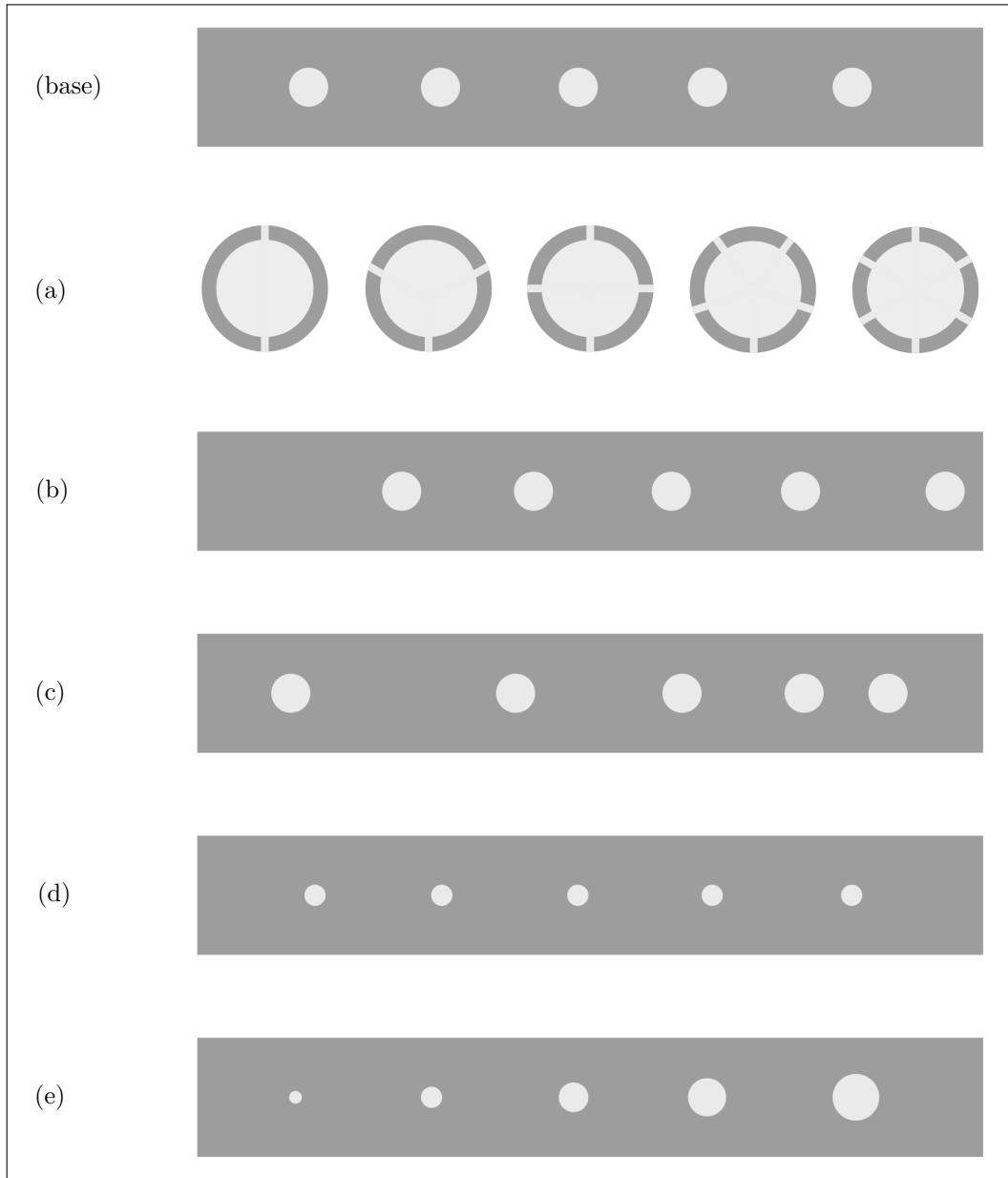
Figure 2.6: Different geometric modifications for a typical extraction well: (base) uniform distribution with equal perforation radius; (a) different number of perforations; (b) uniform perforation shifting to left or right; (c) non-uniform perforation distribution: linear increase or decrease in perforation intervals; (d) uniform changing of perforation radius with uniform distribution; (e) non-uniform changing of perforation radius with uniform distribution. Dimensions not to scale.

Table 2.3: Well modification types and their derivatives.

Well modification type	Description
(a): different number of perforations	a(1): $n = 3$
	a(2): $n = 4$
	a(3): $n = 5$
	a(4): $n = 6$
(b): uniform shifting of perforations	b(1): 10 m to the left
	b(2): 5 m to the left
	b(3): 5 m to the right
	b(4): 10 m to the right
(c): non-uniform perforation distribution	c(1): linear decrease in perforation intervals
	c(2): linear increase in perforation intervals
(d): uniform changing of perforation radius	d(1): $(R_\mathrm{h})_\mathrm{second} = 0.7(R_\mathrm{h})_\mathrm{base}$
	d(2): $(R_\mathrm{h})_\mathrm{second} = 1.5(R_\mathrm{h})_\mathrm{base}$
	d(3): $(R_\mathrm{h})_\mathrm{second} = 2(R_\mathrm{h})_\mathrm{base}$
(e): non-uniform changing of perforation radius	e(1): linear increase $0.7(R_\mathrm{h})_\mathrm{base} \rightarrow (R_\mathrm{h})_\mathrm{base}$
	e(2): linear decrease $(R_\mathrm{h})_\mathrm{base} \rightarrow 0.7(R_\mathrm{h})_\mathrm{base}$

Chapter 3

Results and discussion

3.1 Sub-unit simulation results

Based on the aforementioned methodology, a comparison between the simplified 2D numerical solution and the 1D analytical solution is made. For this comparison the vertical orange line in the middle of the sub-unit geometry shown in figure 2.5 is utilized as the reference profile. Figure 3.1 represents the results of the numerical and analytical solutions: both pressure profiles are visually indistinguishable for any applied gas generation rate. There are two conclusions: one, the COMSOL porous media flow solution is correct in the simple case, giving confidence in the definition of the set-up; two, the simplified 2D numerical solution is validated by the 1D analytical solution, so that a 1D analytical solution can be used in the construction of a semi-analytical tool in the future.
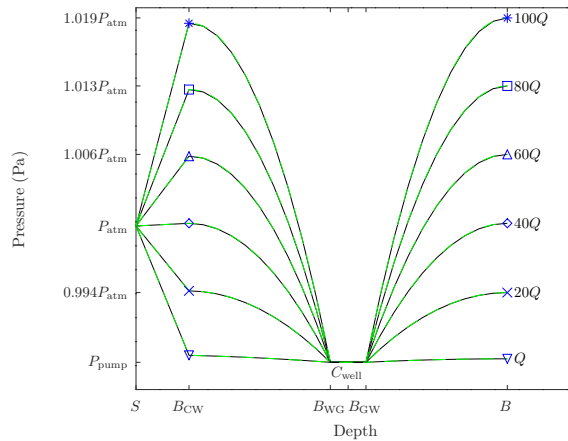
Figure 3.1: Pressure profiles for comparison between 1D analytical solution (solid black lines) and simplified 2D numerical solution (dashed green lines). Markers on both sides have been added to distinguish plots from each other. S: Surface; B_{CW}: boundary between cover and upper waste; B_{WG}: boundary between upper waste and upper gravel; B_{Gwell}: boundary between upper gravel and well; B_{wellG}: boundary between well and lower gravel; B_{GW}: boundary between lower gravel and lower waste; B: bottom. P_{atm} and P_{pump} are atmospheric pressure and the given pump pressure, respectively; C_{well} refers to the centroid of the equivalent well cross-section; Q is gas generation rate.

16

To show how each well modification affects fluid flow in a landfill, some simulations are conducted on the derivatives of modifications defined in figure 2.6 and table 2.3. For tracing the modification impact, the vertical velocity and pressure values along the surface and well center are calculated, respectively. Velocity and pressure profiles are shown in figures 3.2 and 3.3. Items (a) to (e) correspond to the well modifications presented in figure 2.6. Panel (f) in figure 3.2 depicts the ratio of surface mass flux ($\dot{m}$) for each derivative to the surface mass flux obtained from the basic configuration ($\dot{m}_{\text{base}}$) of the well. In vertical velocity profiles, the minimum value is subtracted from the actual values and shown at the top of each panel. Similarly in pressure profiles, pump pressure, as the minimum value within the well, is subtracted from the pressure values for each derivative. This shift of the reference point allows for a better visualization of the velocity and pressure variation in the landfill-well system. The loci of extrema and their shifting, and the overall proportional positioning of the curves are of importance for hereunder interpretations.

In panels (a) and (d) of figures 3.2 and 3.3, when the number of perforations or the perforation radius increase uniformly, higher surface velocity values are seen. This is because a well with a higher number of perforations or larger perforations has a higher collection capability for a given pump strength or equivalently a lower overall resistance to flow. Moreover, the trend of velocity profiles in these panels shows that there is a more significant maximum velocity for a well with a higher number of perforations or uniformly larger perforations. Furthermore, since the higher number of perforations or larger perforations close to the pump allows for more gas to be drawn into the well, the maxima in these velocity profiles shift toward the well outlet. Pressure profiles show that a higher number of perforations or uniformly larger perforations lead to a higher pressure in the well. The reason is the same as above.

Based on panel (b) in figure 3.2 shifting perforations toward the well outlet results in higher velocity above the well outlet and vice versa. Nevertheless the absolute values of those changes are intangible: the minima and maxima of all the curves are close. Moreover in figure 3.3(b) a lower pressure within the well is obtained due to the group of perforations closer to the well outlet.

In panel (c) of figure 3.2 there is a minor change in velocity profiles as a result of linearly increased or decreased intervals between perforation sets. It can be inferred that a higher concentration of perforations close to the well outlet leads to a higher vertical velocity at the surface. Panel (c) in figure 3.3 implies that as the concentration of perforations gets higher near the outlet, the pressure becomes higher within the well.

Panel (e) in figure 3.2 shows that when the radius of perforations increases linearly from the well outlet to the blocked end, higher surface velocity is expected above the blocked end and vice versa. This happens because the resistance diminishes toward the blocked end as a result of the existence of larger perforations. As mentioned before, higher surface velocity is expected above the larger perforations. Pressure profiles in figure 3.3(e) show that a higher pressure within the well occurs in the case of the linearly increasing perforation radius upstream. The reason is that the head induced by the pump is distributed more uniformly than in case of

a linearly decreased perforation radius along the well; the largest perforation is the closest one to the outlet and smaller perforations play less of a role.

Based on panel (f) modifications (a), (d), and (e) in figure 2.6 have the most significant impact on surface mass flux. Conversely modifications (b) and (c) have an intangible influence on surface mass flux.

According to the results presented in figures 3.2 and 3.3, it can be concluded that:

- Increasing the number of perforations or size of perforations leads to higher pressure within the well, having an incremental effect on the surface velocity of the incoming air. This happens due to drawing more mass into the well. Consequently a higher air intrusion rate and mass flux occur (refer to panels (a), (d), (e), and (f) in figures 3.2 and 3.3).

- Changing perforation distribution or shifting perforation sets has an intangible impact on mass flux rate at the surface. Although perforations closer to the suction source result in a lower pressure within the well, reducing air intrusion rate and mass flux at the surface (refer to panels (b), (c), and (f) in figures 3.2 and 3.3).

(a) changing number of perforations

(b) uniform shifting of perforations

(c) non-uniform perforation distribution

(d) uniform changing of perforation radius

(e) non-uniform changing of perforation radius

(f) normalized surface mass flux
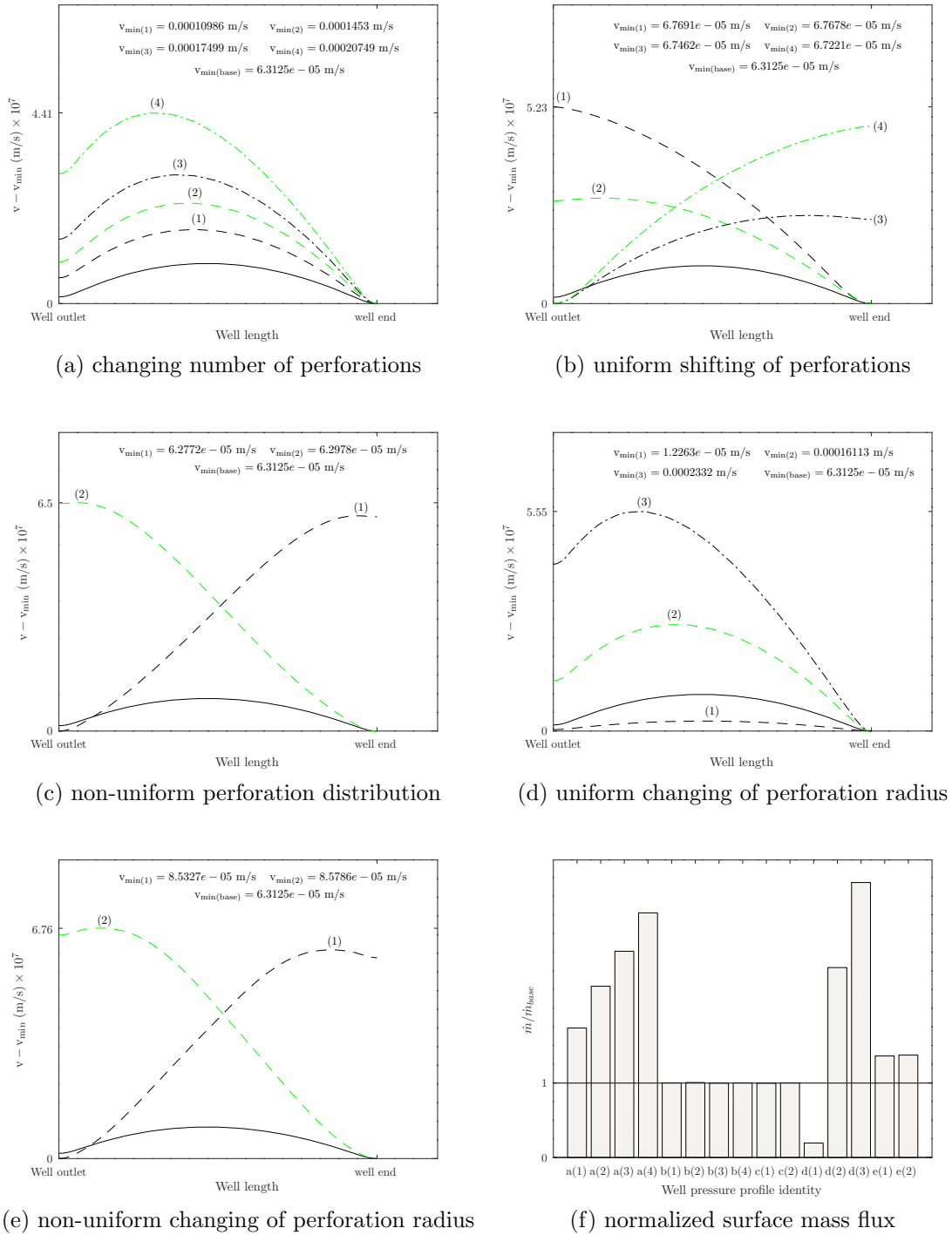
Figure 3.2: Vertical velocity at the surface for different well modifications. Panels (a) to (e) conform to geometric modifications (a) to (e) in figure 2.6. The solid black line in every plot corresponds to the primary well configuration (base). Panel (f) shows the normalized surface mass flux for each configuration.
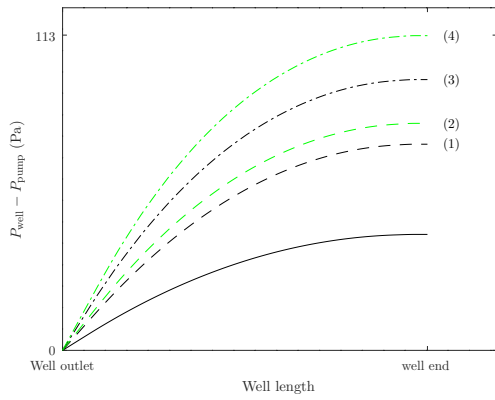
(a) changing number of perforations
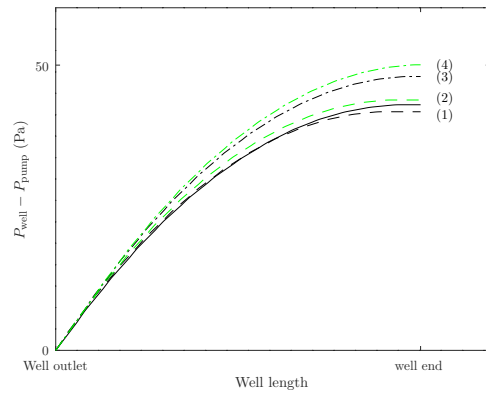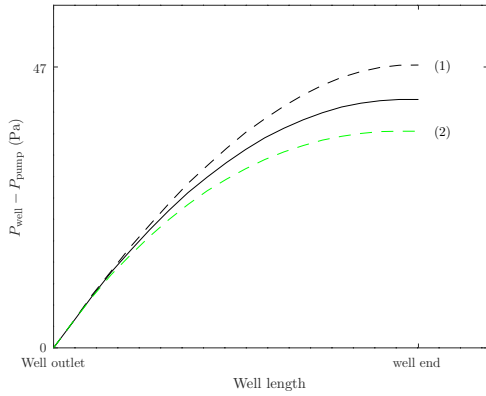
(b) uniform shifting of perforations

(c) non-uniform perforation distribution
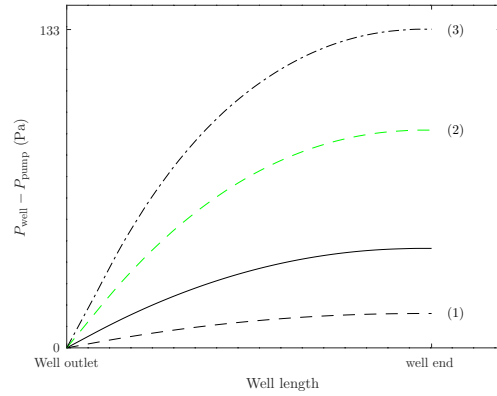
(d) uniform changing of perforation radius
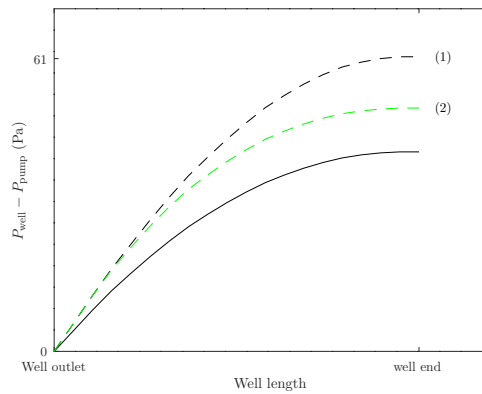
(e) non-uniform changing of perforation radius

Figure 3.3: Pressure profiles along the well center for different well modifications. Panels (a) to (e) conform to geometric modifications (a) to (e) in figure 2.6. The solid black line in every plot corresponds to the primary well configuration (base).

3.1.1 Analytical solution: non-linear vs. linear

It is known that the flow in the landfill system is only weakly compressible: the largest pressure drop either equals or slightly exceeds the suction imposed. This raises the question whether it would be reasonable to use incompressible flow equations. For the particular application of a horizontal landfill well it has been shown that would lead to an inaccurate representation of the pressure distribution in the collection system, since the pipe length is significant (Nec and Huculak, 2017). Below an analytical 1D solutions for the weakly compressible and incompressible flow types through a porous medium are compared. In case the gas density is constant equation (2.3) will be replaced with $\rho = \text{const}$ and the final governing equation for fluid flow in porous media then follow from equation (2.1):

$$\frac{\mathrm{d}^2 P}{\mathrm{d}y^2} = -\frac{\mu Q}{\rho K}. \tag{3.1}$$

To show the difference between linear and non-linear solutions a comparison was made for low and high suction strength. The discrepancy for the former is small and the more significant effect for the latter is shown in figure 3.4. As the generation rate increases, the discrepancy between the two solutions becomes more evident. Thus it is wise to use the non-linear version of the flow equation, i.e. the effect of pressure on the gas density should not be overlooked.
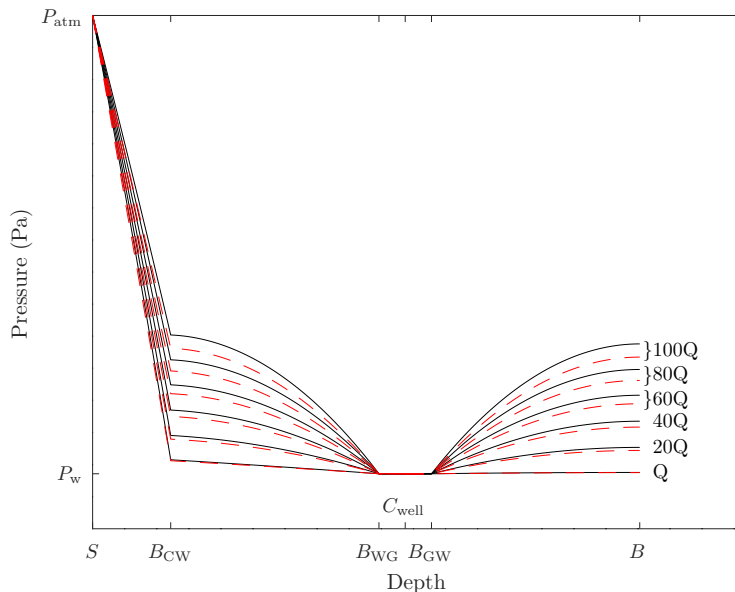
Figure 3.4: Comparison of non-linear (solid black lines) and linear (red black lines) analytical solutions. S: Surface; B_{CW}: boundary between cover and upper waste; B_{WG}: boundary between upper waste and upper gravel; B_{Gwell}: boundary between upper gravel and well; B_{wellG}: boundary between well and lower gravel; B_{GW}: boundary between lower gravel and lower waste; B: bottom. P_{atm} and P_{pump} are atmospheric pressure and the given pump pressure (-12.5 kPa), respectively; C_{well} refers to the centroid of the equivalent well cross-section; Q is gas generation rate.

3.2 Validation of computational mesh

The simulations conducted at stage one permit to prioritize the studied modifications and their potential combinations as follows. This prioritization is based on the observed impact of each modification on the surface mass flux and pressure values throughout the landfill. Consequently modification (c) is excluded from the later simulations. Prior to sensitivity analyses for each modification that are conducted at stage two, there should be a validation process for the computational meshes used to make sure that the simulation is adequately accurate. In general two meshes with a different number of elements are utilized. For each modification the models in COMSOL are run on these two meshes: base and fine. In some cases these meshes are customized for low and high suction strength separately. Table 3.1 shows the meshing information for different modifications. The maximum relative and absolute errors are based on the pressure drop within the well. Modification names correspond to those in figure 2.6 and table 2.3.

Table 3.1: Meshing information for different well modifications and corresponding maximum errors between the base and fine meshes.

Modification	Value	P_{pump}	Num. of elements	Max. rel. error	Max. abs. error
(a)	$n=2$	Low: -1.25 kPa	Base: 294894 Fine: 506270	$9.0516E-03$	1.47 Pa
		High: -12.5 kPa	Base: 225676 Fine: 410940	$4.5505E-05$	0.04 Pa
	$n=4$	Low: -1.25 kPa	Base: 294894 Fine: 506270	$5.1812E-03$	1.54 Pa
		High: -12.5 kPa	Base: 209952 Fine: 398576	$4.4434E-04$	0.8 Pa
	$n=6$	Low: -1.25 kPa	Base: 297550 Fine: 395788	$2.6775E-03$	0.93 Pa
		High: -12.5 kPa	Base: 204818 Fine: 392424	$5.2140E-04$	1.41 Pa
(b)	375 m	Low: -1.25 kPa	Base: 164774 Fine: 257806	$1.4104E-04$	$9E-03$ Pa
		High: -12.5 kPa	Base: 164774 Fine: 257806	$1.4104E-04$	$9E-03$ Pa
	390 m	Low: -1.25 kPa	Base: 158482 Fine: 236536	$7.3113E-09$	$4E-07$ Pa
		High: -12.5 kPa	Base: 158482 Fine: 236536	$7.3113E-09$	$4E-07$ Pa
	405 m	Low: -1.25 kPa	Base: 152418 Fine: 229368	$4.1615E-05$	$2E-03$ Pa
		High: -12.5 kPa	Base: 152418 Fine: 229368	$4.1615E-05$	$2E-03$ Pa
(e)	decr.	Low: -1.25 kPa	Base: 257564 Fine: 332862	$2.7809E-05$	$7E-03$ Pa
		High: -12.5 kPa	Base: 257564 Fine: 332862	$2.8651E-04$	0.7 Pa
	incr.	Low: -1.25 kPa	Base: 260298 Fine: 335596	$2.5301E-05$	0.01 Pa
		High: -12.5 kPa	Base: 260298 Fine: 335596	$7.0870E-05$	0.2 Pa
(b)+(e)	225 m and decr.	Low: -1.25 kPa	Base: 187878 Fine: 240160	$4.5890E-06$	$2E-04$ Pa
		High: -12.5 kPa	Base: 187878 Fine: 240160	$4.5890E-06$	$2E-04$ Pa
	225 m and incr.	Low: -1.25 kPa	Base: 187920 Fine: 240202	$1.6625E-05$	$7E-04$ Pa
		High: -12.5 kPa	Base: 187920 Fine: 240202	$1.6625E-05$	$7E-04$ Pa

According to the relative errors calculated for modification (a), going from low suction to high with the same value of n the error decreases by two orders of magnitude with $n = 2$ and by one order of magnitude with $n = 4$ and $n = 6$. Moreover maximum obtained absolute and relative errors are $9.0516E - 03$ and 1.54 Pa, respectively which depict a reasonable accuracy for the conducted simulations. To evaluate the precision of base and fine meshes for each modification, pressure values for the centerline of the well and a top-to-bottom profile at $x = 15$ m are calculated. As an example, panels in figure 3.5 demonstrate the validation result for modification (a) when $n = 2$: the pressure profiles corresponding to base and fine meshes match. This is one of the worst cases in table 3.1. In the field a precision of 1 Pa is ample with anything below that being untraceable by standard instrumentation. This figure shows that the simulation results obtained with the base mesh are adequately accurate. Therefore all results discussed hereinafter are done on the base meshes. Graphs corresponding to the remaining validation pairs listed in table 3.1 are not included in the thesis.
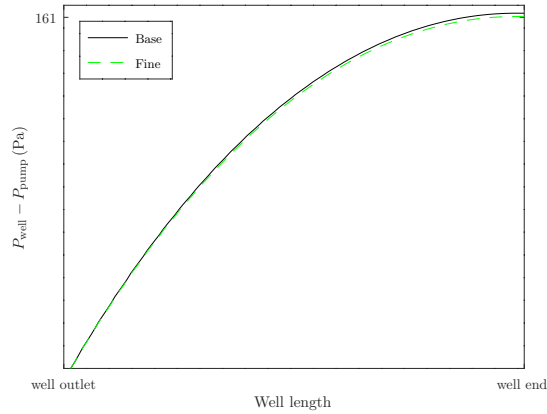
(a) longitudinal pressure proflie in the well
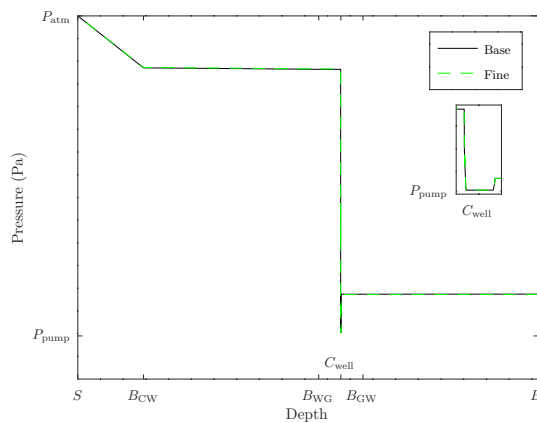
(b) vertical pressure profile from top to bottom

Figure 3.5: Validation of the base mesh using the fine mesh. Applying low suction strength (-1.25 kPa) and a set of two perforations ($n=2$) for each production section, the top panel is longitudinal pressure drop along the well center and the bottom panel is vertical pressure values for a profile from surface to landfill bottom (at $x = 15$ m).

23

3.3 Full length simulation: introduction

In the following sections, results obtained based on the aforesaid methodology are discussed for different modifications. In order to understand the insight following from the results, it is necessary first to understand the general behavior of the flow in the coupled landfill-well system. The purpose of this section is to explain this behavior using basic pressure drop arguments along specifically defined paths in the system. The pressure at the surface is known and equals atmospheric. The only other point, where the pressure is known a priori is at the outlet. Since the bottom of the landfill has a no flux condition, the pressure there can vary depending on the overall resistance. The bottom and top parts are only connected through the perforated sections of the well. In order to be able to interpret the physicality of the results, five intervals within the system are introduced.

Figure 3.6 shows a schematic view of a longitudinal cross-section of the landfill comprising the well and its first collecting slit. This figure demonstrates the intervals on which pressure difference is calculated. For the upper part of the landfill, moving downward from the surface to the well on interval 1, the pressure difference is investigated for the porous media. Interval 2 is a vertical line from the upper well ingress to the intercept which is the intersection of well centreline and slit centreline; followed by interval 3 which is a horizontal distance from the intercept to the well outlet. On intervals 2 and 3 pressure difference is evaluated based on the continuum flow in the well. Similarly for the lower part of the landfill, moving upward from the bottom to the well on interval 4, pressure difference is assessed for the porous media. Moreover pressure difference within the well from the lower well ingress to the intercept is appraised on interval 5. As mentioned before, interval 3 is used for pressure difference investigation between the intercept and the outlet.

To investigate this phenomenon, divide the landfill into two parts: one part above the well and the other below the well. Aiming to facilitate tracing the trajectories on which pressure drops are calculated, four arbitrary paths are defined based on the introduced intervals, as represented in table 3.2.

Table 3.2: Paths based on intervals.

Path name	Intervals
Γ_1	1→2→3
Γ_2	4→5→3
Γ_3	2→3
Γ_4	5→3

It is known that the total pressure drop in an open system equals the sum of pressure drop across the landfill porous media and pressure drop within the well. Therefore, total pressure drop in the upper and lower parts are:

$$\begin{cases} \Delta P_{\text{U, total}} = \Delta P_{\text{U, pore}} + \Delta P_{\text{U, well}}, & x, y \in \Gamma_1, \\[2em] \Delta P_{\text{L, total}} = \Delta P_{\text{L, pore}} + \Delta P_{\text{L, well}}, & x, y \in \Gamma_2, \end{cases} \tag{3.2}$$
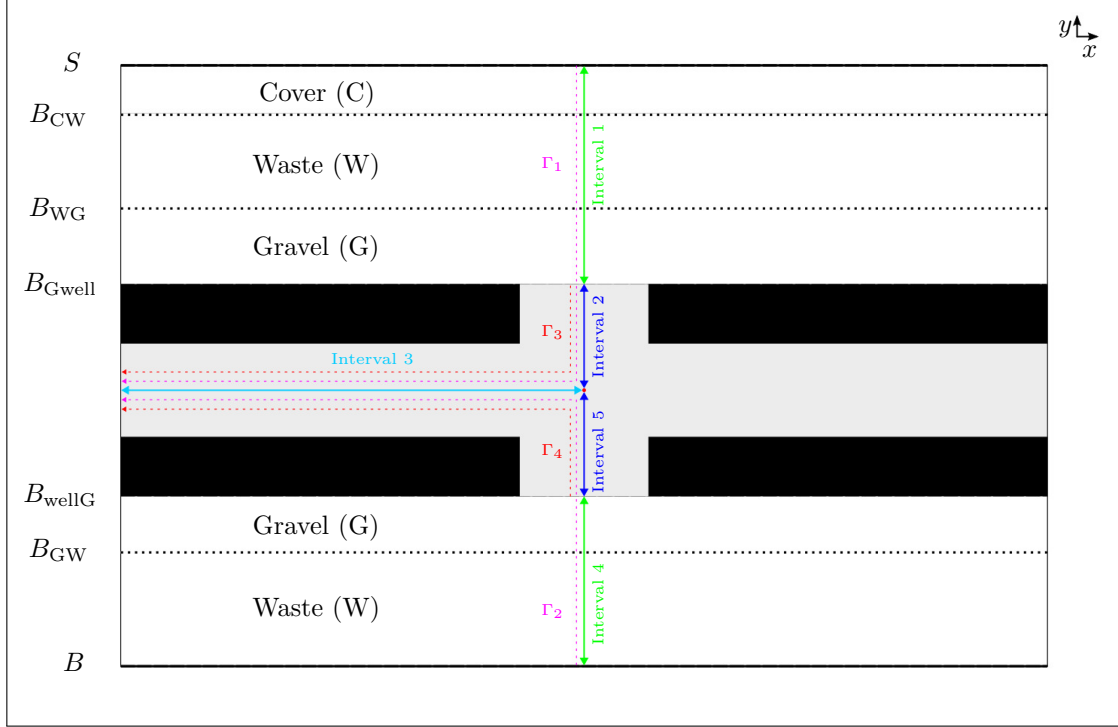
Figure 3.6: Schematic of trajectories/paths for pressure profiles. All horizontal layer labels are as in figure 2.5. Intervals 1 and 5 are vertical lines that refer to porous layers in the upper and lower parts of the landfill, respectively. Intervals 2 and 4 are vertical lines that represent the distance from the well ingresses to the intercept in the upper and lower parts, respectively. Interval 3 is a horizontal distance from the intercept to the outlet. Red point on well centerline shows the intercept. Dimensions not to scale.

where indices U and L stand for upper and lower, respectively. Well pressure drop refers to pressure difference in well between pump pressure and pressure at the common boundaries between gravel layer and well:

$$\begin{cases} \Delta P_{\text{U, well}} = (P_{\text{Gwell}} - P_{\text{intc}}) + (P_{\text{intc}} - P_{\text{pump}}), & x, y \in \Gamma_3, \\ \\ \Delta P_{\text{L, well}} = (P_{\text{wellG}} - P_{\text{intc}}) + (P_{\text{intc}} - P_{\text{pump}}), & x, y \in \Gamma_4. \end{cases} \tag{3.3}$$

where P_{intc} refers to the pressure at the intercept point. In the upper and lower parts, pressure differences of porous media are expresessed as:

$$\begin{cases} \Delta P_{\text{U, pore}} = \Delta P_{\text{C}} + \Delta P_{\text{W}} + \Delta P_{\text{G}} \\ \qquad = (P_{\text{S}} - P_{\text{CW}}) + (P_{\text{CW}} - P_{\text{WG}}) \qquad \{x, y \in \text{Interval } i \,|\, i = 1\}, \\ \qquad + (P_{\text{WG}} - P_{\text{Gwell}}), \\ \\ \Delta P_{\text{L, total}} = \Delta P_{\text{W}} + \Delta P_{\text{G}} \\ \qquad = (P_{\text{B}} - P_{\text{GW}}) + (P_{\text{GW}} - P_{\text{wellG}}), \qquad \{x, y \in \text{Interval } i \,|\, i = 4\}. \end{cases} \tag{3.4}$$

where indices C, W, and G stand for cover, waste, and gravel layers, respectively.

In the upper part on path Γ_1, total pressure drop depends on the pump and surface pressures. Since pressure at the surface is always constant and equal to atmospheric ($P_S = P_{atm}$), for a given pump pressure total pressure drop in the upper part must be constant. In the lower part on path Γ_2, there is a no flux boundary at the bottom. By Darcy's law, in the absence of gravity, the normal velocity is zero and consequently vertical pressure gradient equals zero ($dP/dy = 0$). Generally the pressure along the bottom is not constant. However, since the inlet and outlet planes are blocked, there is very little horizontal pressure gradient. With adding gravity pressure gradient is not zero, so that variation in pressure value with and without gravity is expected at the bottom of the landfill. In figure 3.7 pressure difference profiles for the base configuration with and without gravity at the bottom of the landfill are plotted; the pressure difference is based on the minimum value of each profile and this shift of the reference point allows for a better visualization of the pressure variation along the bottom. The plotted profiles clearly show that in a landfill with blocked ends pressure at the bottom of the landfill is not constant. Moreover, the pressure variation is very small – less than 1Pa, which is the resolution of existing instrumentation in the field – allowing to conclude that for all practical purposes the pressure on the bottom of the landfill is constant. The difference between extrema for both profiles represents a variation that is by far less than the maximum absolute error provided in table 3.1. Furthermore, both pressure profiles match, meaning that the difference between pressure values at the bottom in models with and without gravity corresponds to the hydrostatic pressure.

	Bottom Pressure (Pa)	
	min	max
Without gravity	100159.926	100160.097
With gravity	100405.814	100405.985
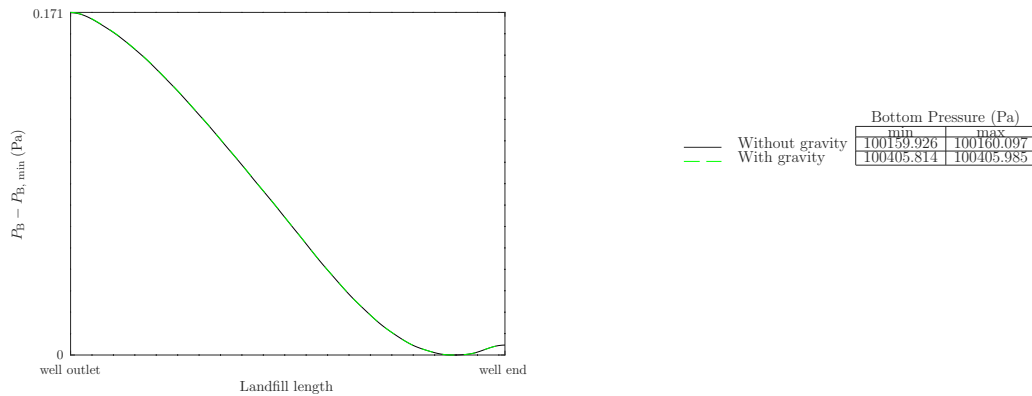
Figure 3.7: Comparison of pressure difference at the bottom of the landfill for the base configuration with and without gravity. The table on the right side contains minimum and maximum values for the normalization applied to each curve.

It is perceived that total pressure drop in the upper part on path Γ_1 is constant. Furthermore, In the lower part on path Γ_2 total pressure drop is virtually constant as the pressure value at the bottom of the landfill is not an absolute constant. The porous layer constitutes a barrier to fluid flow and permeability represents the amount of its resistance. Overall when the resistance in the open system increases, there is a reduction in surface flux. Based on Darcy's law, any layer's permeability and pressure gradient are interrelated. Beginning with the layer that is closest to the surface, as cover permeability changes there should be a counter change in pressure

difference in porous medium to compensate for the impact of permeability on flow rate to keep it fixed. Notwithstanding, surface flux reduction occurs as a result of decreasing permeability in the system. In such a case it can be concluded that the pressure drop compensation in porous media has been insufficient. In other words, pressure gradient has a reaction effect on flow rate, which in some cases might not entirely compensate for the porous media permeability changes, leading to a variation in surface flux.

The surface flux is based on the pressure gradient immediately beneath the surface and should be interpreted as the type of surface flux, be it air intrusion or gas escaping. When the gas generation considered for the model is small, the pump is capable of extracting all generated landfill gas along with some air, leading to negative surface flux in most cases. If precise tracing of air intrusion and mixing with the landfill gas was to be attempted, this would require an additional dispersion equation. This modeling would not make sense side by side with an effective constant gas generation rate and composition. To initialize the dispersion model one will require input from field measurements, which is cost prohibitive given that landfill properties change over time. The amount of intruding air can approximately be calculated based on mass conservation across the surface, but was not done here, since this project does not aim to provide quantitative predictions.

Based on the results provided in section 3.1, it is expected that increasing the number of perforations (modification (a) in figure 2.6) will lead to a higher surface flux. This is also valid for a uniform change in perforation size (modification (d) in figure 2.6). For perforation shifting (modification (b) in figure 2.6) there might be an impact on surface flux when extreme shifting is applied. A linear increase in perforation size (modification (e) in figure 2.6) results in a higher air intrusion. Furthermore, combining these modifications might increase the chance to have more control over surface flux.

3.4 Changing number of perforations

The first modification ((a) in figure 2.6) is investigated in this section. This modification reduces the local resistance at the ingress into the well by increasing the collection area on the surface of the well. It is expected that this effect will be felt at the surface as an increased influx of air or diminished escape of landfill gas, depending on the scenario seen with the base configuration under the same conditions. Throughout this section modification (a) is investigated and several sensitivity analyses are conducted when perforation numbers in each production segment equal 2, 4 or 6.

Below the immediate conclusions following from the numerical solutions are discussed. For a comprehensive explanation on the physics of flow in the coupled system and the interplay of head losses over different trajectories within the open system see section 3.3. Figures 3.8, 3.9, and 3.10 demonstrate the effect of cover permeability (K_C), waste permeability (K_W) and pump pressure (P_{pump}) on surface mass flux. Figure 3.8 shows the impact of cover permeability on well pressure, vertical pressure from top to bottom at x=15 m, and surface flux for a pump pressure of -1.25 kPa for base configuration when number of apertures in each perforated

production segment is two (n=2). In this figure each line style corresponds to a value of cover permeability. In panel (a), changing permeability of cover leads to a significant impact on well pressure. Maximum well pressure drop with respect to pump pressure occurs at the blocked end.

In panel (b) the slope of the line in the S-B_{CW} region shows the intensity of cover permeability effect on pressure in the landfill. The progression of lines shows that the pressure profile slope becomes steeper as the permeability decreases. For lower cover permeabilities most of the pressure drop happens in the landfill cover, so the well pressure drop should reduce to keep the total pressure drop constant. Therefore decreasing cover permeability reduces pressure within the well.

Surface flux decreases with a diminishing permeability, as shown by the progression of curves in the inset of panel (c) - the inset demonstrates the actual surface flux profiles to visualize them in a single window. The reason is that for the open system upstream pressure equals atmospheric and downstream pressure equals the pressure at the common boundaries between the well and gravel layer, which is not fixed. In such a case the pressure drop in the porous media fuse compensate for the negative impact of the cover permeability reduction on fluid flow, leading to a decrease in the surface flux. In light of the explanation above, for lower cover permeabilities the effect on the pressure drop and surface flux is higher than that of the production well; the well has a lower impact on the surface flux and location of maximum surface flux moves away from well outlet.

A similar set of results for a progression of waste permeability values is given in figure 3.9. It is seen that there is no tangible difference in well pressure, except for the tightest waste permeability, as represented by dotted-dashed black line in panel (a). Nonetheless no variation can be seen in the surface flux (inset of panel (c)). In the case of lowest waste permeability, pressure drop within the well is more dominant than that in waste layer. Based on figure 3.10 a higher suction strength leads to a higher well pressure drop, as represented by a progression of curves from bottom to top in panel (a). Furthermore, for an increased pump pressure there is a higher pressure drop within the well in comparison to porous media, as shown by a progression of curves from top to bottom in panel (b). Changing pump pressure directly affects surface mass flux: by a progression of curves from top to bottom in the inset of panel (c), a higher suction strength leads to a higher surface flux. Moreover, based on panel (c) the maximum surface flux locus shifts toward the well end.

The above analysis was subsequently conducted for the modifications with $n = 4$ and $n = 6$ and resulted in similar findings. For the highest cover permeability, comparing the three modifications reveals that an increased number of perforations augments the impact on well pressure. The reason is that for the highest permeability, the well plays a more dominant role in fluid flow throughout landfill. However for the lower cover permeabilities, the opposite is correct. Changing waste permeability for modifications with a higher number of perforations provides the same result as for the base configuration. The same pressure and surface flux trends are observed in the landfill: as the number of perforations increases, surface mass flux increases since more fluid is drawn in as expected and the locus of the maximum flux shifts toward the well outlet.

(a) long. pressure in the well (n=2)

(b) vertical pressure profile (n=2)

(c) surface mass flux (n=2)

		Surface mass flux (kg/m$^2 \cdot$ s)	
		min	max
———	KC=1e−11 m^2	−7.5875e−5	−7.5825e−5
− − −	KC=1e−12 m^2	−3.2161e−5	−3.2158e−5
− − −	KC=1e−13 m^2	−4.2819e−6	−4.2817e−6
———	KC=1e−14 m^2	−4.3953e−7	−4.3951e−7
−·−·−	KC=1e−15 m^2	−4.4065e−8	−4.4063e−8
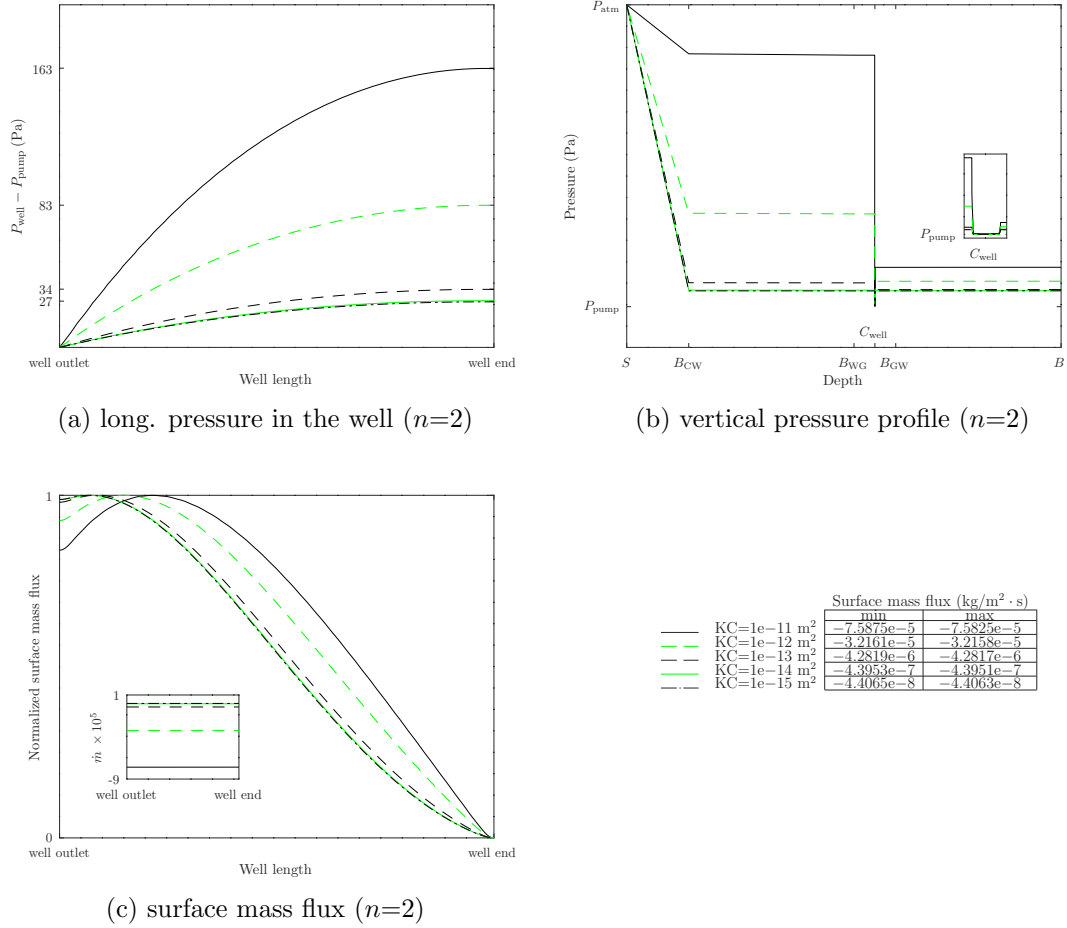
Figure 3.8: Effect of cover permeability on pressure and surface flux for base configuration with n=2. Panel (a) shows the well pressure profile at the centerline. Panel (b) represents the pressure profile along a vertical line from top to bottom of landfill at x=15 m; inset represents the pressure values in the well and its slits. Panel (c) shows the normalized surface flux, $(\dot{m} - \dot{m}_{\min})/(\dot{m}_{\max} - \dot{m}_{\min})$, and the table contains scaling values for each plot. The inset demonstrates the actual surface flux profiles.

(a) long. pressure in the well (n=2)

(b) vertical pressure profile (n=2)

(c) surface mass flux (n=2)
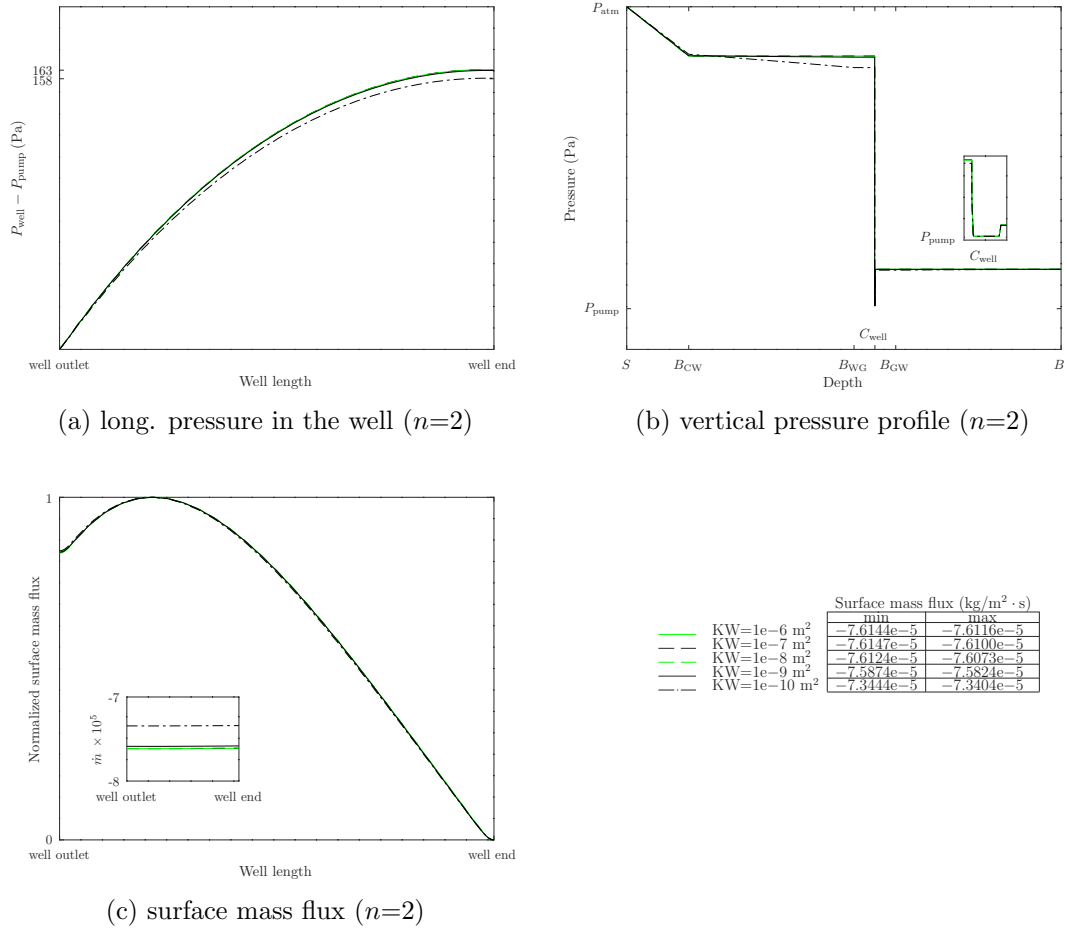
Figure 3.9: Effect of waste permeability on pressure and surface flux for n=2. Panel (a) shows the well pressure profile at the centerline. Panel (b) represents the pressure profile along a vertical line from top to bottom of landfill at x=15 m; inset represents the pressure values in the well and its slits. Panel (c) shows the normalized surface flux, $(\dot{m} - \dot{m}_{\min})/(\dot{m}_{\max} - \dot{m}_{\min})$, and the table contains scaling values for each plot. The inset demonstrates the actual surface flux profiles.

(a) long. pressure in the well (n=2)

(b) vertical pressure profile (n=2)

(c) surface mass flux (n=2)

Figure 3.10: Effect of suction strength on pressure and surface flux for n=2. Panel (a) shows the well pressure profile at the centerline. Panel (b) represents the pressure profile along a vertical line from top to bottom of landfill at x=15 m; inset represents the pressure values in the well and its slits. Panel (c) shows the normalized surface flux, $(\dot{m} - \dot{m}_{\min})/(\dot{m}_{\max} - \dot{m}_{\min})$, and the table contains scaling values for each plot. The inset demonstrates the actual surface flux profiles.

In addition to the previous investigation, double-parameter sensitivity analyses are done for K_C-K_W, K_C-P_{pump}, and K_W-P_{pump} combinations, summarized in figures 3.11, 3.12, and 3.13, respectively. As mentioned in the beginning of section 3.3, there are two key concepts in a landfill interacting with the atmosphere: the total pressure drop in the entire open system is constant for a given suction strength; by Darcy's law there is a direct relationship between permeability and surface flux.

Panels (a) and (c) in figure 3.11 imply that the impact of the cover permeability in comparison to the waste permeability on pressure drop within the well and surface flux is stronger. Comparing lines corresponding to different combinations (solid black / dashed green and solid green / dashed black sets of lines), it is the cover permeability variation that makes a significant difference in well pressure profile and surface mass flux, not the waste permeability. The reason is that a higher permeability leads to less resistance to fluid flow. Furthermore, at the lowest level of cover permeability, varying waste permeability almost does not affect well pressure drop, as well as surface flux. From solid green and dashed black lines in panel (b) it follows that having a tighter cover reduces the pressure drop portion of the waste layer. For a given pump pressure the tightest cover results in a minimum surface flux and the waste permeability is not of importance. Maximum surface flux location shifts toward the well outlet for combinations with lower cover permeabilities.

Panel (a) in figure 3.12 demonstrates that increasing pump pressure leads to a higher pressure drop within the well (solid green line), but this phenomenon diminishes dramatically for a lower permeability (dashed black line). In the case of the tightest cover (green and black dashed lines) in panel (b), as the landfill is almost sealed, changing the suction strength leads to a minor variation in the well pressure drop, since most of the head is lost in the cover. It means that the incoming surface flux approaches zero, and as a result of the constant gas generation rate in the waste layer, the pressure drop within the well is roughly kept fixed (green and black dashed lines in panel (a)). As for surface flux, for a higher cover permeability upon increasing pump pressure the air intrusion is more pronounced, as shown by solid black and solid green lines in the inset of panel (c). However in the case of a tighter cover, changing suction strength does not majorly affect the surface flux (dashed black and dashed green lines). In terms of locus of maximum surface flux, by increasing suction strength for a tighter cover, it moves away from the well outlet (solid black and solid green lines in panel (c)); this happens since farther perforations with respect to well outlet can increase their involvement in the suction process. For a looser cover despite changing the pump pressure, there is no shifting in the surface flux profile (dashed black and dashed green lines).

Figure 3.13 shows that the pump pressure is critical in controlling surface flux. The sets of solid green-dashed black and solid black-dashed green lines in panels (a) and (b) it indicates that a significant variation in well pressure drop and landfill pressure occurs as a result of a change in the suction strength. The waste permeability has a minor impact on the pressure drop within the well and throughout the landfill. Therefore surface flux can not be controlled by waste permeability, as shown by solid black-dashed green and solid green-dashed black sets of lines in the inset of panel (c). Despite the fact that in practice the landfill designers and operators have very little control over the waste permeability. Increasing pump

pressure leads to a shifting of the maximum surface flux locus toward the blocked end (solid black-dashed green and solid green-dashed black sets of lines panel (c)).

(a) long. pressure in the well ($n=2$)

(b) vertical pressure profile ($n=2$)

(c) surface mass flux ($n=2$)

	Surface mass flux (kg/m² · s)	
	min	max
—— KC=1e−11 m², KW=1e−6 m²	−7.6144e−5	−7.6116e−5
– – KC=1e−11 m², KW=1e−10 m²	−7.3444e−5	−7.3404e−5
—— KC=1e−15 m², KW=1e−6 m²	−4.4075e−8	−4.4074e−8
– – KC=1e−15 m², KW=1e−10 m²	−4.3968e−8	−4.3966e−8
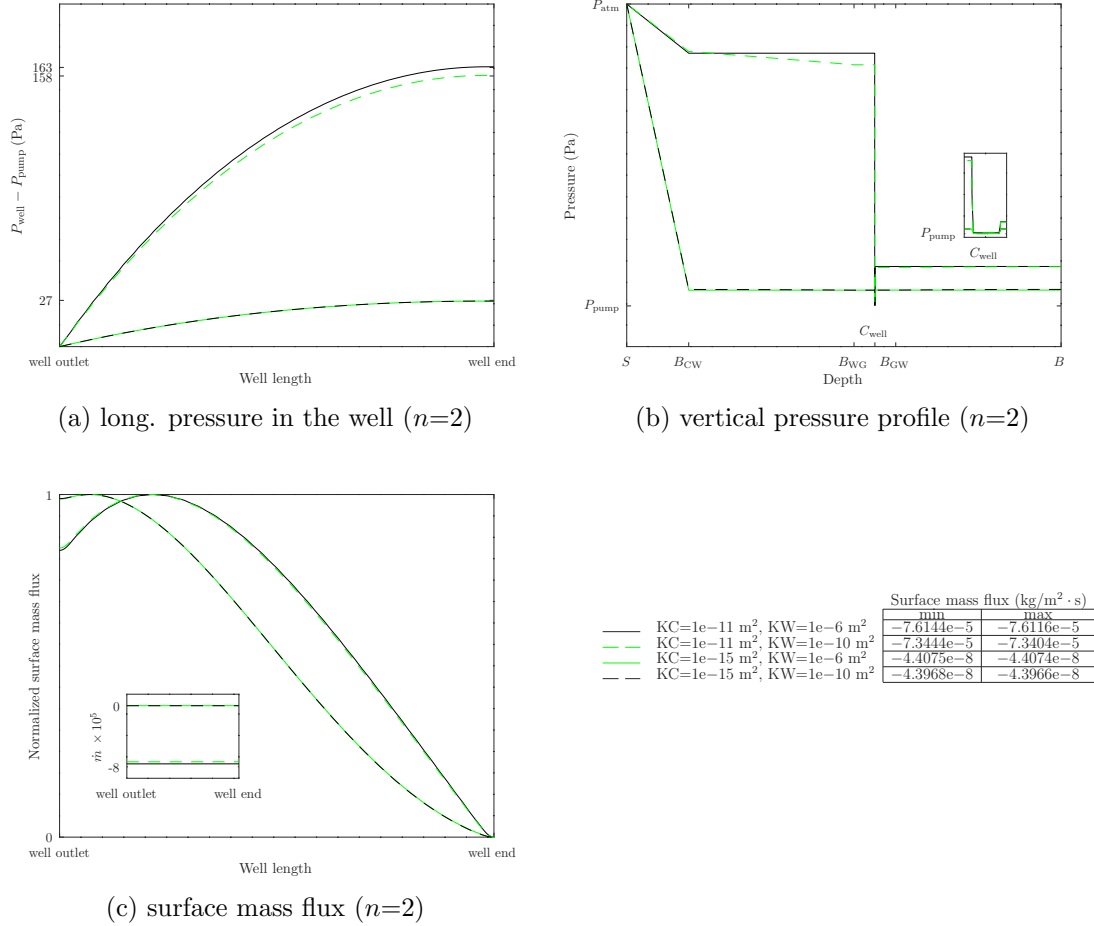
Figure 3.11: Effect of waste-cover permeability combinations on pressure and surface flux for $n=2$. Panel (a) shows the well pressure profile at the centerline. Panel (b) represents the pressure profile along a vertical line from top to bottom of landfill at x=15 m; inset represents the pressure values in the well and its slits. Panel (c) shows the normalized surface flux, $(\dot{m} - \dot{m}_{min})/(\dot{m}_{max} - \dot{m}_{min})$, and the table contains scaling values for each plot. The inset demonstrates the actual surface flux profiles.

Based on the obtained results for double-parameter sensitivity analyses by utilizing $n=4$ or $n=6$ it can be concluded that a higher number of perforations leads to a higher well pressure drop for the highest cover permeability. The impact of waste permeability on pressure drop is more obvious for a higher number of perforations. Surface flux maxima loci are shifted toward the well outlet for a higher number of perforations. As expected, the most obvious means of controlling the surface flux is the permeability of the cover layer.

It was observed that increasing the number of perforations led to a higher air intrusion. The reason is that a well with a higher number of perforations collects more mass, increasing overall flow throughout the system. Therefore this modification provides a means to control surface flux in cases where landfill gas escapes, but

increasing the pump suction is not an option. Reducing the local resistance at the ingress into the well will then create the requisite reversal of flow direction at the surface.

(a) long. pressure in the well (n=2)

(b) vertical pressure profile (n=2)

(c) surface mass flux (n=2)
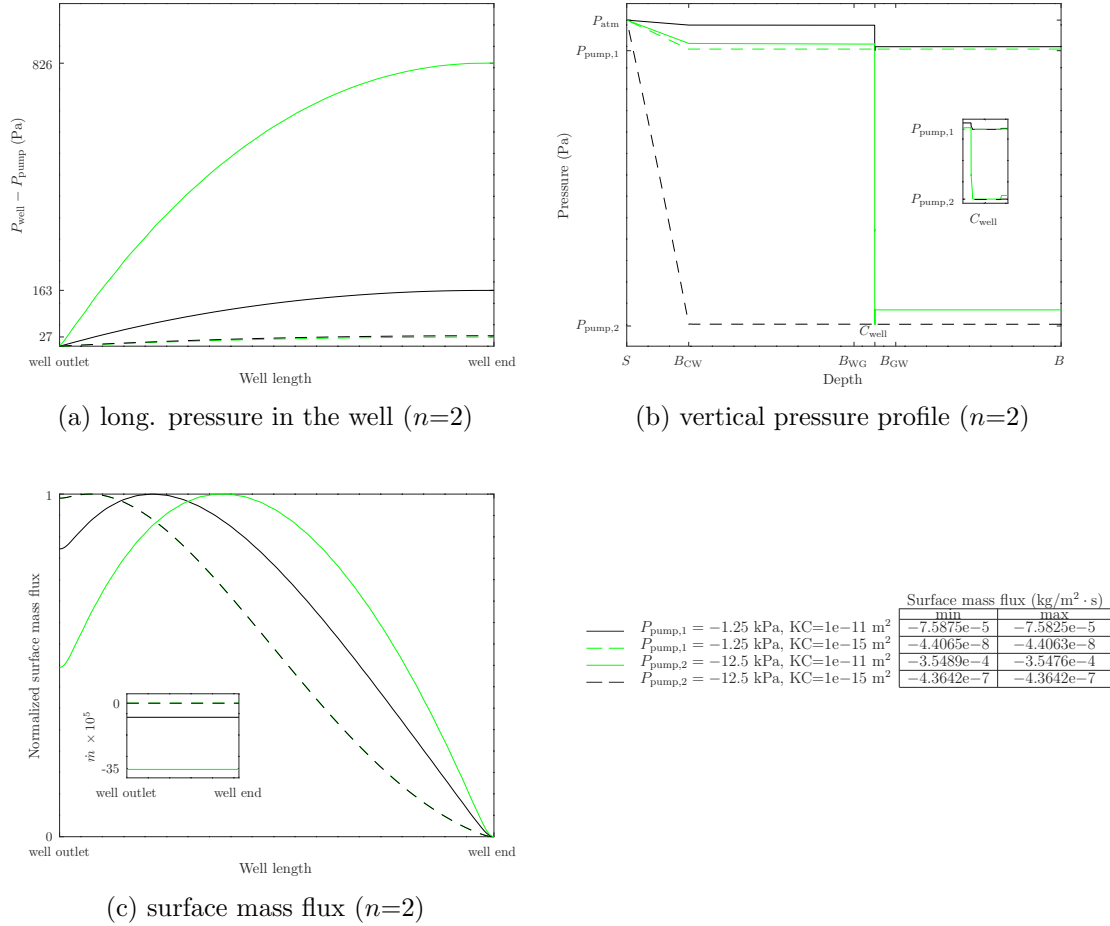
Figure 3.12: Effect of cover permeability-pump pressure combinations on pressure and surface flux for n=2. Panel (a) shows the well pressure profile at the centerline. Panel (b) represents the pressure profile along a vertical line from top to bottom of landfill at x=15 m; inset represents the pressure values in the well and its slits. Panel (c) shows the normalized surface flux, $(\dot{m} - \dot{m}_{min})/(\dot{m}_{max} - \dot{m}_{min})$, and the table contains scaling values for each plot. The inset demonstrates the actual surface flux profiles.

34

(a) long. pressure in the well (n=2)

(b) vertical pressure profile (n=2)

(c) surface mass flux (n=2)
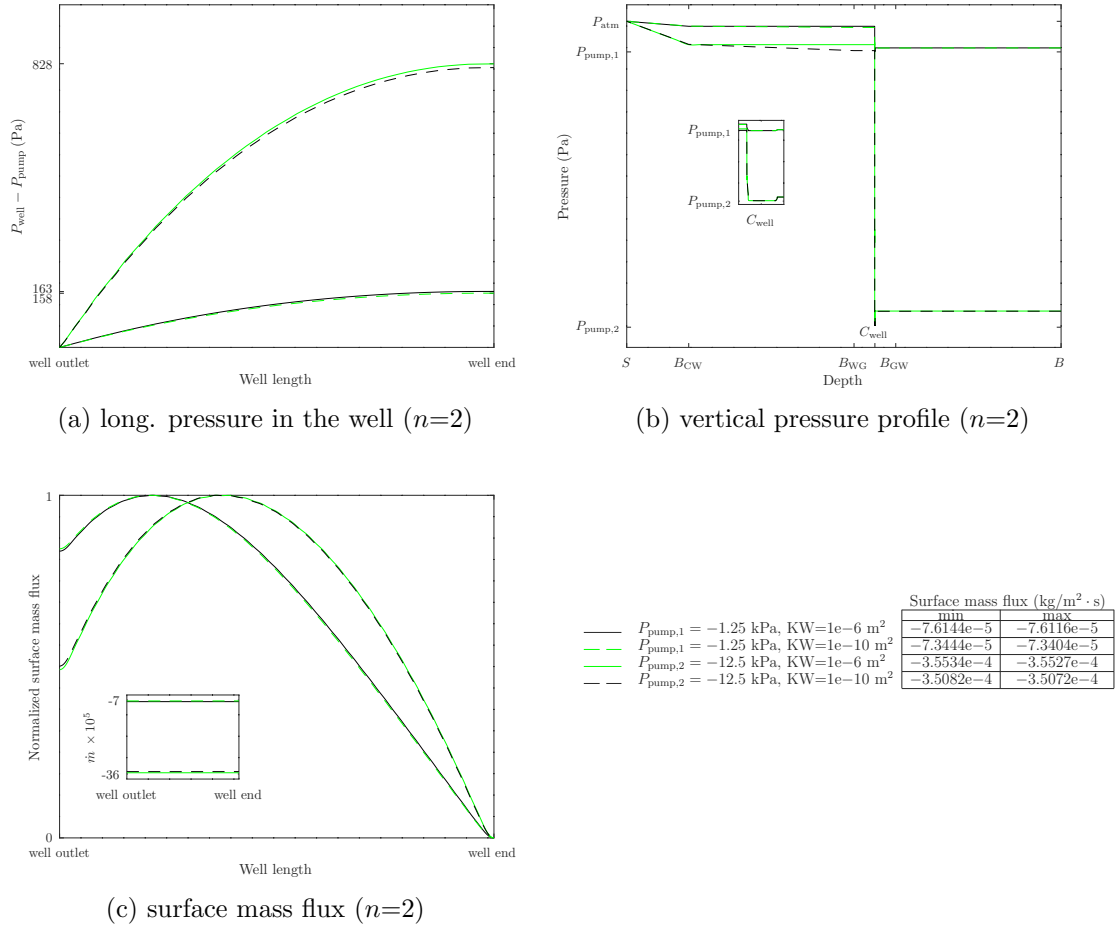
Figure 3.13: Effect of waste permeability-pump pressure combinations on pressure and surface flux for n=2. Panel (a) shows the well pressure profile at the centerline. Panel (b) represents the pressure profile along a vertical line from top to bottom of landfill at x=15 m; inset represents the pressure values in the well and its slits. Panel (c) shows the normalized surface flux, $(\dot{m} - \dot{m}_{\min})/(\dot{m}_{\max} - \dot{m}_{\min})$, and the table contains scaling values for each plot. The inset demonstrates the actual surface flux profiles.

3.5   Changing perforation size uniformly

This section discusses the impact of various aperture sizes (modification (d) in figure 2.6) on the landfill-well coupled open system. By increasing the collection area on the well's surface, this modification lowers the local resistance at the ingress into the well. According to the equivalent width formula, $W_{ep} = (n\pi R_h^2)/(2W_{ew})$, for a fixed aperture width, the radius of the holes is proportional to the square root of the number of perforations; perforation number variation from 2 to 6 corresponds to perforation radius change from $R_{h,base}$ to $2.45R_{h,base}$. Based on this argument in terms of modeling, changing perforation radius provides the same result as the variation of perforation number. According to obtained results from section 3.4, a bigger perforation radius leads to a higher well pressure drop for the highest cover permeability. But for the lower cover permeabilities, it is the other way around. For both large and small perforations, changing waste permeability does not show tangible impact on pressure and surface flux. Furthermore, pressure and surface flux trends in the landfill are the same for different waste permeabilities. As the perforation radius increases, so does the surface mass flux and the location of the highest surface flux moves away from the well end. Despite the fact that in 3D the local effect would be different but the surface is far away from the well so that this local effect on surface flux is intangible and it can be neglected. As expected, a higher perforation size improves the well effective collection ability, leading to a higher air intrusion.

3.6   Changing perforation size non-uniformly

Linear perforation size change (modification (e) in figure 2.6) is investigated in this section. This modification affects pressure drop distribution non-uniformly along the well length. If the linear increase in perforation size is applied, the local ingress resistance reduces at the end of the well, since this is the location of the larger perforations. By comparison to the base configuration, a higher air intrusion or lower gas escaping at the surface is expected near the blocked end.

Detailed explanations of the physics of flow in a coupled system and the interplay of head losses within an open system can be found in section 3.3. In the case of a linear decrease in perforation size, based on panels (a) and (b) in figure 3.14 reducing cover permeability–from top to bottom–leads to a higher pressure drop in landfill and consequently lower pressure drop in well for a landfill in contact with the atmosphere. The reason is that the total pressure drop in the system is constant and it is equal to pressure difference between the atmosphere and pump. According to the inset of panel (c) from bottom to top, surface flux becomes lower and approaches zero for smaller cover permeabilities. Maxima loci of the surface flux are fairly above well outlet where the maximum suction is applied due to the largest perforations near the outlet, leading to a reverse S-shaped curves incline toward the well outlet (panel (c)).

Panels (a) and (b) in figure 3.15 represent that increasing waste permeability causes tiny variation in well and landfill pressure except for the tightest waste layer

(dotted-dashed black line), which provides a lower pressure drop throughout the waste layer and within the well. It is deemed that reducing waste permeability has a subtractive impact on surface flux, as shown from bottom to top in the inset of panel (c). There is not a noticeable shift in the reverse S-shaped surface flux profiles (panel (c)). According to panels (a) and (b) in figure 3.16, changing suction strength leads to a significant effect on the pressure within the well and throughout landfill; from top to bottom profiles correspond to lower pump pressures. Increased pump pressure provides a higher pressure drop within the well and throughout the landfill. From top to bottom in the inset of panel (c), there is an incremental variation in surface flux; no shifting for surface flux maxima loci as well. Reverse S-shaped curves of surface flux incline toward the well outlet with a maximum above the larger perforations, as represented in panel (c).

(a) long. pressure in the well ($n=2$)

(b) vertical pressure profile ($n=2$)

(c) surface mass flux ($n=2$)

	Surface mass flux (kg/m² · s)	
	min	max
KC=1e−11 m²	−2.3329e−4	−2.3095e−4
KC=1e−12 m²	−4.3922e−5	−4.3855e−5
KC=1e−13 m²	−4.5949e−6	−4.5927e−6
KC=1e−14 m²	−4.6104e−7	−4.6088e−7
KC=1e−15 m²	−4.6119e−8	−4.6103e−8
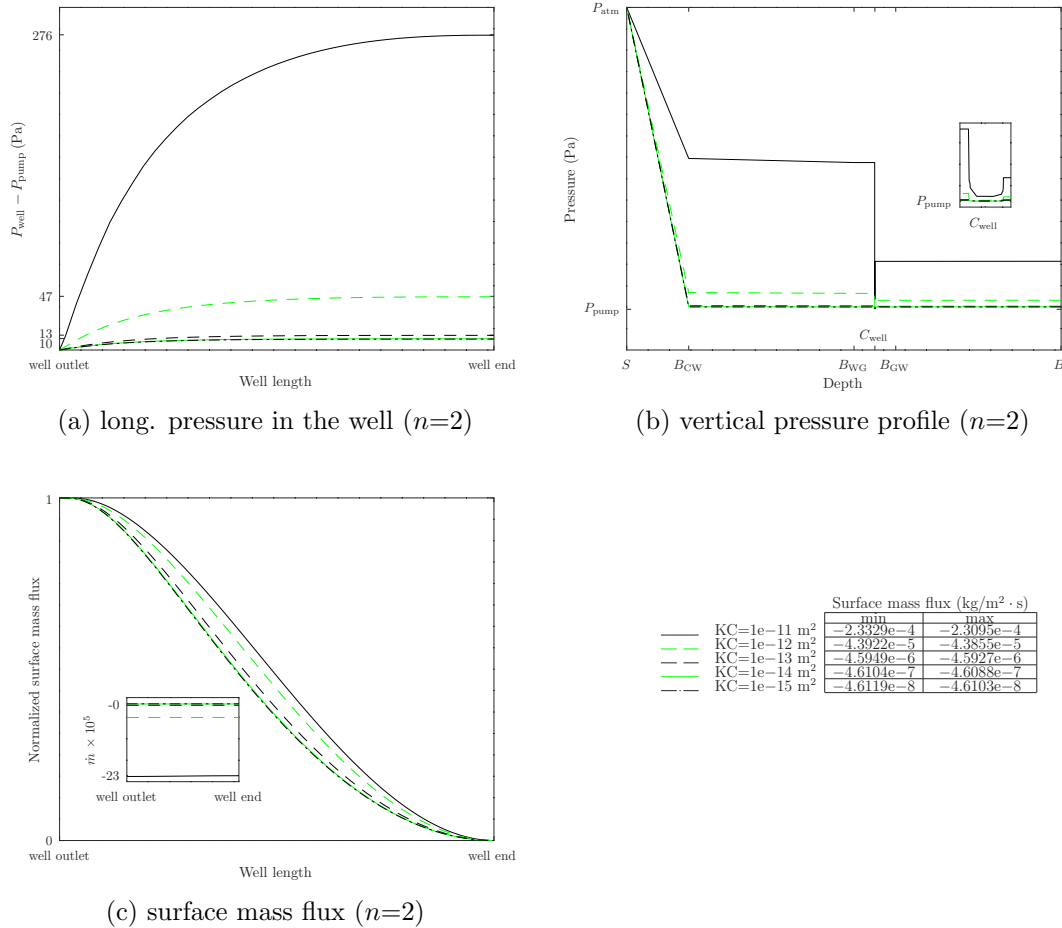
Figure 3.14: Effect of cover permeability on pressure and surface flux for linear perforation size decrease ($n=2$). Panel (a) shows the well pressure profile at the centerline. Panel (b) represents the pressure profile along a vertical line from top to bottom of landfill at x=15 m; inset represents the pressure values in the well and its slits. Panel (c) shows the normalized surface flux, $(\dot{m} - \dot{m}_{min})/(\dot{m}_{max} - \dot{m}_{min})$, and the table contains scaling values for each plot. The inset demonstrates the actual surface flux profiles.

(a) long. pressure in the well (n=2)

(b) vertical pressure profile (n=2)

(c) surface mass flux (n=2)
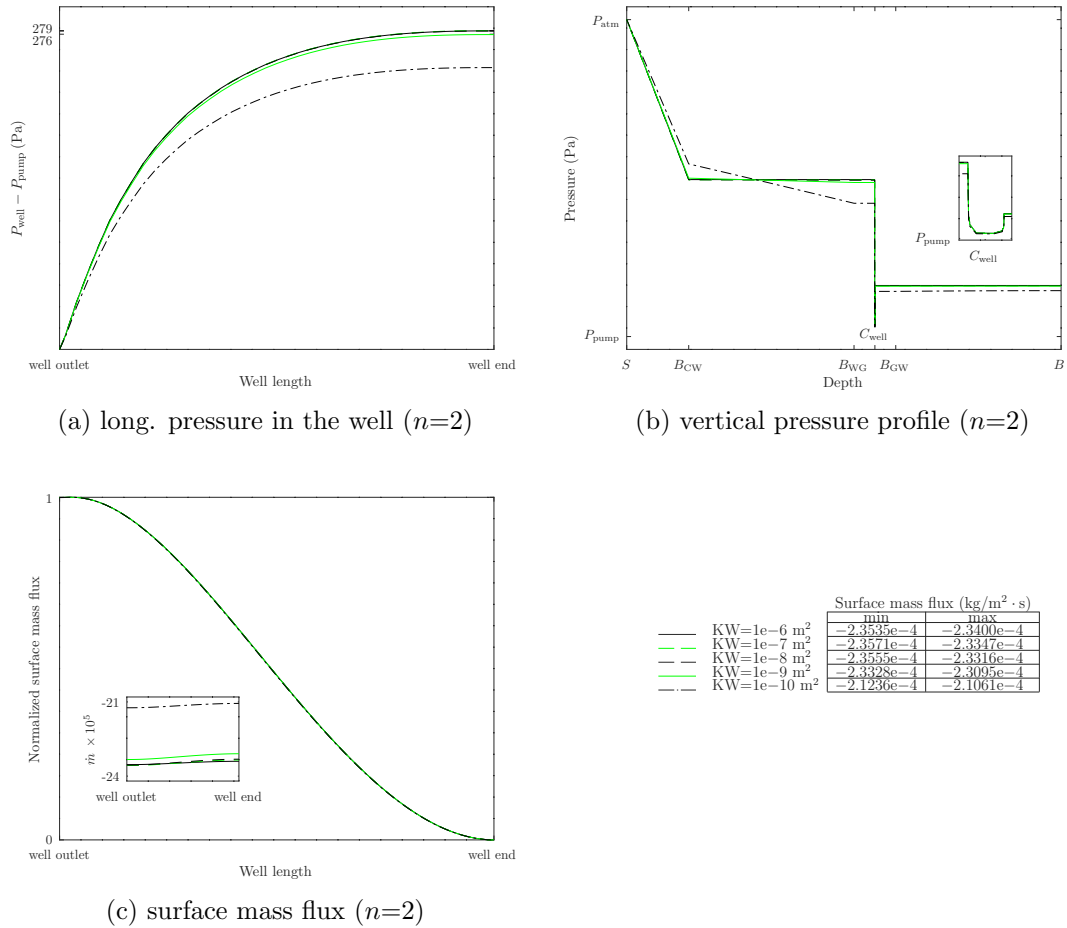
Figure 3.15: Effect of waste permeability on pressure and surface flux for linear perforation size decrease (n=2). Panel (a) shows the well pressure profile at the centerline. Panel (b) represents the pressure profile along a vertical line from top to bottom of landfill at x=15 m; inset represents the pressure values in the well and its slits. Panel (c) shows the normalized surface flux, $(\dot{m} - \dot{m}_{\min})/(\dot{m}_{\max} - \dot{m}_{\min})$, and the table contains scaling values for each plot. The inset demonstrates the actual surface flux profiles.

38

(a) long. pressure in the well (n=2)

(b) vertical pressure profile (n=2)

(c) surface mass flux (n=2)
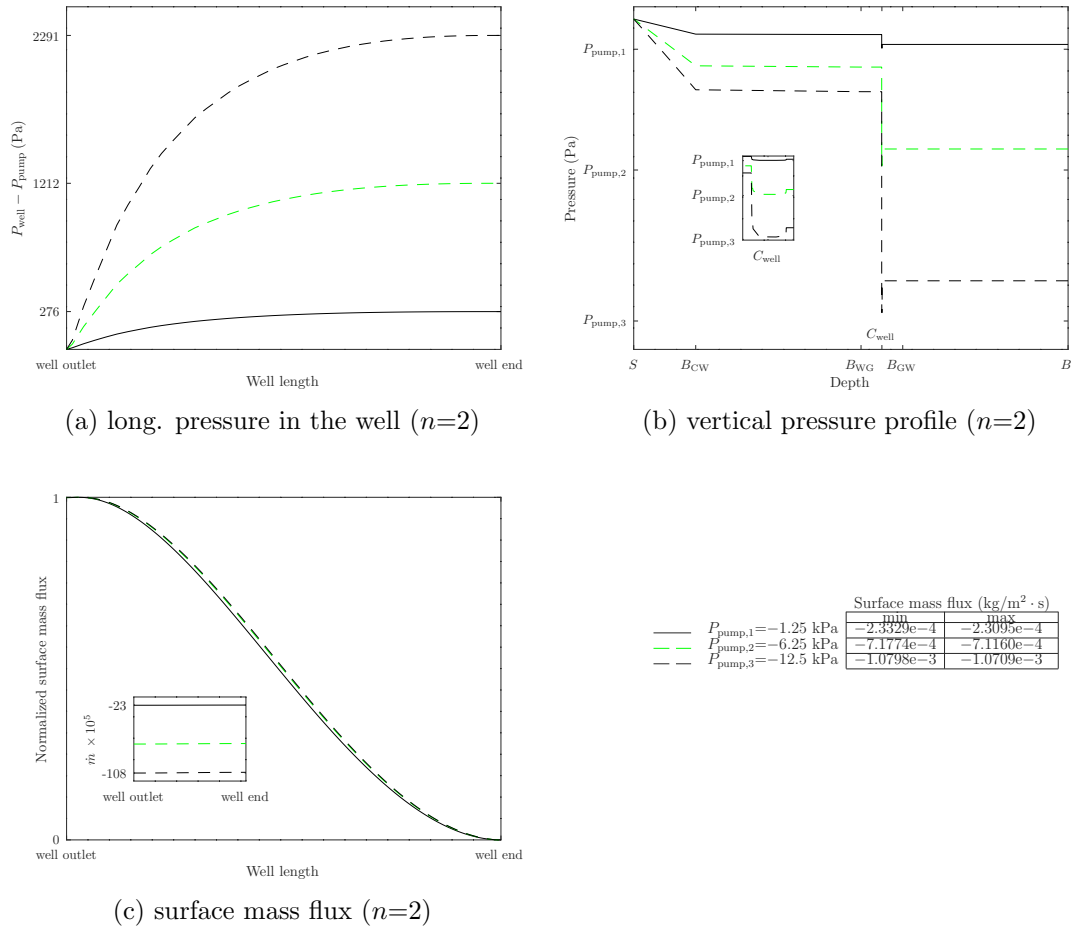
Figure 3.16: Effect of suction strength on pressure and surface flux for linear perforation size decrease (n=2). Panel (a) shows the well pressure profile at the centerline. Panel (b) represents the pressure profile along a vertical line from top to bottom of landfill at x=15 m; inset represents the pressure values in the well and its slits. Panel (c) shows the normalized surface flux, $(\dot{m} - \dot{m}_{\min})/(\dot{m}_{\max} - \dot{m}_{\min})$, and the table contains scaling values for each plot. The inset demonstrates the actual surface flux profiles.

Moreover two-parameter sensitivity analyses are conducted for the linear decreasing perforation size modification. Through the K_C-K_W combination (figure 3.17) it is understood that for the tightest cover most of the pressure drop in the system occurs in the cover layer, and neither waste permeability nor well pressure has a tangible effect on pressure drop and consequently surface flux (solid green and dashed black lines in panels (a), (b), and (c)). However according to solid black and dashed green lines in panels (a) and (b) for the looser cover, decreasing waste permeability leads to a higher and a lower pressure drop throughout the waste layer and within the well, respectively; there is a lower surface mass flux for the open system, as shown by the inset of panel (c). Reverse S-shaped curves in panel (c) demonstrate that Location of maximum surface flux is above the outlet where the largest perforation is the nearest.

(a) long. pressure in the well (n=2)

(b) vertical pressure profile (n=2)

(c) surface mass flux (n=2)

	Surface mass flux (kg/m$^2 \cdot$ s)	
	min	max
KC=1e−11 m^2, KW=1e−6 m^2	−2.3535e−4	−2.3400e−4
KC=1e−11 m^2, KW=1e−10 m^2	−2.1236e−4	−2.1061e−4
KC=1e−15 m^2, KW=1e−6 m^2	−4.6129e−8	−4.6120e−8
KC=1e−15 m^2, KW=1e−10 m^2	−4.6022e−8	−4.6006e−8
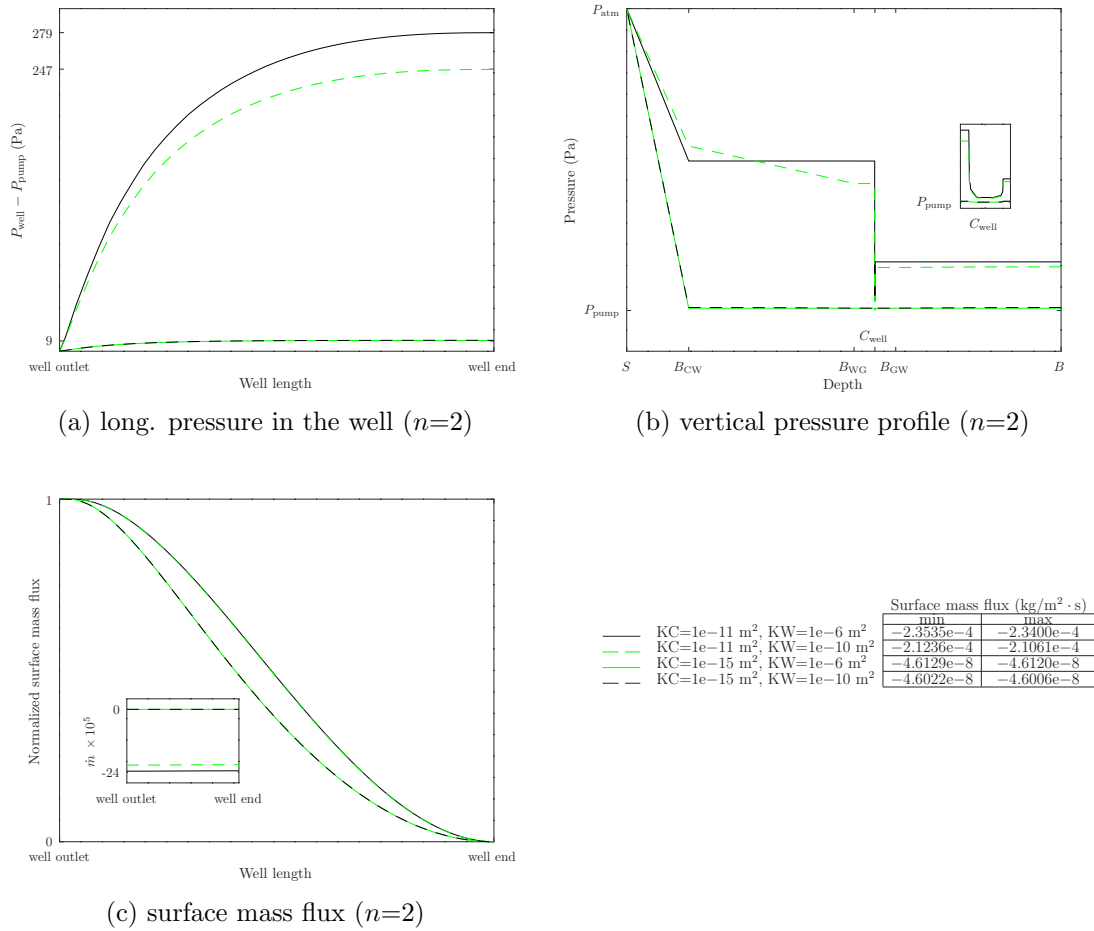
Figure 3.17: Effect of waste-cover permeability combinations on pressure and surface flux for linear perforation size decrease (n=2). Panel (a) shows the well pressure profile at the centerline. Panel (b) represents the pressure profile along a vertical line from top to bottom of landfill at x=15 m; inset represents the pressure values in the well and its slits. Panel (c) shows the normalized surface flux, $(\dot{m} - \dot{m}_{\min})/(\dot{m}_{\max} - \dot{m}_{\min})$, and the table contains scaling values for each plot. The inset demonstrates the actual surface flux profiles.

In the case of the K_{C}-P_{pump} combination–figure 3.18–when the lowest cover permeability is applied pressure drop in the cover layer is dominant and pump pressure is not critical. Therefore at the very low level of cover permeability changing suction strength does not cause any effect on surface flux and it reaches zero (dashed green and dashed black lines in panel (b) and inset of panel (c)). On the other hand, for the loosest cover layer pump pressure plays a crucial role in the system; for a given pump pressure, pressure drop within the well and surface flux increase (solid green and solid black lines in panel (b) and inset of panel (c)). The reason for previous arguments is that the total pressure drop in the system is constant. Based on the figure 3.19 for a given waste permeability, increasing suction strength leads to a significant increase in pressure drop throughout the landfill-well system and a higher surface flux (sets of solid and dashed lines). According to the sets of solid black-dashed green and solid green-dashed black lines in panels (a), (b), and inset of panel (c), waste permeability changing leads to a tiny impact on pressure and surface mass flux. Well pressure drop possess the dominant portion of total pressure drop in the open system. In figures 3.18 and 3.19 reverse S-shaped curves of surface flux (panel (c)) incline toward the well outlet with a maximum above the larger perforations.

By ending the investigation of the linear decrease of perforation size, for the linear increase of perforation size figures 3.20, 3.21, and 3.22 show the sensitivity of pressure and surface flux to cover permeability, waste permeability and suction strength, respectively. In figure 3.20 panels (a) and (b) represents that reduced cover permeability results in higher pressure drop in cover layer and lower pressure drop in well. In terms of surface flux as the perforation size increases along the well, more mass can be drawn into the larger holes located at the blocked end (solid black and dashed green lines). In this case the surface flux profiles differ from the previous trends for the aforementioned modifications. Therefore surface flux maxima loci are above well end, as shown by S-shaped curves in panel (c). Reducing the cover permeability, it is shifted toward the well outlet (dashed black, solid green, and dotted-dashed black lines).

Regarding panel (a) in figure 3.21 changing waste permeability has a tiny influence on the well pressure. Panel (b) demonstrates that by applying reduced permeability, pressure drop in the waste layer was not tangible unless for the tightest case (dotted-dashed black line). Moreover in this case well pressure drop is more noticeable, as shown by the dotted-dashed black line in panel (a). According to the surface flux profiles in panel (c) S-shaped trends are roughly the same and differ from a typical profile, since well production capacity diminishes by moving toward the outlet; minimum surface flux values are obtained for the lowest waste permeability, as represented by dotted-dashed black line in the inset of panel (c). Based on figure 3.22 it is concluded that increasing suction strength leads to a higher pressure drop within the well and subsequently a higher total pressure drop in the landfill-well coupled system, as represented from bottom to top in panels (a) and (b). Due to the increased total pressure drop in the open system the surface mass flux significantly increases, which is shown from top to bottom in the inset of panel (c). Notwithstanding the surface mass flux S-shaped trends are fairly the same in panel (c): the surface flux maxima and minima loci correspond to the maximum

and minimum perforation sizes at the blocked end and outlet, respectively.

(a) long. pressure in the well (n=2)

(b) vertical pressure profile (n=2)

(c) surface mass flux (n=2)
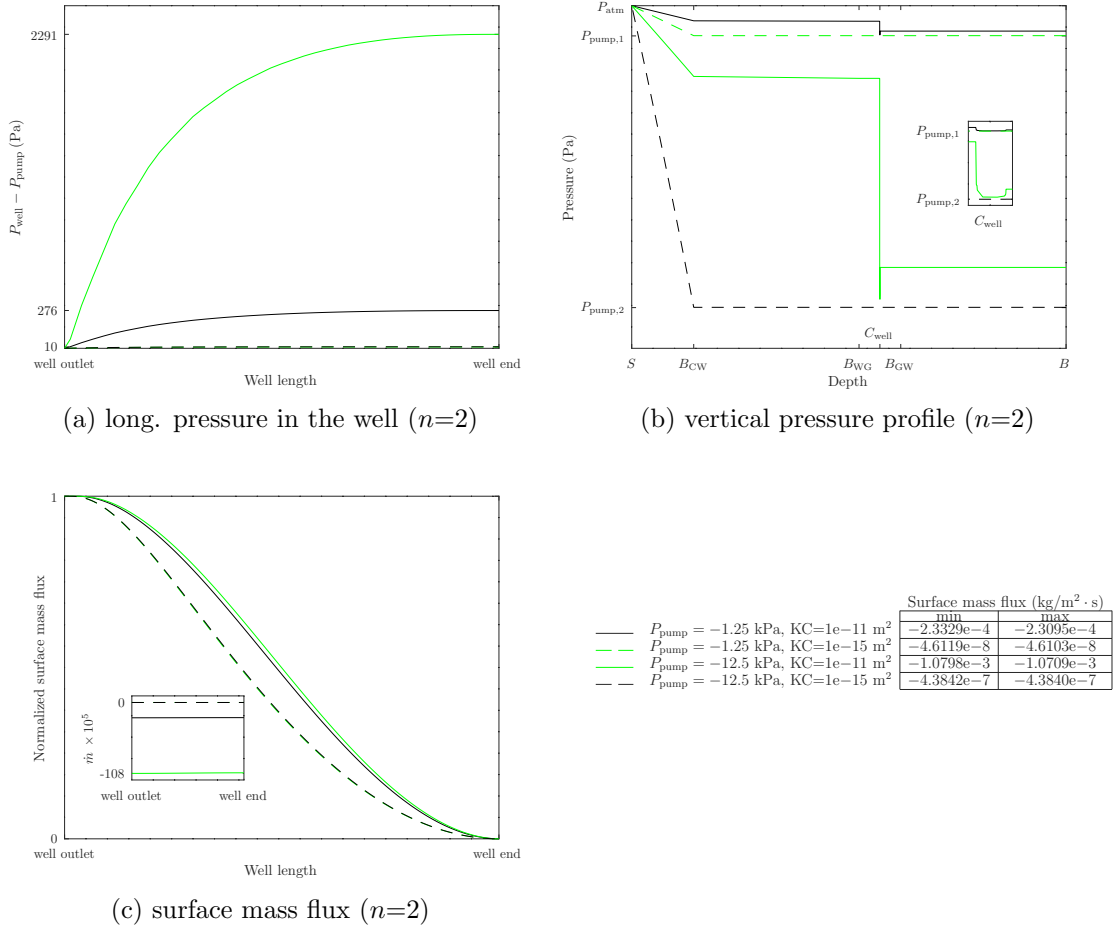
Figure 3.18: Effect of cover permeability-suction strength combinations on pressure and surface flux for linear perforation size decrease (n=2). Panel (a) shows the well pressure profile at the centerline. Panel (b) represents the pressure profile along a vertical line from top to bottom of landfill at x=15 m; inset represents the pressure values in the well and its slits. Panel (c) shows the normalized surface flux, $(\dot{m} - \dot{m}_{min})/(\dot{m}_{max} - \dot{m}_{min})$, and the table contains scaling values for each plot. The inset demonstrates the actual surface flux profiles.

(a) long. pressure in the well ($n=2$)

(b) vertical pressure profile ($n=2$)

(c) surface mass flux ($n=2$)
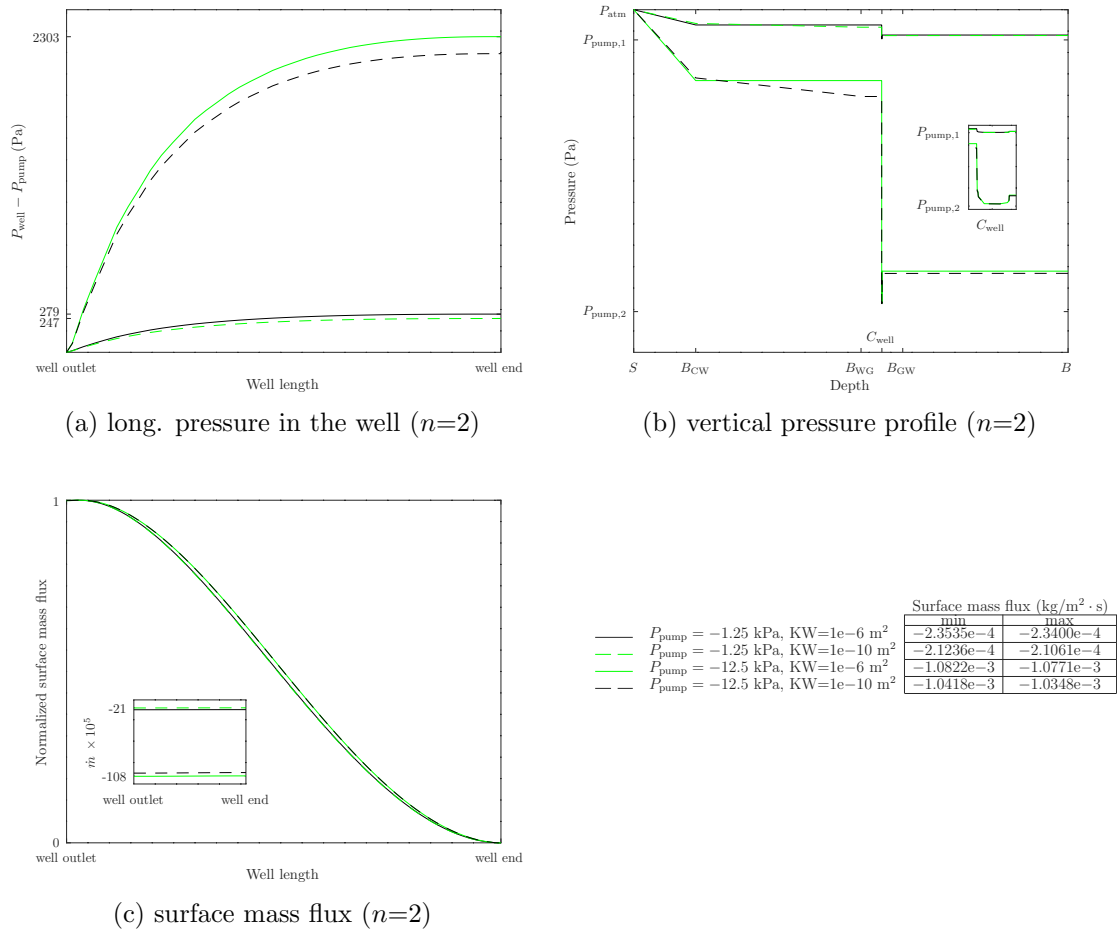
Figure 3.19: Effect of waste permeability-suction strength combinations on pressure and surface flux for linear perforation size decrease ($n=2$). Panel (a) shows the well pressure profile at the centerline. Panel (b) represents the pressure profile along a vertical line from top to bottom of landfill at x=15 m; inset represents the pressure values in the well and its slits. Panel (c) shows the normalized surface flux, $(\dot{m} - \dot{m}_{\min})/(\dot{m}_{\max} - \dot{m}_{\min})$, and the table contains scaling values for each plot. The inset demonstrates the actual surface flux profiles.

(a) long. pressure in the well (n=2)

(b) vertical pressure profile (n=2)

(c) surface mass flux (n=2)
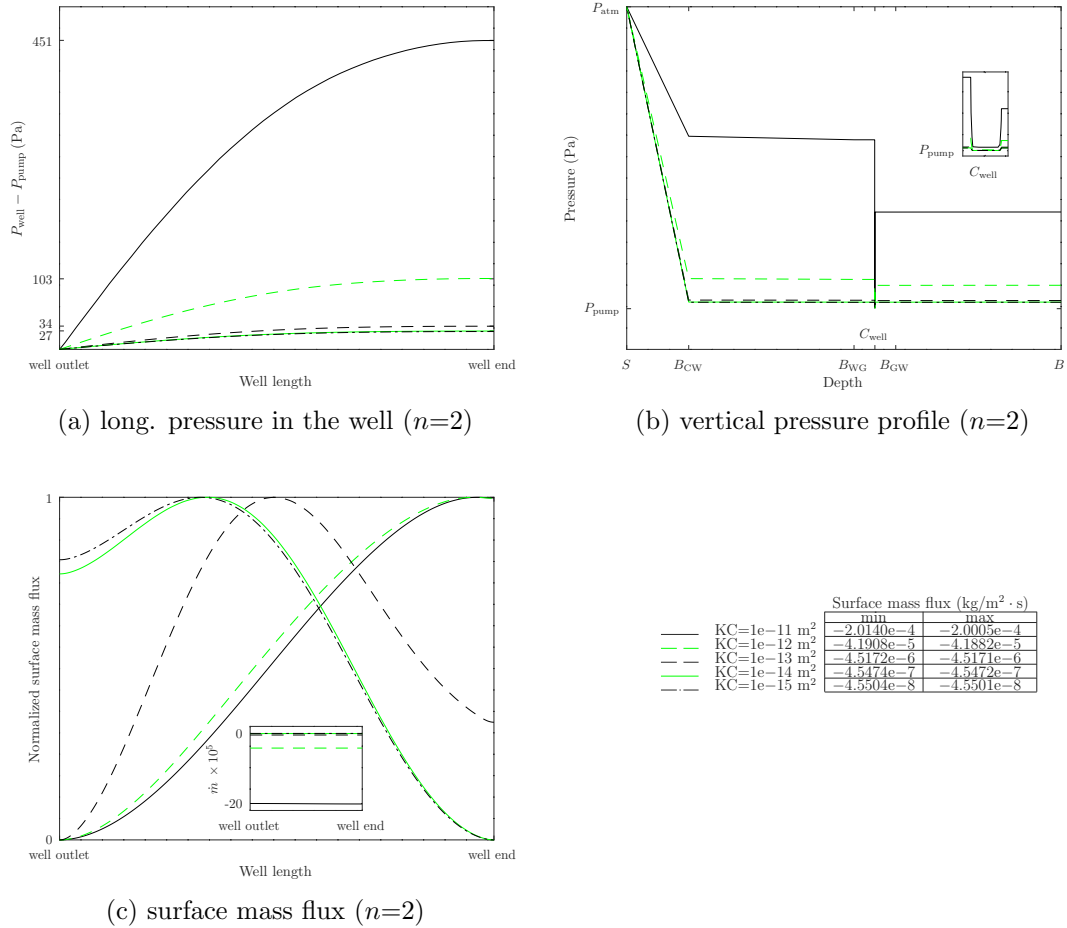
Figure 3.20: Effect of cover permeability on pressure and surface flux for linear perforation size increase (n=2). Panel (a) shows the well pressure profile at the centerline. Panel (b) represents the pressure profile along a vertical line from top to bottom of landfill at x=15 m; inset represents the pressure values in the well and its slits. Panel (c) shows the normalized surface flux, $(\dot{m} - \dot{m}_{\min})/(\dot{m}_{\max} - \dot{m}_{\min})$, and the table contains scaling values for each plot. The inset demonstrates the actual surface flux profiles.

(a) long. pressure in the well (n=2)

(b) vertical pressure profile (n=2)

(c) surface mass flux (n=2)
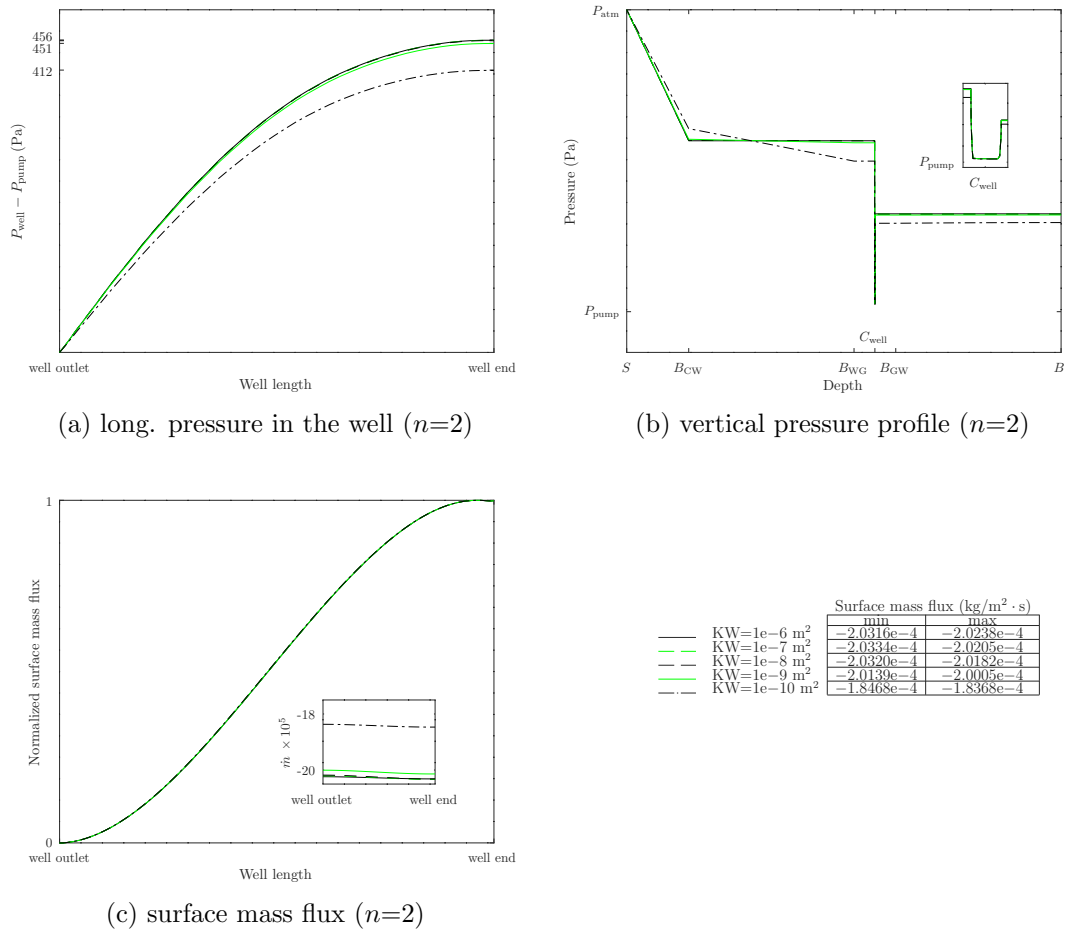
Figure 3.21: Effect of waste permeability on pressure and surface flux for linear perforation size increase (n=2). Panel (a) shows the well pressure profile at the centerline. Panel (b) represents the pressure profile along a vertical line from top to bottom of landfill at x=15 m; inset represents the pressure values in the well and its slits. Panel (c) shows the normalized surface flux, $(\dot{m} - \dot{m}_{\min})/(\dot{m}_{\max} - \dot{m}_{\min})$, and the table contains scaling values for each plot. The inset demonstrates the actual surface flux profiles.

(a) long. pressure in the well (n=2)

(b) vertical pressure profile (n=2)

(c) surface mass flux (n=2)
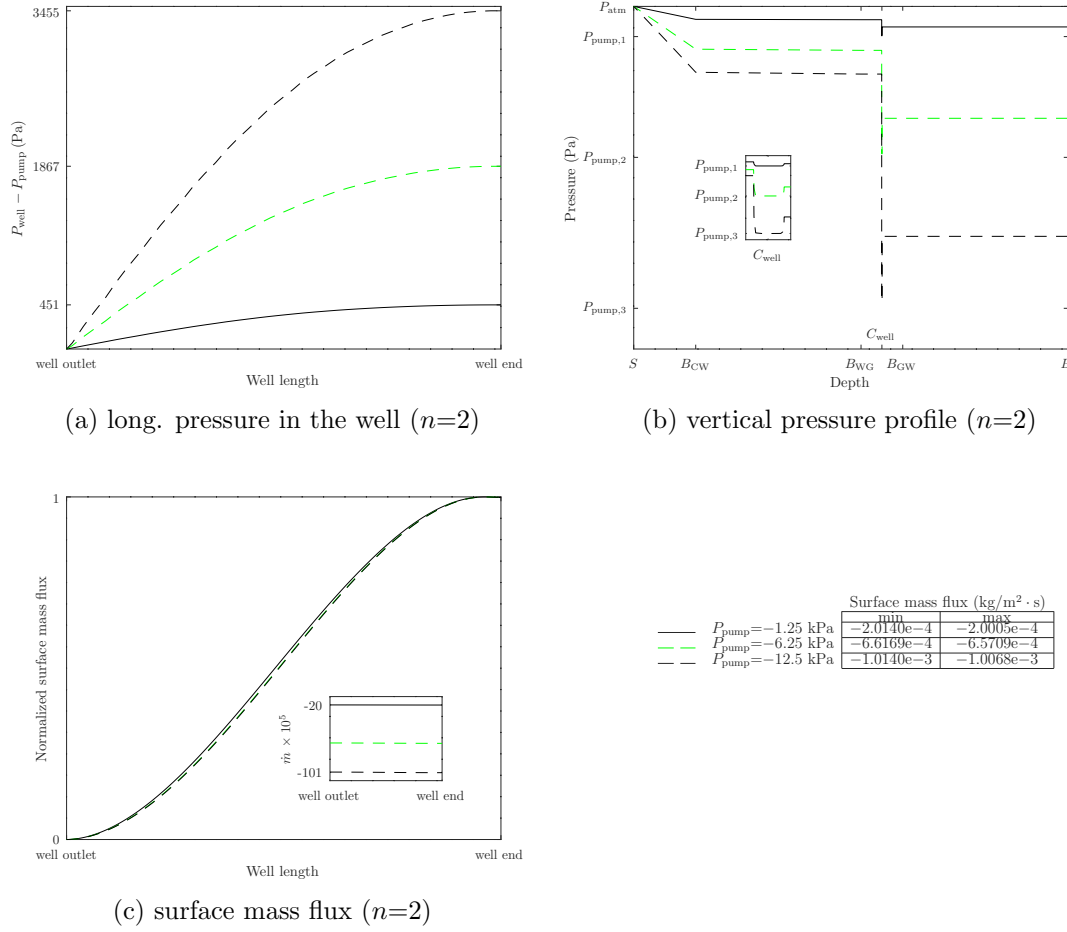
Figure 3.22: Effect of suction strength on pressure and surface flux for linear perforation size increase (n=2). Panel (a) shows the well pressure profile at the centerline. Panel (b) represents the pressure profile along a vertical line from top to bottom of landfill at x=15 m; inset represents the pressure values in the well and its slits. Panel (c) shows the normalized surface flux, $(\dot{m} - \dot{m}_{min})/(\dot{m}_{max} - \dot{m}_{min})$, and the table contains scaling values for each plot. The inset demonstrates the actual surface flux profiles.

Two-parameters sensitivity analyses are conducted on K_C-K_W, K_C-P_{pump} and K_W-P_{pump} combinations. Panels (a) and (b) in figure 3.23 show that cover permeability has a significant impact on pressure and surface flux. Applying a tighter cover layer leads to a higher pressure drop throughout the layer and a lower pressure drop within the well, which is shown by solid green and dashed black lines. In the case of utilizing a higher cover permeability, as represented by solid black and dashed green lines, the effect of waste permeability is more tangible: the lower waste permeability causes a higher pressure drop within the waste layer, as represented by dashed green line in panel (b). According to the solid black-dashed green and solid green-dashed black sets of lines in the inset of panel (c), surface flux is highly influenced by cover permeability: a higher surface flux as a result of higher cover permeability. Whilst the perforation size increases along the well from the outlet toward the blocked end, a higher surface flux is expected at the blocked end for the

highest cover permeability, as well as an S-shaped curve (solid black and dashed green lines). Although the solid green and dashed black lines in panel (c) represent that for a lower cover permeability the maximum surface flux happens somewhere in the middle.

(a) long. pressure in the well (n=2)

(b) vertical pressure profile (n=2)

(c) surface mass flux (n=2)

	Surface mass flux (kg/m$^2 \cdot$ s)	
	min	max
KC=1e−11 m^2, KW=1e−6 m^2	−2.0316e−4	−2.0238e−4
KC=1e−11 m^2, KW=1e−10 m^2	−1.8468e−4	−1.8368e−4
KC=1e−15 m^2, KW=1e−6 m^2	−4.5514e−8	−4.5513e−8
KC=1e−15 m^2, KW=1e−10 m^2	−4.5407e−8	−4.5404e−8
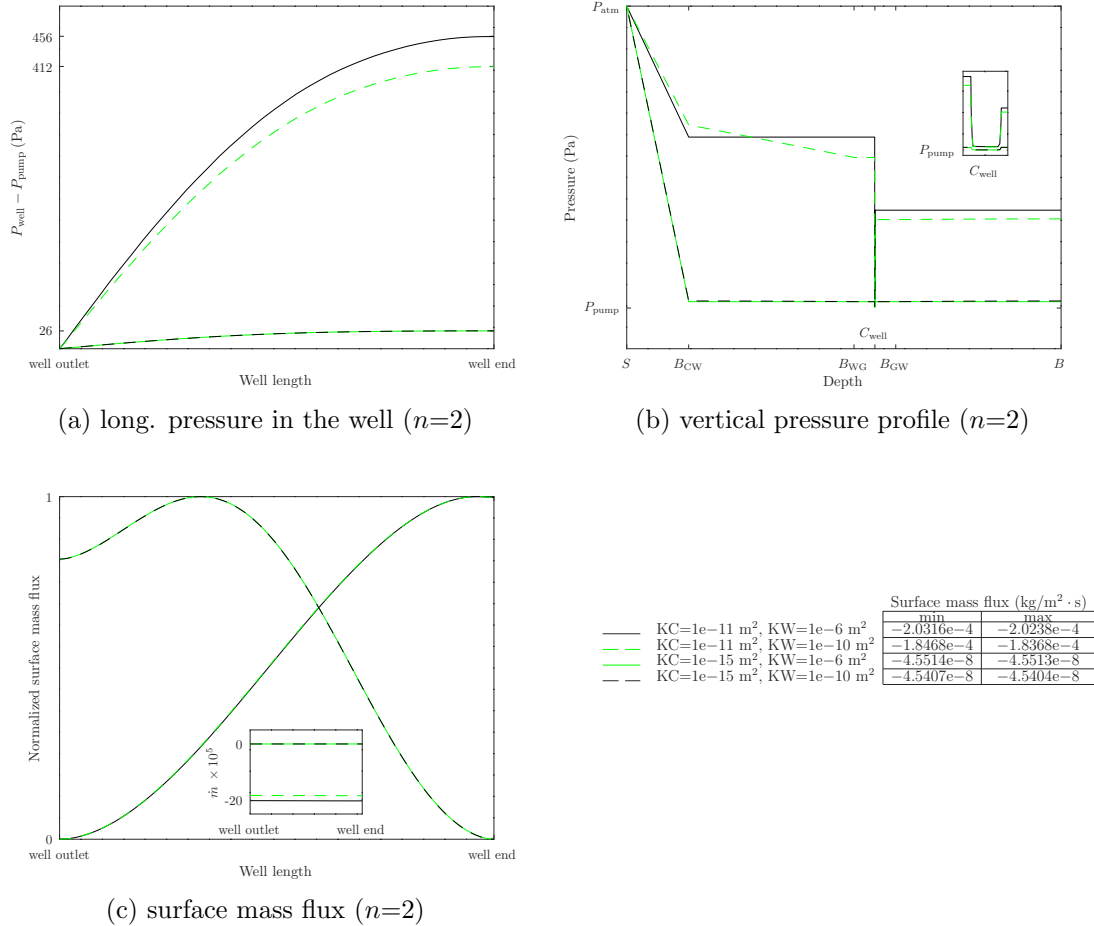
Figure 3.23: Effect of waste-cover permeability combinations on pressure and surface flux for linear perforation size increase (n=2). Panel (a) shows the well pressure profile at the centerline. Panel (b) represents the pressure profile along a vertical line from top to bottom of landfill at x=15 m; inset represents the pressure values in the well and its slits. Panel (c) shows the normalized surface flux, $(\dot{m} - \dot{m}_{\min})/(\dot{m}_{\max} - \dot{m}_{\min})$, and the table contains scaling values for each plot. The inset demonstrates the actual surface flux profiles.

According to panel (c) in figure 3.24 it can be deduced that surface flux trends and values are governed by cover permeability and suction strength. Based on the dashed black and green lines in panel (a), there is a lower well pressure drop for a tighter cover layer. As represented in panel (b) pressure drop in the landfill-well coupled system highly depends upon cover permeability values. Once the cover permeability decreases most of the pressure drop occurs throughout the layer (dashed black and green lines in panel (b)) and the pressure drop within the well is at its minimum level. A higher surface mass flux is obtained using increased suction

strength for a lower cover permeabilitiy, as represented by solid green line in the inset of panel (c). Since there are larger perforations along the well from the outlet to blocked end, a higher surface flux is provided moving toward the blocked end, which are shown by the S-shaped curves in panel (c). By decreasing cover permeability, the surface flux maxima loci are shifted toward the well outlet (dashed black and green lines). Based on figure 3.25 the well pressure influence is dominant in comparison to the waste permeability. According to the solid green and dashed black lines in panels (a) and (b) increasing suction strength leads to a higher pressure drop within the well and pressure drop throughout the system. Moreover as shown in the inset of panel (c) the surface flux are increased. Based on panel (c) notwithstanding, due to the tiny impact of waste permeability on the total pressure drop the S-shaped trends of the surface flux are fairly the same: a higher surface flux value corresponds to a larger perforation size along the well.

A linear increase in perforation size leads to a higher well collection capability due to a more uniform pressure distribution in the well. It means that less gas escapes at the surface. If changing pump suction is not an option, this modification offers a way to control surface flux in situations where landfill gas escape at the blocked end is significant.

(a) long. pressure in the well ($n=2$)

(b) vertical pressure profile ($n=2$)



(c) surface mass flux ($n=2$)
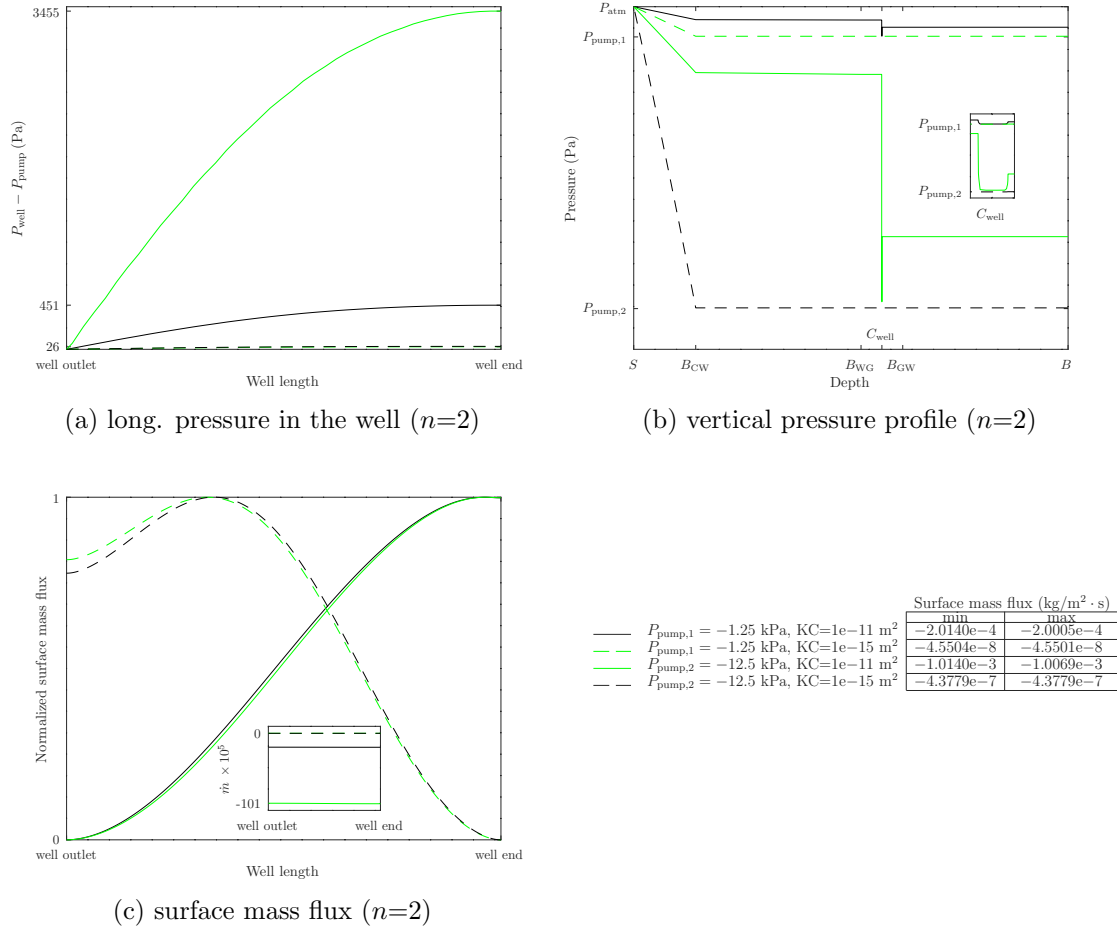
Figure 3.24: Effect of cover permeability-suction strength combinations on pressure and surface flux for linear perforation size increase ($n=2$). Panel (a) shows the well pressure profile at the centerline. Panel (b) represents the pressure profile along a vertical line from top to bottom of landfill at x=15 m; inset represents the pressure values in the well and its slits. Panel (c) shows the normalized surface flux, $(\dot{m} - \dot{m}_{\min})/(\dot{m}_{\max} - \dot{m}_{\min})$, and the table contains scaling values for each plot. The inset demonstrates the actual surface flux profiles.

(a) long. pressure in the well (n=2)

(b) vertical pressure profile (n=2)

(c) surface mass flux (n=2)
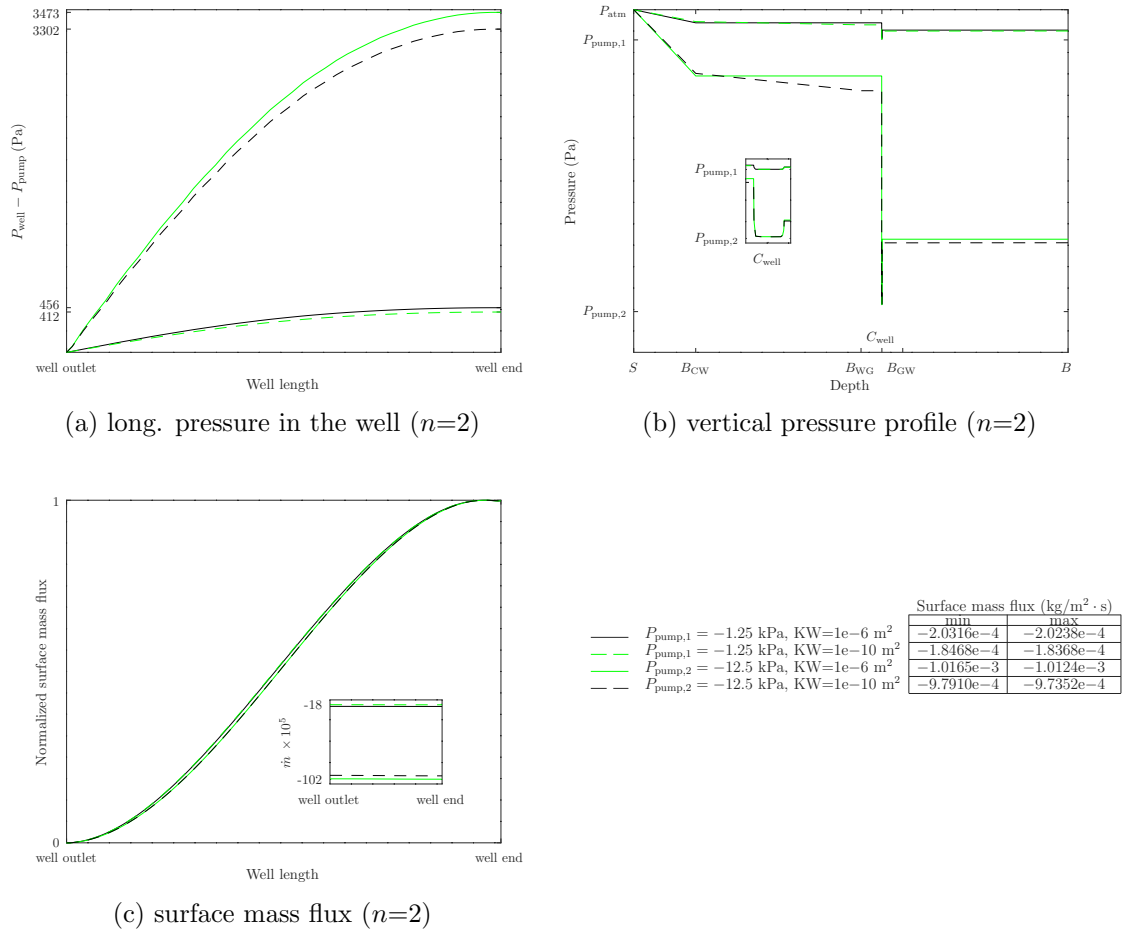
Figure 3.25: Effect of waste permeability-suction strength combinations on pressure and surface flux for linear perforation size increase (n=2). Panel (a) shows the well pressure profile at the centerline. Panel (b) represents the pressure profile along a vertical line from top to bottom of landfill at x=15 m; inset represents the pressure values in the well and its slits. Panel (c) shows the normalized surface flux, $(\dot{m} - \dot{m}_{\min})/(\dot{m}_{\max} - \dot{m}_{\min})$, and the table contains scaling values for each plot. The inset demonstrates the actual surface flux profiles.

3.7   Perforation shifting

In this section the influence of well perforation shifting–modification (b) in figure 2.6–on the landfill-well system is assessed. This modification reduces the collection area on the surface of the well by shifting perforations and thus removing some perforations, leading to a lower well suction capability. It is expected that this effect weaken collection ability near the outlet but maintain it near the blocked end due to the proximity of the perforations thereto. Based on section 3.1 shifting perforation up to 10 meters has led to a small or zero impact on pressure and surface mass flux. Therefore to show whether more shifting of perforations can have any effect on the system, perforations are moved farther away from the outlet. In this case since the interval between each consecutive set of perforation is 15 meters, due to more shifting some perforation are removed from the well geometry. This continuous shifting is done every 15 meters until only one perforation is left 15 meters away from the blocked end. It is noticed that at one step due to reducing well production capability, there are both gas efflux and air influx at the surface, simultaneously. This is considered as a threshold stage for the same given fluid dynamic conditions and here to demonstrate the pressure and flux variation in the entire system, only three modifications are taken into account: pre-threshold, threshold, and post-threshold.

Figures 3.26 to 3.31 are shown for the pre-threshold stage where surface mass flux at the surface is still resulted from air influx. In this case only three perforations have been left at the 370 m, 395 m, and 405 m away from the blocked end. In panels (a) and (b) of figure 3.26 from bottom to top, as the cover permeability increases the well pressure drop increases and the pressure drop throughout the cover layer decreases. This behavior is similar to the findings obtained from previous modifications. One of the crucial differences between the following pressure drop profiles and the previous ones is that as a result of removing perforations along the well once shifting is in progress, pressure profile trends become linear. This linear head loss is due to hydrodynamic friction. Furthermore due to the low number of perforations and consequently a highly reduced well production capability, pressure drop within the well is not changed dramatically like the profiles represented for the previous modifications. Surface flux profiles are fairly close together, as shown by the S-shaped curves in panel (c); nonetheless lower surface flux levels are expected due to a tighter cover layers, as presented in the inset. Maximum surface flux locates at the blocked end where the perforations exist.

Figure 3.27 shows the impact of waste permeability on the pressure and surface flux. In panels (a) and (b) pressure drop in the landfill and well do not experience a tangible variation. According to panel (c) The surface flux levels do not show a dramatic change as a result of waste permeability variation and maxima loci are at blocked end, as represented by the S-shaped curves. On the other hand panels (a) and (b) in figure 3.28 demonstrate that suction strength significantly impact pressure drop and surface flux in the landfill-well system. By increasing pump pressure which is denoted from bottom to top in panels (a) and (b), head loss within the well and throughout landfill increase significantly. Subsequently surface flux values increase, as represented in the inset of panel (c). Despite the S-shaped curves in panel (c)

indicate that the location of the maximum surface flux is almost fixed above the blocked end.

(a) long. pressure in the well (n=2)


(b) vertical pressure profile (n=2)

(c) surface mass flux (n=2)
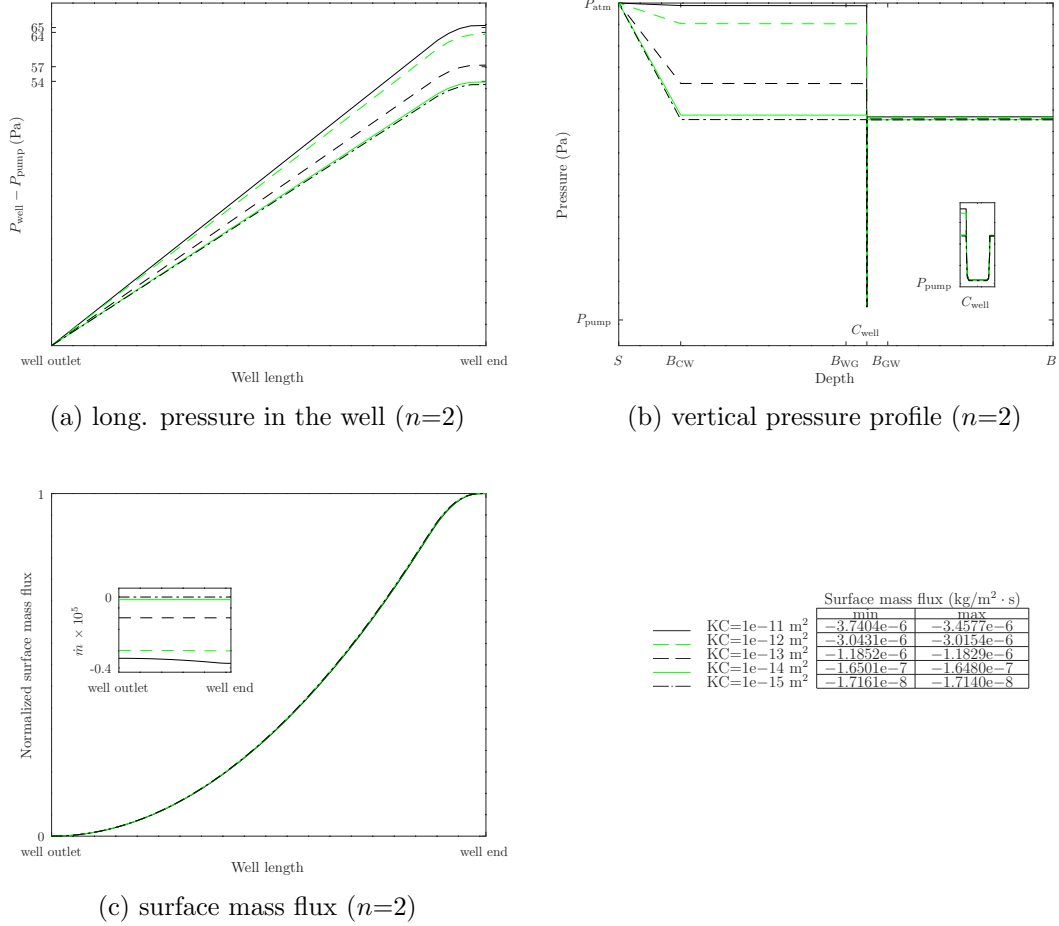
Figure 3.26: Effect of cover permeability on pressure and surface flux for perforation shifting of 375 meters (n=2). Panel (a) shows the well pressure profile at the centerline. Panel (b) represents the pressure profile along a vertical line from top to bottom of landfill at x=375 m; inset represents the pressure values in the well and its slits. Panel (c) shows the normalized surface flux, $(\dot{m} - \dot{m}_{\min})/(\dot{m}_{\max} - \dot{m}_{\min})$, and the table contains scaling values for each plot. The inset demonstrates the actual surface flux profiles.

(a) long. pressure in the well (n=2)

(b) vertical pressure profile (n=2)

(c) surface mass flux (n=2)
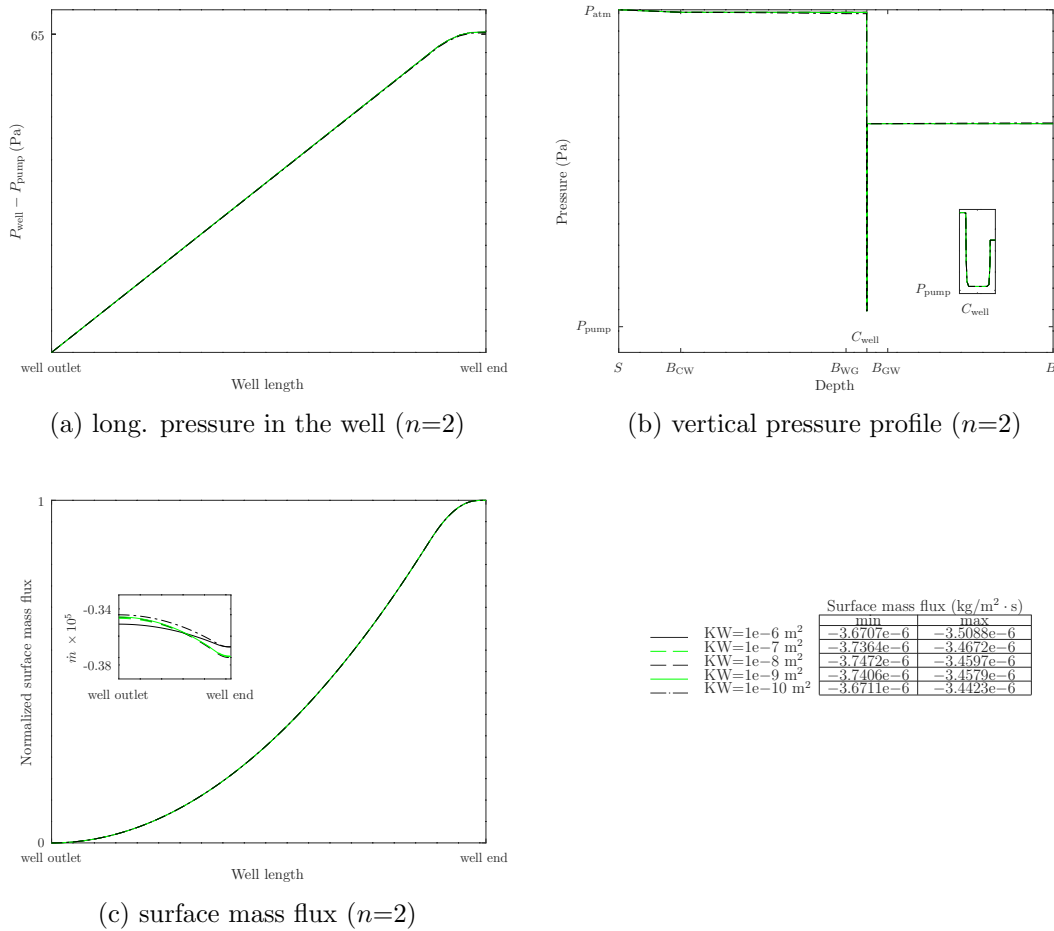
Figure 3.27: Effect of waste permeability on pressure and surface flux for perforation shifting of 375 meters (n=2). Panel (a) shows the well pressure profile at the centerline. Panel (b) represents the pressure profile along a vertical line from top to bottom of landfill at x=375 m; inset represents the pressure values in the well and its slits. Panel (c) shows the normalized surface flux, $(\dot{m} - \dot{m}_{\min})/(\dot{m}_{\max} - \dot{m}_{\min})$, and the table contains scaling values for each plot. The inset demonstrates the actual surface flux profiles.

(a) long. pressure in the well (n=2)

(b) vertical pressure profile (n=2)



(c) surface mass flux (n=2)
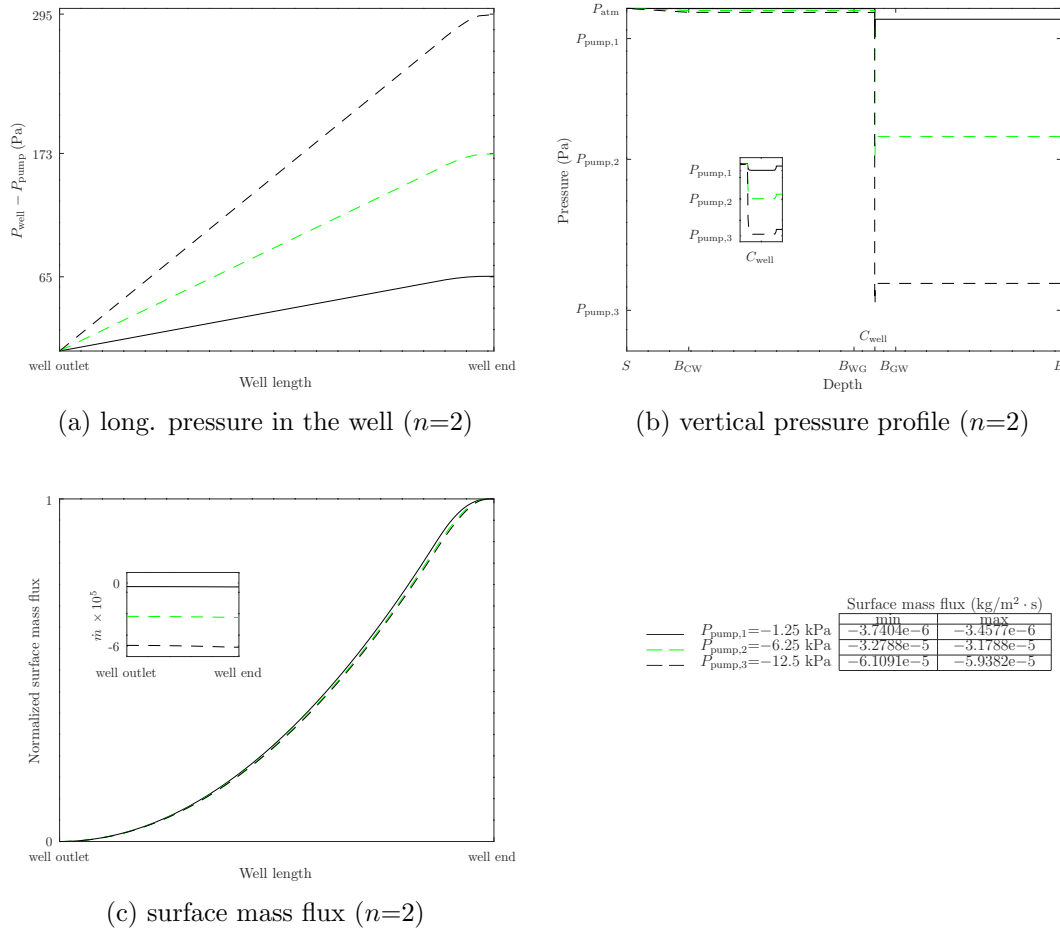
Figure 3.28: Effect of suction strength on pressure and surface flux for perforation shifting of 375 meters (n=2). Panel (a) shows the well pressure profile at the centerline. Panel (b) represents the pressure profile along a vertical line from top to bottom of landfill at x=375 m; inset represents the pressure values in the well and its slits. Panel (c) shows the normalized surface flux, $(\dot{m} - \dot{m}_{\min})/(\dot{m}_{\max} - \dot{m}_{\min})$, and the table contains scaling values for each plot. The inset demonstrates the actual surface flux profiles.

Double-parameter investigations are done and three different combinations are studied: cover-waste permeabilities, cover permeability-pump pressure and waste permeability-pump pressure. Based on figure 3.29 pressure drop and surface flux are mainly governed by the cover permeability. According to solid black-dashed green and solid green-dashed black sets of lines in panels (a), (b) and inset of panel (c), changing waste permeability has an intangible effect on the system. Comparing solid black-solid green and dashed green-dashed black sets of lines, as the cover layer gets tighter, pressure drop increases throughout the landfill cover and decreases within the well. As the total pressure drop in the entire system is constant the surface flux reduces due to a lower cover permeability, as shown by solid green and dashed black lines in the inset of panel (c). Nevertheless due to the decreased capability of well production, S-shaped surface flux profiles are the same and the maxima loci incline toward the blocked end (panel(c)). Based on the inset of panel (c) in figure

3.30 it can be deduced that both pump pressure and cover permeability variation significantly affect surface mass flux. Pressure drop in the landfill is governed by these two parameters, so that when the tightest cover permeability is applied most of the pressure drop occurs throughout the cover layer (dashed lines in panel (b)) and for the suction strength a higher pump pressure causes a higher pressure drop within the well (solid lines in panel (a)). In such case that only three perforations are utilized at the very end of the well, surface flux maxima loci are above the blocked end, as represented by S-shaped curves in panel (c); the trends of surface flux profiles are relatively the same as a result of the low number of perforations.

(a) long. pressure in the well (n=2)

(b) vertical pressure profile (n=2)

(c) surface mass flux (n=2)

	Surface mass flux ($\text{kg/m}^2 \cdot \text{s}$)	
	min	max
—— KC=1e−11 m², KW=1e−6 m²	−3.6707e−6	−3.5088e−6
– – KC=1e−11 m², KW=1e−10 m²	−3.6711e−6	−3.4423e−6
—— KC=1e−15 m², KW=1e−6 m²	−1.7177e−8	−1.7166e−8
– – KC=1e−15 m², KW=1e−10 m²	−1.7065e−8	−1.7044e−8
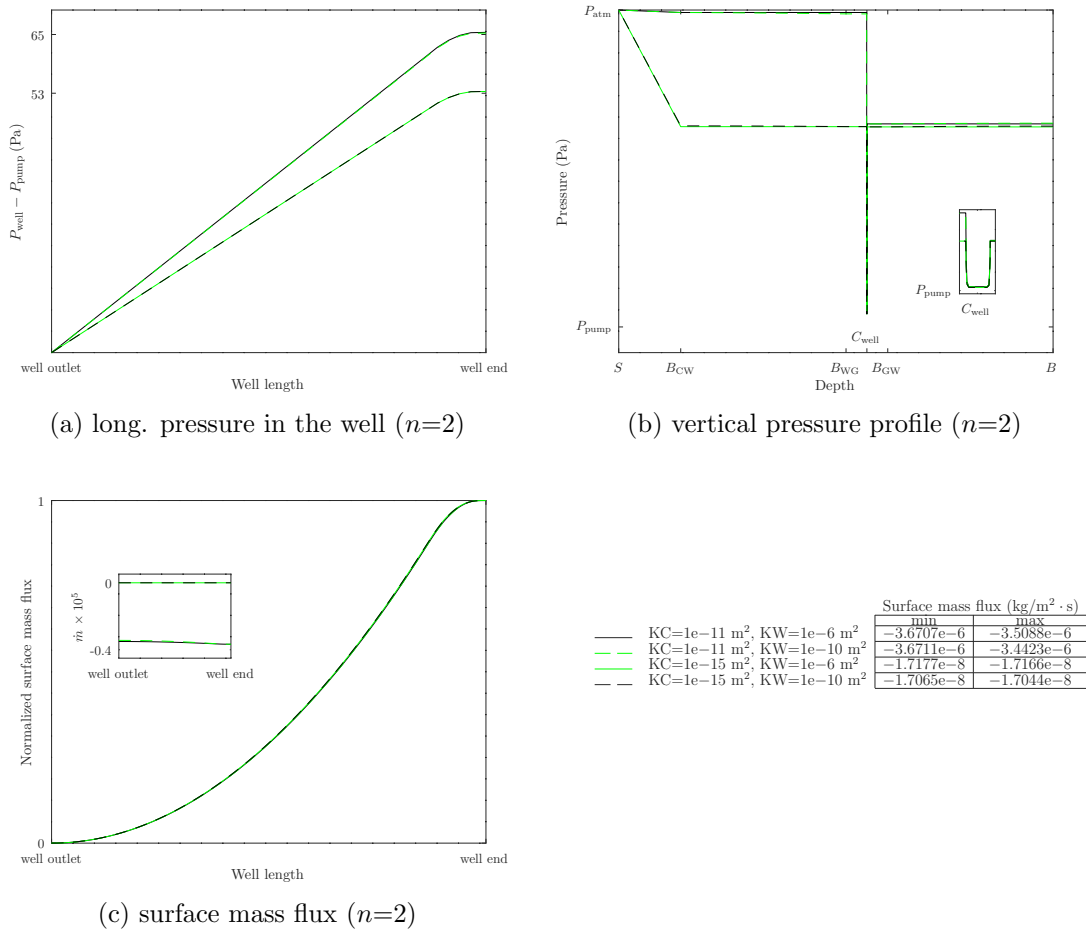
Figure 3.29: Effect of waste-cover permeability combinations on pressure and surface flux for perforation shifting of 375 meters (n=2). Panel (a) shows the well pressure profile at the centerline. Panel (b) represents the pressure profile along a vertical line from top to bottom of landfill at x=375 m; inset represents the pressure values in the well and its slits. Panel (c) shows the normalized surface flux, $(\dot{m} - \dot{m}_{\min})/(\dot{m}_{\max} - \dot{m}_{\min})$, and the table contains scaling values for each plot. The inset demonstrates the actual surface flux profiles.

(a) long. pressure in the well (n=2)

(b) vertical pressure profile (n=2)

(c) surface mass flux (n=2)
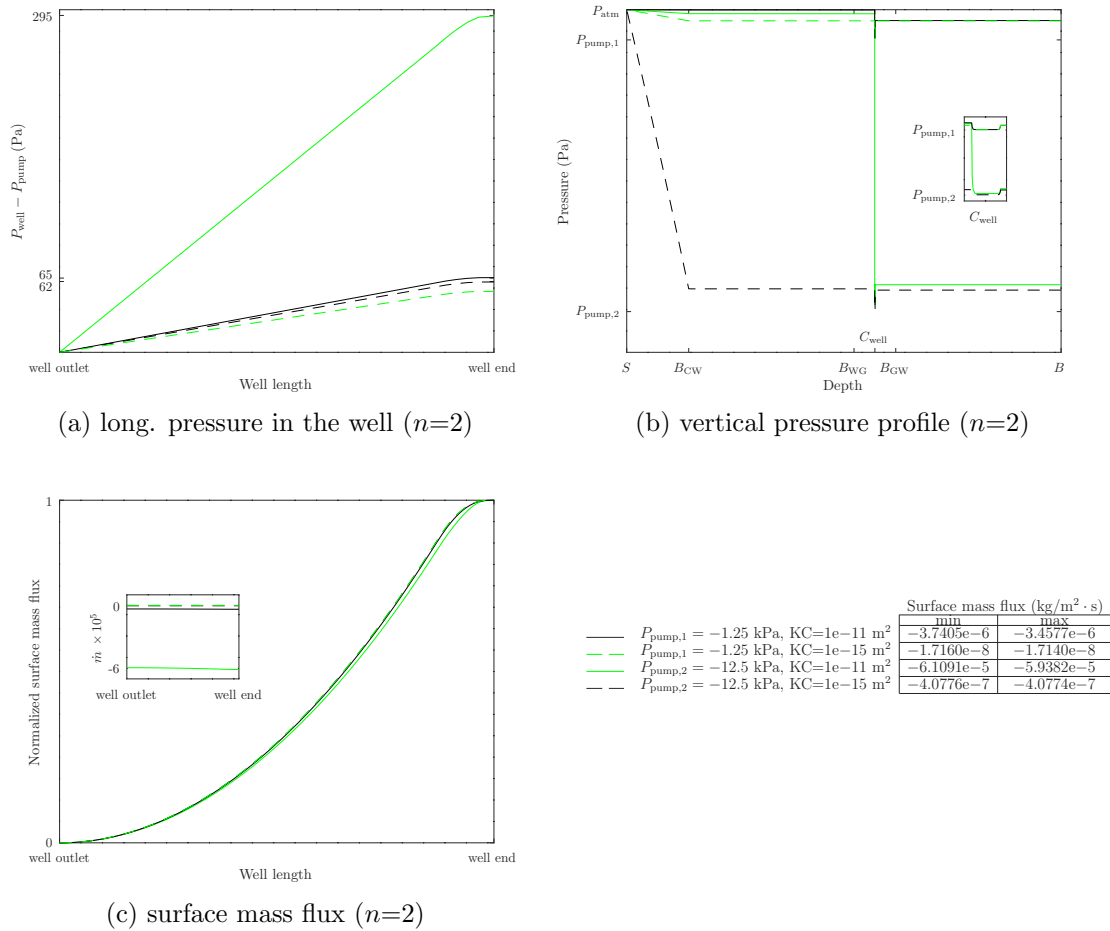
Figure 3.30: Effect of cover permeability-suction strength combinations on pressure and surface flux for perforation shifting of 375 meters (n=2). Panel (a) shows the well pressure profile at the centerline. Panel (b) represents the pressure profile along a vertical line from top to bottom of landfill at x=375 m; inset represents the pressure values in the well and its slits. Panel (c) shows the normalized surface flux, $(\dot{m} - \dot{m}_{\min})/(\dot{m}_{\max} - \dot{m}_{\min})$, and the table contains scaling values for each plot. The inset demonstrates the actual surface flux profiles.

Based on figure 3.31 solid black-dashed green and solid green-dashed black sets of lines in panel (a) represent that waste permeability changes have an intangible effect on pressure drop within the well. However solid black-solid green and dashed green-dashed black sets of lines in panels (a) and (b) and the inset of panel (c) depict that suction strength governs pressure drop and surface mass flux. An increased pump pressure leads to a higher pressure drop within the well and surface flux, as represented by solid green and dashed black lines in panel (a) and inset of panel (c). Panel (a) demonstrates that the low number of perforations along the well–three at the very end–causes a linear pressure profile for the non-perforated well segment. Due to the low number of perforations and influence of waste permeability there is no difference in the S-shaped trends of surface flux profiles, as shown in panel (c).

(a) long. pressure in the well ($n=2$)

(b) vertical pressure profile ($n=2$)

(c) surface mass flux ($n=2$)

|	Surface mass flux (kg/m² · s)	
	min	max
$P_{pump,1} = -1.25$ kPa, KW=1e−6 m²	−3.6707e−6	−3.5088e−6
$P_{pump,1} = -1.25$ kPa, KW=1e−10 m²	−3.6711e−6	−3.4423e−6
$P_{pump,2} = -12.5$ kPa, KW=1e−6 m²	−6.0658e−5	−5.9680e−5
$P_{pump,2} = -12.5$ kPa, KW=1e−10 m²	−6.0695e−5	−5.9311e−5
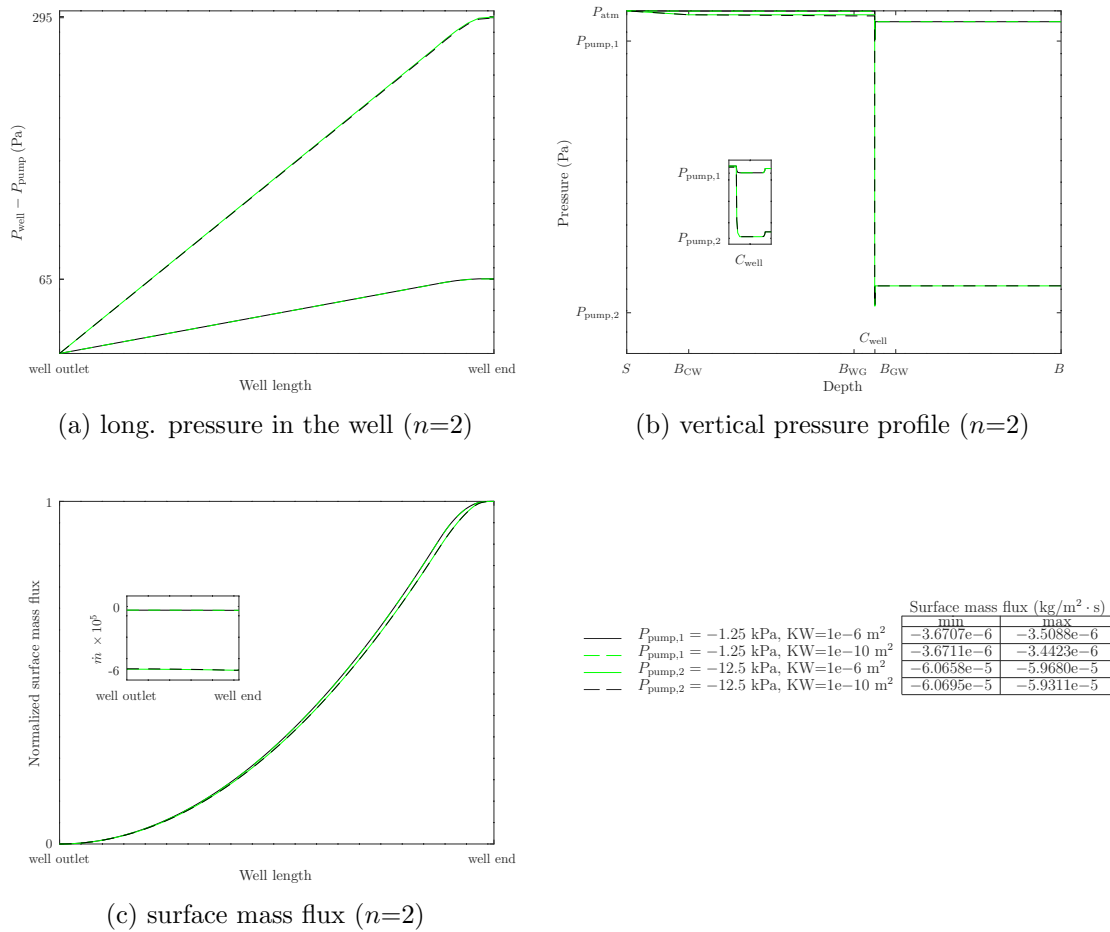
Figure 3.31: Effect of waste permeability-suction strength combinations on pressure and surface flux for perforation shifting of 375 meters ($n=2$). Panel (a) shows the well pressure profile at the centerline. Panel (b) represents the pressure profile along a vertical line from top to bottom of landfill at x=375 m; inset represents the pressure values in the well and its slits. Panel (c) shows the normalized surface flux, $(\dot{m} - \dot{m}_{min})/(\dot{m}_{max} - \dot{m}_{min})$, and the table contains scaling values for each plot. The inset demonstrates the actual surface flux profiles.

In the threshold case there are two perforations at the end of the well. Figure 3.32 represents the effects of different cover permeabilities on the pressure drop and surface flux. According to panel (a) despite changing cover permeability, there is no variation in pressure drop within the well. This is due to the fact that there are only two holes in the well wall, which results in a low capability of the well for gas extraction. Based on the vertical pressure profiles in panel (b) most of the head loss occurs within the well. Panel (c) indicates that there are two conditions for surface flux: one, when both gas efflux and air influx happen simultaneously and two, when only gas efflux occurs across the landfill. Due to the lack of well production capacity there is a small radius of influence for the well. Based on solid black line in panel (c) when the highest cover permeability is applied both air and landfill gas have a chance to flow into or out of the landfill. In such case surface flux is divided into two parts. The first part includes gas efflux far from the perforations (positive flux) and the second part comprises air influx near the extraction zone (negative flux), so that a V-shaped profile is expected for the surface flux. For a tighter cover layer landfill gas can only escape from the landfill (positive flux). This is because during gas generation pressure in landfill is higher than atmospheric and the pump does not have a strong suction capability to draw more mass into well; a pressure build-up leads to the gas escaping.

Figure 3.33 demonstrates that changing waste permeability can not significantly affect pressure drop and surface flux. Pressure drop within the well is roughly equal for all waste permeability values, as shown in panel (a). Moreover according to panel (b) most of the pressure drop in the system occurs within the well. Since landfill is not sealed enough on top, gas efflux and air influx occur at the surface (panel (c)). In this case V-shaped profiles are expected for all modifications: gas escapes from the surface horizontally far from the perforations and air is drawn into the landfill above the perforations where there is a stronger suction. In figure 3.34 significant pressure drop and surface flux variation are obtained as a result of applying different suction strengths. Based on panels (a) and (b) from bottom to top as the pump pressure increases, pressure drop within the well becomes higher and the portion of well pressure drop is more than that in porous media. For the lowest pump pressure surface efflux and influx co-occur, so that there is a V-shaped profile (solid black line in panel (c)). As the suction strength gets higher more mass is drawn into the well and therefore only air influx happens (negative flux, as represented in the inset of panel (c).

Dual sensitivity analyses are conducted to investigate the effect of three combinations of cover permeability, waste permeability, and pump pressure. According to panels (a) and (b) in figure 3.35, changing cover and waste permeabilities have roughly no impact on the pressure drop. Although based on solid black-dashed green and solid green-dashed black sets of lines in panels (c) it is deduced that surface flux is influenced by the cover permeability, not the waste permeability. Due to a higher cover permeability–solid green and dashed black lines–there are two types of surface mass flux: air influx (negative flux) and gas efflux (positive flux). The reason is that the cover layer is permeable enough to allow gas to move inward or outward of landfill and the well suction is insufficient to collect all generated gas. In this case at the surface one part where is far from the well perforations experiences

gas efflux and the other part near the perforations undergoes air influx. Therefore surface flux profile is V-shaped. As presented by solid green and dashed black lines the cover seals landfill and prevents air inflow for the tightest cover permeability. However gas escaping is expected due to a higher pressure below the surface as a result of gas generation, as shown in the inset of panel (c).

(a) long. pressure in the well (n=2)

(b) vertical pressure profile (n=2)

(c) surface mass flux (n=2)
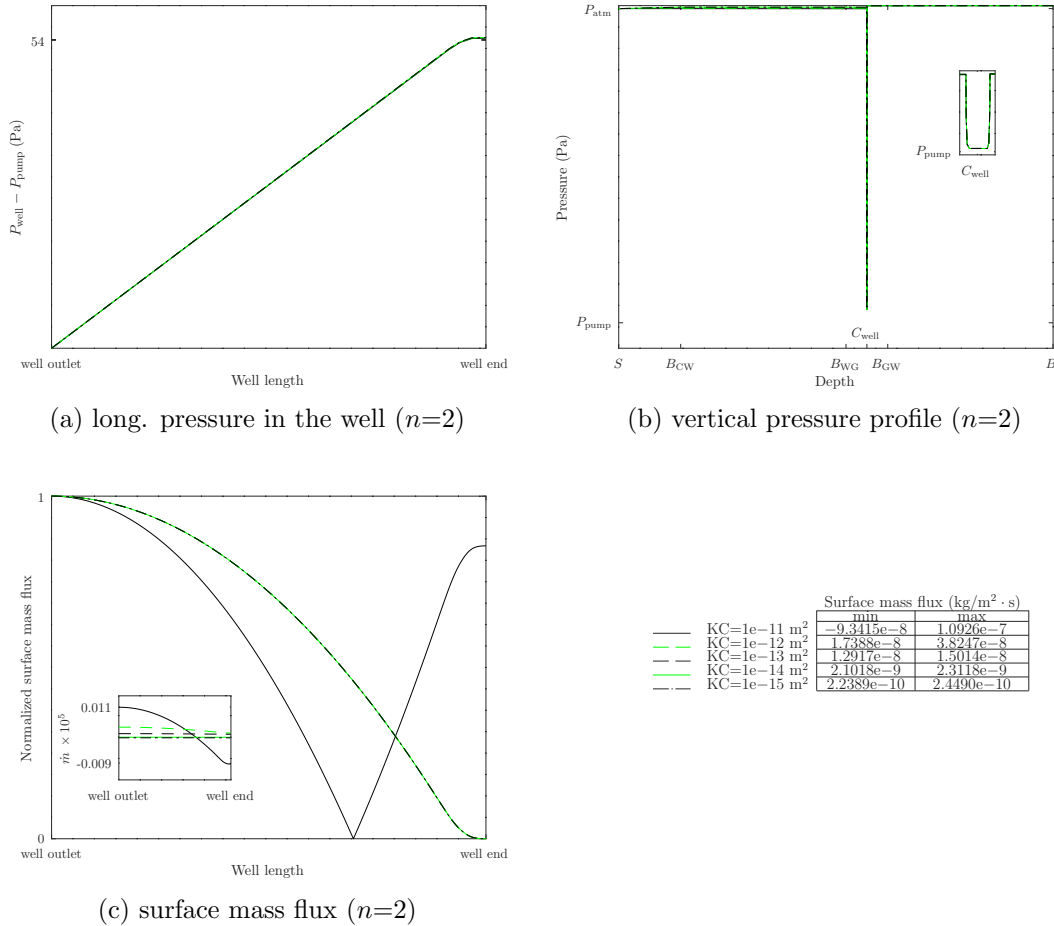
Figure 3.32: Effect of cover permeability on pressure and surface flux for perforation shifting of 390 meters (n=2). Panel (a) shows the well pressure profile at the centerline. Panel (b) represents the pressure profile along a vertical line from top to bottom of landfill at x=390 m; inset represents the pressure values in the well and its slits. Panel (c) shows the normalized surface flux, $(\dot{m} - \dot{m}_{\min})/(\dot{m}_{\max} - \dot{m}_{\min})$, and the table contains scaling values for each plot. The inset demonstrates the actual surface flux profiles.

(a) long. pressure in the well (n=2)

(b) vertical pressure profile (n=2)

(c) surface mass flux (n=2)
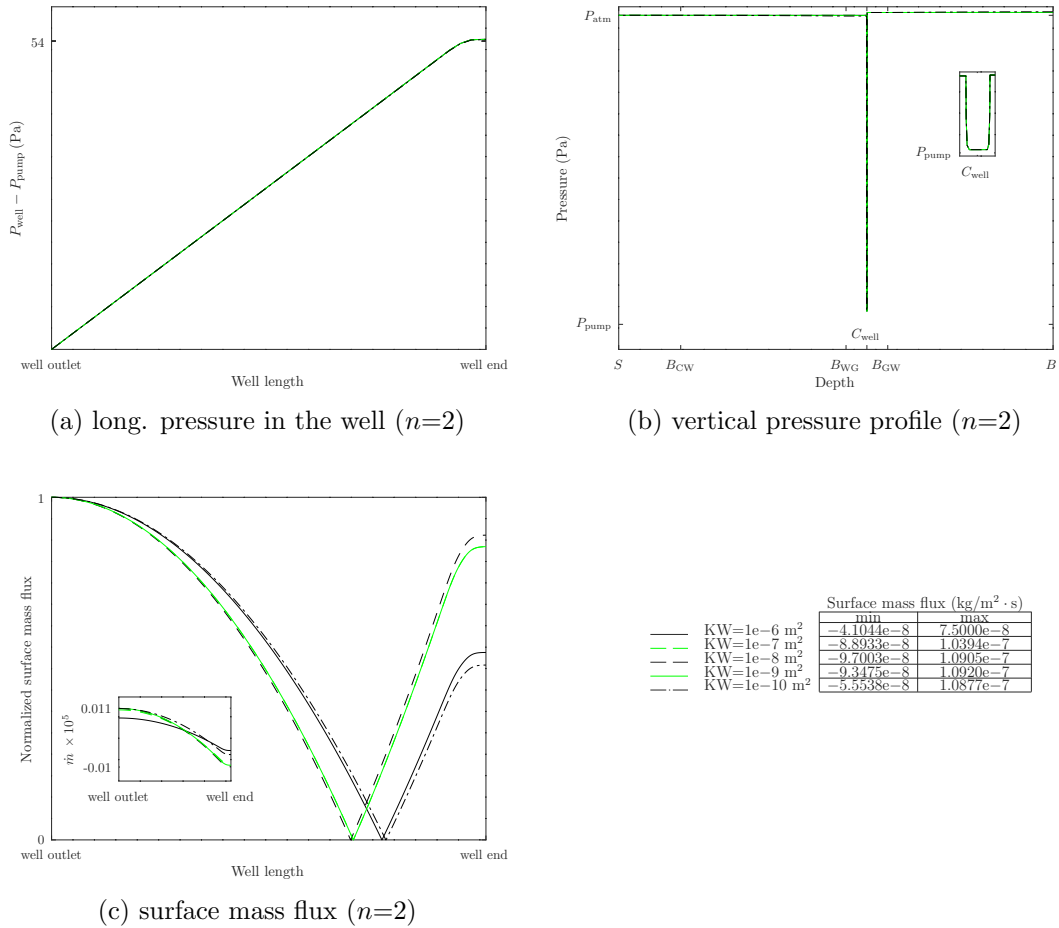
Figure 3.33: Effect of waste permeability on pressure and surface flux for perforation shifting of 390 meters (n=2). Panel (a) shows the well pressure profile at the centerline. Panel (b) represents the pressure profile along a vertical line from top to bottom of landfill at x=390 m; inset represents the pressure values in the well and its slits. Panel (c) shows the normalized surface flux, $(\dot{m} - \dot{m}_{\min})/(\dot{m}_{\max} - \dot{m}_{\min})$, and the table contains scaling values for each plot. The inset demonstrates the actual surface flux profiles.

(a) long. pressure in the well (n=2)

(b) vertical pressure profile (n=2)



(c) surface mass flux (n=2)
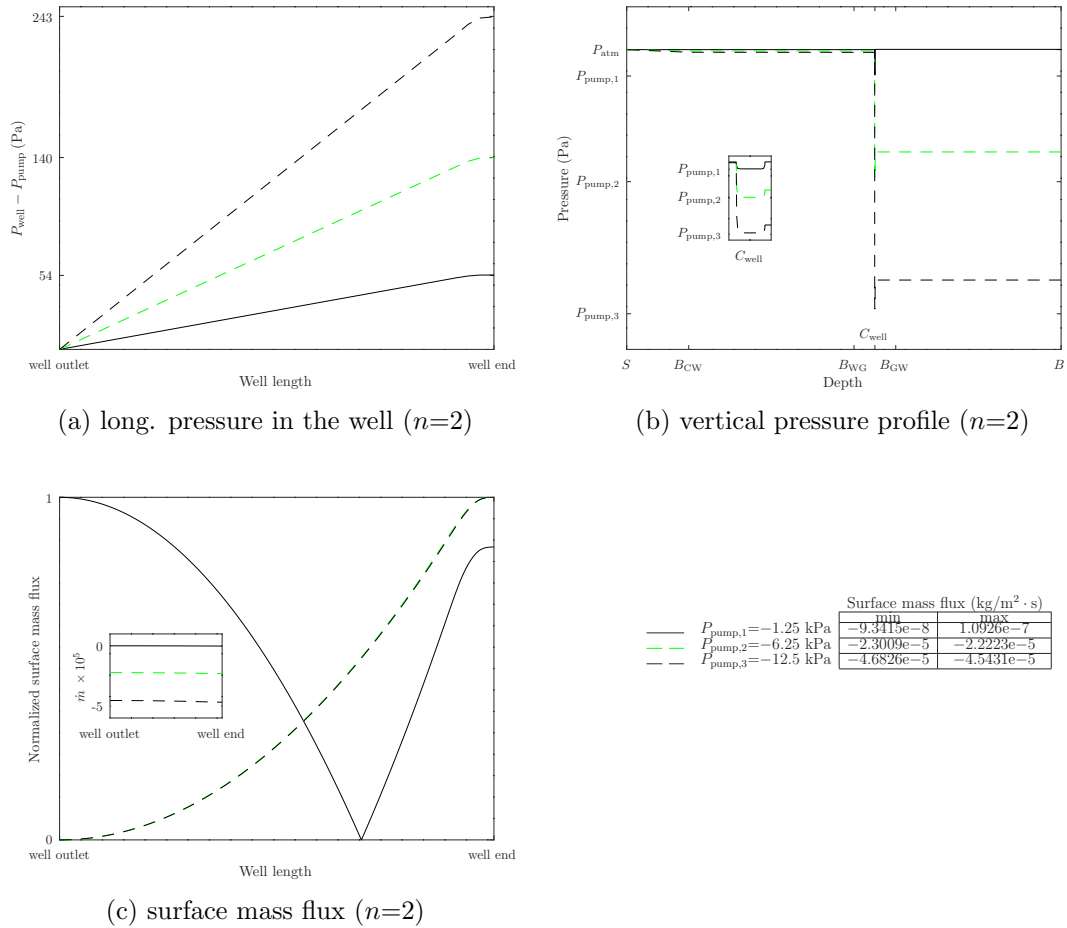
Figure 3.34: Effect of suction strength on pressure and surface flux for perforation shifting of 390 meters (n=2). Panel (a) shows the well pressure profile at the centerline. Panel (b) represents the pressure profile along a vertical line from top to bottom of landfill at x=390 m; inset represents the pressure values in the well and its slits. Panel (c) shows the normalized surface flux, $(\dot{m} - \dot{m}_{\min})/(\dot{m}_{\max} - \dot{m}_{\min})$, and the table contains scaling values for each plot. The inset demonstrates the actual surface flux profiles.

(a) long. pressure in the well ($n=2$)

(b) vertical pressure profile ($n=2$)

(c) surface mass flux ($n=2$)
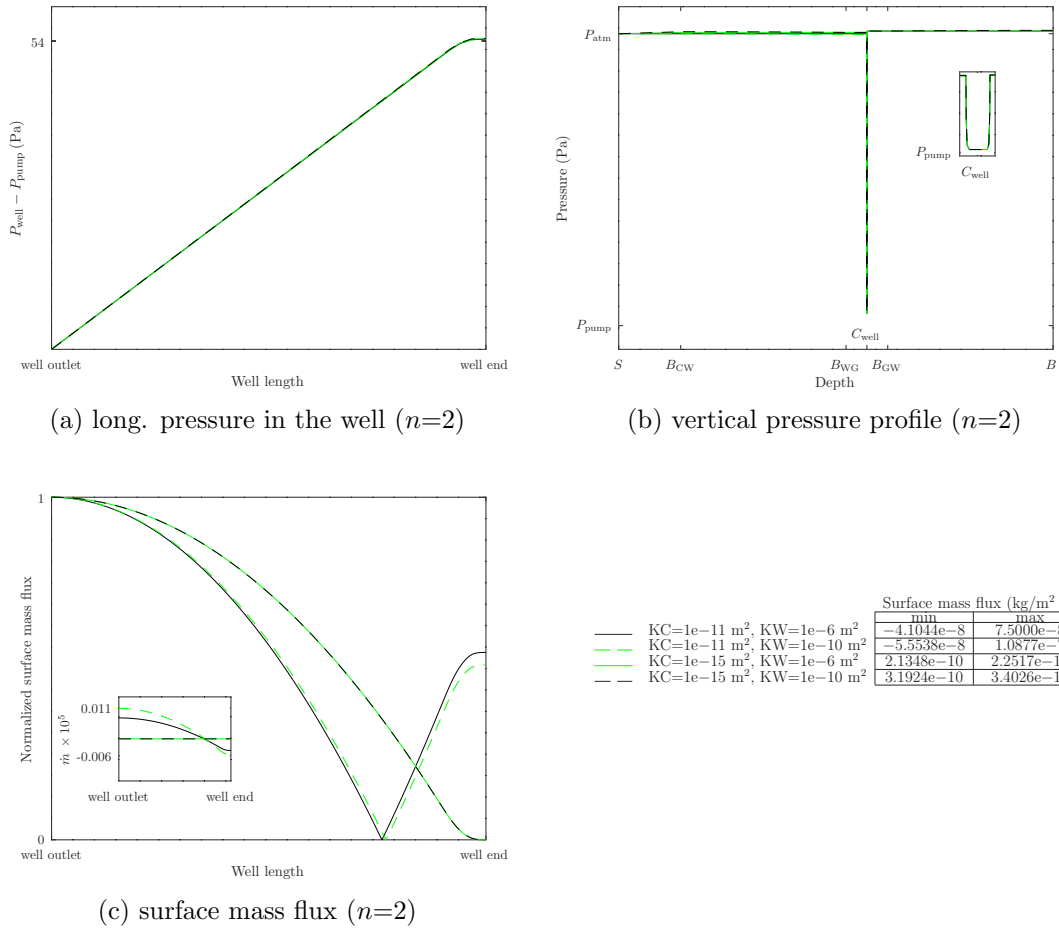
Figure 3.35: Effect of waste-cover permeability combinations on pressure and surface flux for perforation shifting of 390 meters ($n=2$). Panel (a) shows the well pressure profile at the centerline. Panel (b) represents the pressure profile along a vertical line from top to bottom of landfill at x=390 m; inset represents the pressure values in the well and its slits. Panel (c) shows the normalized surface flux, $(\dot{m} - \dot{m}_{\min})/(\dot{m}_{\max} - \dot{m}_{\min})$, and the table contains scaling values for each plot. The inset demonstrates the actual surface flux profiles.

62

Results obtained for the combination of cover permeability and pump pressure are shown in figure 3.36. Based on panel (a) pressure drop within the well is affected by suction strength and cover permeability. Solid green and dashed black lines represents that for a stronger pump pressure there is a higher well pressure drop. This increase in pressure drop is lesser for a tighter cover permeability, as shown by dashed black line in panel (a). Hence the impact of cover permeability variation on well pressure drop is significant. Cover permeability can strongly control pressure drop throughout the landfill, so that for the tightest permeability most of the pressure drop in the entire system happens in the cover layer, which is indicated by dashed lines in panel (b). Based on panel (c) when cover permeability is high and pump pressure is low, since the cover can not properly isolate landfill and well is not strong enough to collect all the generated gas, one part of the surface where is away from the production perforations experiences gas efflux and the other part above the perforations is exposed to air influx. Thence a V-shaped profile for surface mass flux is expected, which is shown by solid black line in panel (c). As both pump pressure and cover permeability are low there is only gas escaping at the surface (dashed green line in panel (c)). The reason is that landfill is sealed enough to prevent incoming air but not sufficiently isolated to cease high-pressure landfill gas escaping. Furthermore due to the low suction strength production well is not capable of collecting all generated gas. Another condition is when pump pressure is high: in this case the amount of cover permeability is not of importance (solid green and dashed black lines). In such condition as a result of high suction strength all generated gas and some air are drawn into the well. When the cover permeability is more permeable, the amount of surface mass flux is higher, as represented by solid green line in the inset of panel (c).

In figure 3.37 results show that waste permeability does not affect well pressure drop, as presented by solid black-dashed green and solid green-dashed black sets of lines in panel (a). However pump pressure significantly governs pressure drop within the well. Vertical pressure profiles in panel (b) confirm this statement since once a higher pump pressure is applied the major portion of the head loss in the open landfill-well system belongs to the well. When suction strength is low there are both gas escaping and air intrusion at the surface from the well outlet toward the end, respectively. Consequently a V-shaped surface flux profile is obtained which is indicated by solid black and dashed green lines in panel (c). On the other hand when the highest pump pressure is applied all generated gas is extracted along with some air from the surface, as shown by solid green and dashed black lines. Comparing solid black-dashed green and solid green-dashed black sets of lines in the inset of panel (c), waste permeability has not any tangible impact on surface mass flux.

(a) long. pressure in the well ($n=2$)

(b) vertical pressure profile ($n=2$)

(c) surface mass flux ($n=2$)
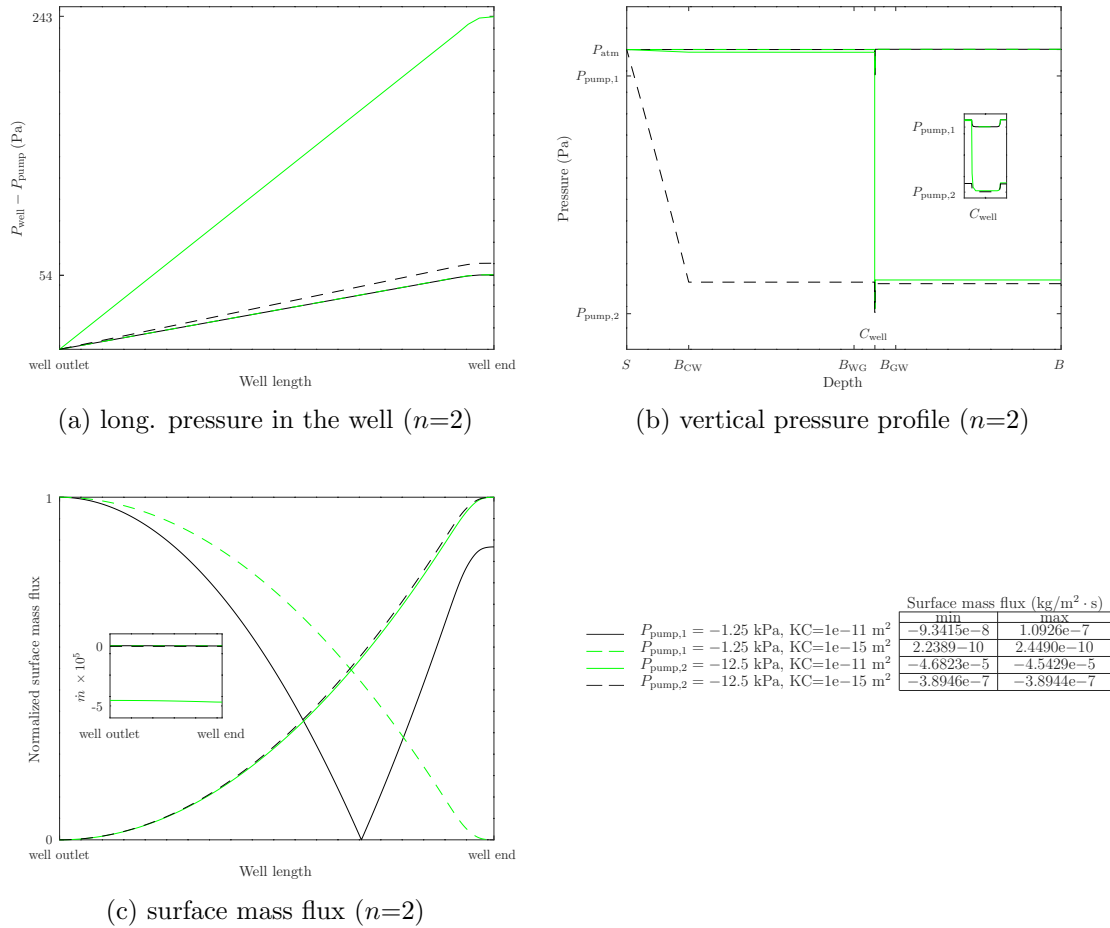
Figure 3.36: Effect of cover permeability-suction strength combinations on pressure and surface flux for perforation shifting of 390 meters ($n=2$). Panel (a) shows the well pressure profile at the centerline. Panel (b) represents the pressure profile along a vertical line from top to bottom of landfill at x=390 m; inset represents the pressure values in the well and its slits. Panel (c) shows the normalized surface flux, $(\dot{m} - \dot{m}_{\min})/(\dot{m}_{\max} - \dot{m}_{\min})$, and the table contains scaling values for each plot. The inset demonstrates the actual surface flux profiles.

(a) long. pressure in the well (n=2)

(b) vertical pressure profile (n=2)

(c) surface mass flux (n=2)
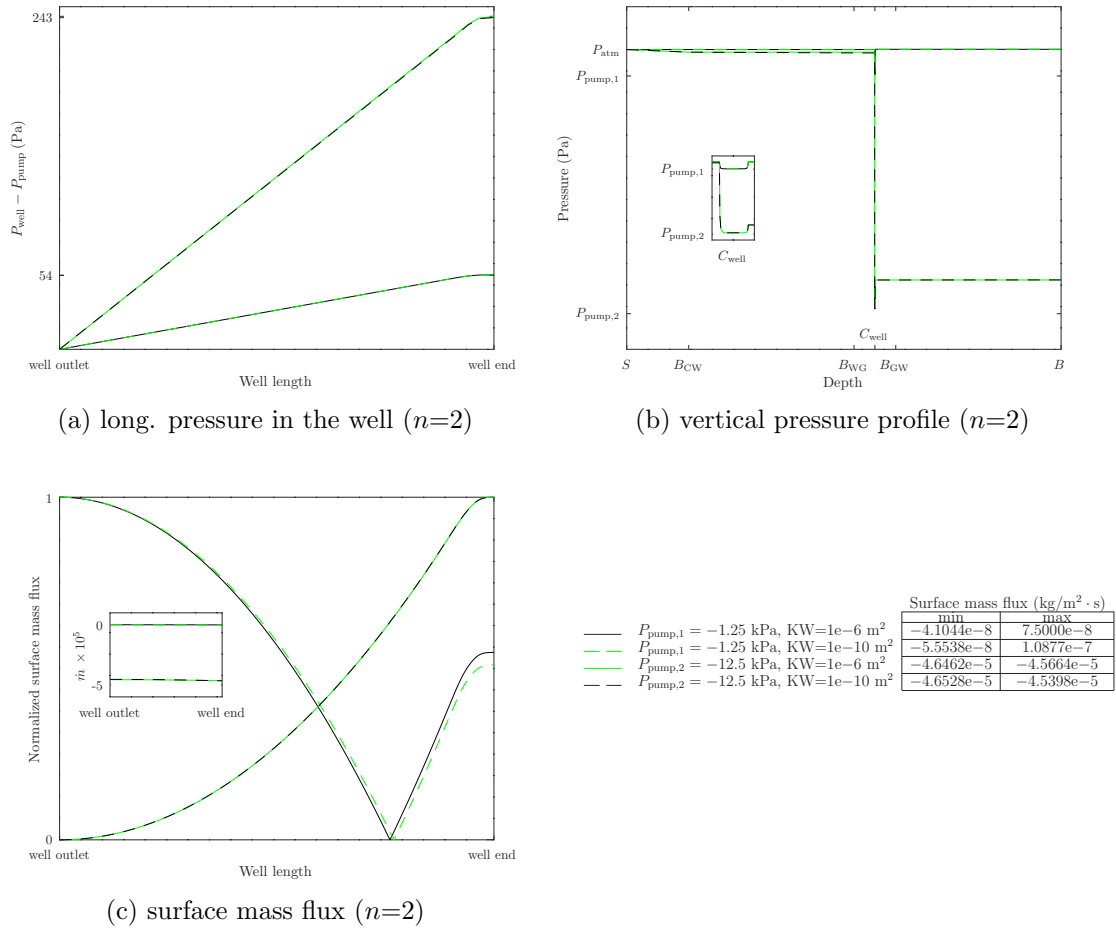
Figure 3.37: Effect of waste permeability-suction strength combinations on pressure and surface flux for perforation shifting of 390 meters (n=2). Panel (a) shows the well pressure profile at the centerline. Panel (b) represents the pressure profile along a vertical line from top to bottom of landfill at x=390 m; inset represents the pressure values in the well and its slits. Panel (c) shows the normalized surface flux, $(\dot{m} - \dot{m}_{\min})/(\dot{m}_{\max} - \dot{m}_{\min})$, and the table contains scaling values for each plot. The inset demonstrates the actual surface flux profiles.

The last well modification contains only one set of perforations at the last producing section. Figures 3.38 to 3.43 represent the effect of this modification along with permeabilities and suction strength variation on the pressure drop and surface flux. In figure 3.38 different well pressure drop profiles correspond to the variation of cover permeability. As the cover permeability decreases from bottom to top in panel (a), the head loss increases within the well. This trend is contrary to the typical instances and the reason is that in this case well suction is not capable enough to outweigh the build-up pressure resulting from gas generation in the landfill. Removing perforation sets and friction result in linear profiles. According to panel (b) vertical pressure profiles indicate pressure above atmospheric throughout the cover and waste layers which refers to the conditions that the amount of gas generated is higher than that of extracted gas. Surface flux maxima are above the well outlet, as represented in panel (c). From top to bottom the inset represents that there are different levels of gas efflux corresponding to the cover layer permeabilities: a lower cover permeability leads to a lower gas efflux.

Based on panels (a) and (b) in figure 3.39 waste permeability changes does not have any impact on pressure drop within the well and throughout landfill. Pressure above atmospheric in vertical pressure profiles in panel (b) refers to the pressure build-up due to the gas generation when the well production capacity is insufficient to collect all generated gas. In such conditions surface mass flux comprises gas escaping from landfill, as shown in the inset of panel (c). Since the single perforation set locates at the very end of the well, minimum suction is on the the outlet side, leading to a maximum surface efflux at this part (panel (c)). In figure 3.40 it is evident that changing suction strength leads to a significant pressure drop and surface flux variation. Increasing pump pressure results in a higher pressure drop within the well, as shown from bottom to top in panel (a). Based on the dashed lines in panels (b) and (c) when sufficient suction strength is applied pressure in the landfill is sub-atmospheric, which means that only air influx occurs at the surface, as represented in the inset of panel (c). For a condition in which pump pressure is insufficient since pressure in waste layer is built up, pressure below the surface is higher than atmospheric, so that gas escaping is expected (solid black line in panel (b) and the inset of panel (c)). If air influx or gas escaping happen at the surface, maxima loci are above the blocked end or outlet, respectively.

Results obtained for dual sensitivity analyses containing K_C-K_W, K_C-P_{pump}, and K_W-P_{pump} combinations are presented in figures 3.41 to 3.43. Based on figure 3.41 cover permeability governs pressure drop and surface flux in the landfill-well open system, as represented by solid black-solid green and dashed green-dashed black sets of lines; conversely, waste permeability causes no change. Decreasing cover permeability leads to a higher pressure build-up in the landfill and higher pressure drop within the well (solid black-solid green and dashed green-dashed black sets of lines in panels (a) and (b); for more details refer to section 3.3). The reason is that well suction capability is not sufficient due to the low number of perforations and the cover is tight. Since the pressure throughout the landfill goes above atmospheric, at the surface there is some gas escaping but not air influx (inset of panel (c)); maxima loci are above the outlet (panel (c)).

(a) long. pressure in the well (n=2)

(b) vertical pressure profile (n=2)

(c) surface mass flux (n=2)

	Surface mass flux (kg/m$^2 \cdot$ s)	
	min	max
KC=1e−11 m^2	4.1162e−6	4.2170e−6
KC=1e−12 m^2	3.9836e−6	3.9945e−6
KC=1e−13 m^2	2.8277e−6	2.8292e−6
KC=1e−14 m^2	8.0699e−7	8.0719e−7
KC=1e−15 m^2	1.0242e−7	1.0244e−7
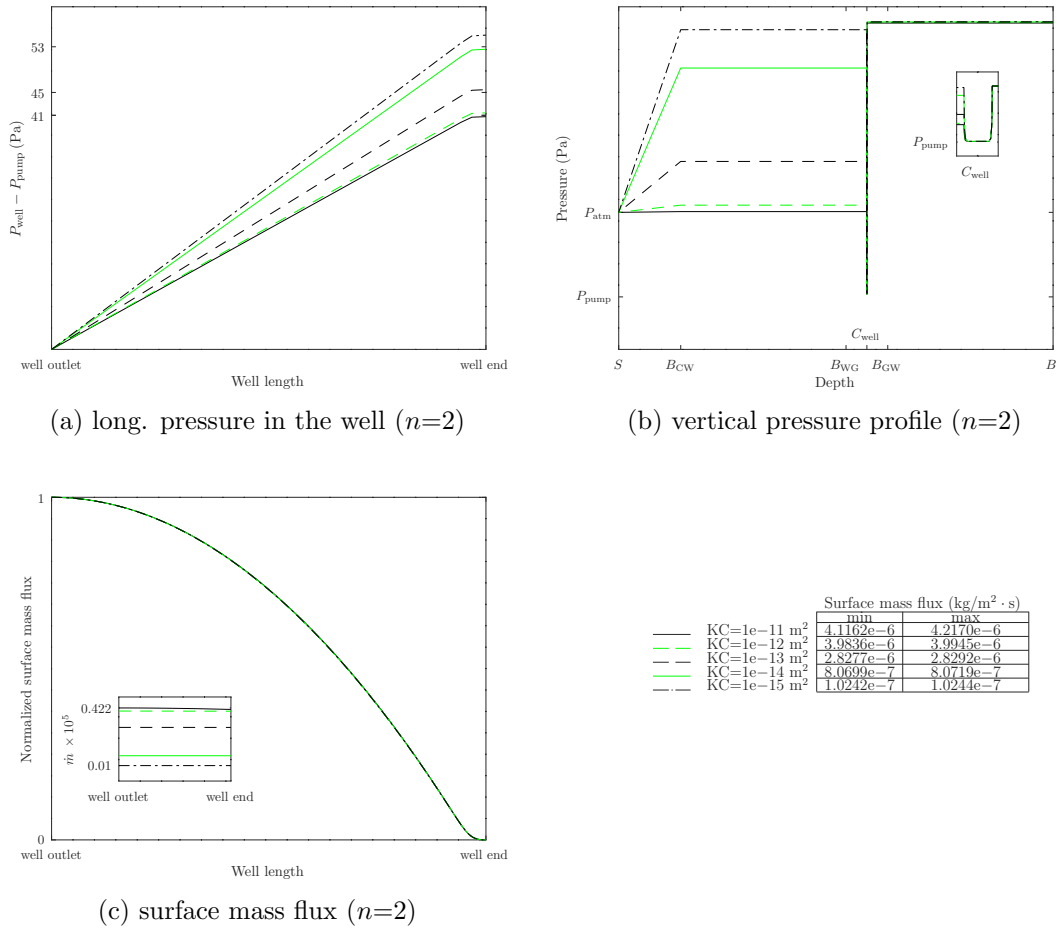
Figure 3.38: Effect of cover permeability on pressure and surface flux for perforation shifting of 405 meters (n=2). Panel (a) shows the well pressure profile at the centerline. Panel (b) represents the pressure profile along a vertical line from top to bottom of landfill at x=405 m; inset represents the pressure values in the well and its slits. Panel (c) shows the normalized surface flux, $(\dot{m} - \dot{m}_{\min})/(\dot{m}_{\max} - \dot{m}_{\min})$, and the table contains scaling values for each plot. The inset demonstrates the actual surface flux profiles.

(a) long. pressure in the well (n=2)

(b) vertical pressure profile (n=2)

(c) surface mass flux (n=2)
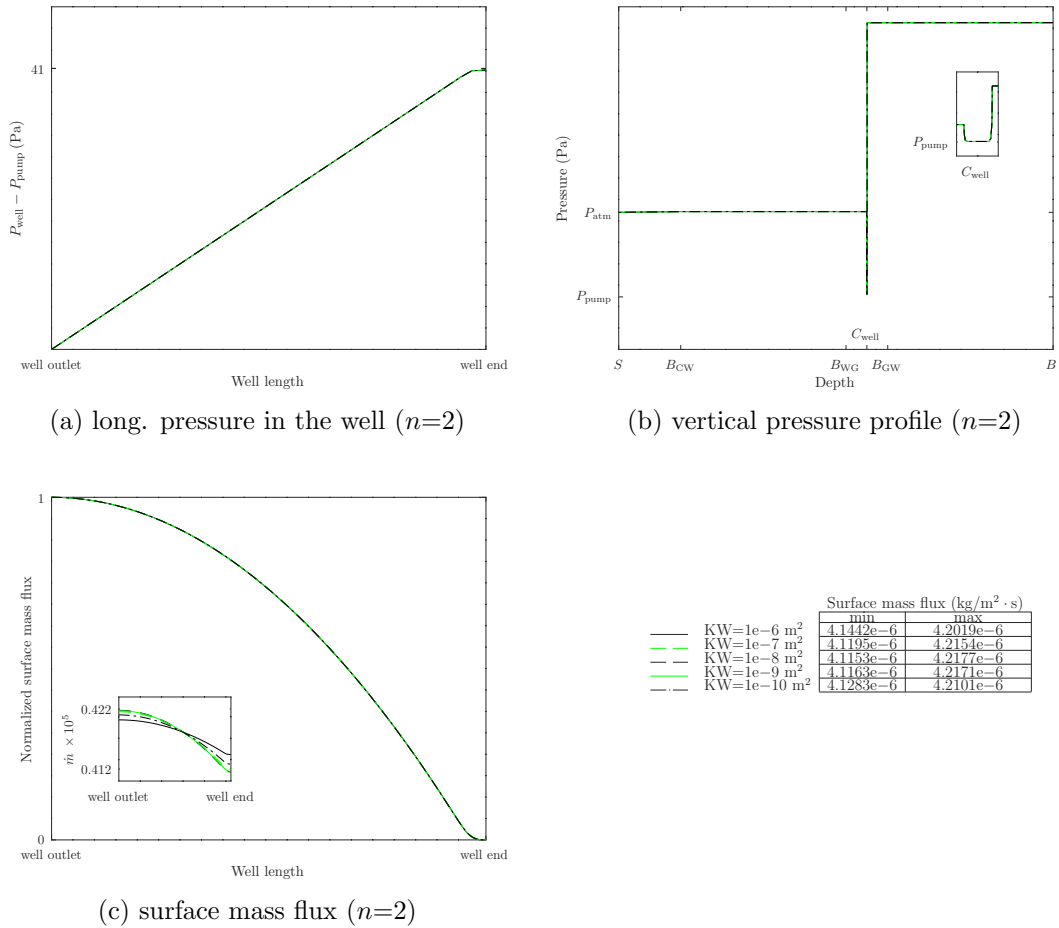
Figure 3.39: Effect of waste permeability on pressure and surface flux for perforation shifting of 405 meters (n=2). Panel (a) shows the well pressure profile at the centerline. Panel (b) represents the pressure profile along a vertical line from top to bottom of landfill at x=405 m; inset represents the pressure values in the well and its slits. Panel (c) shows the normalized surface flux, $(\dot{m} - \dot{m}_{\min})/(\dot{m}_{\max} - \dot{m}_{\min})$, and the table contains scaling values for each plot. The inset demonstrates the actual surface flux profiles.

(a) long. pressure in the well (n=2)

(b) vertical pressure profile (n=2)



(c) surface mass flux (n=2)
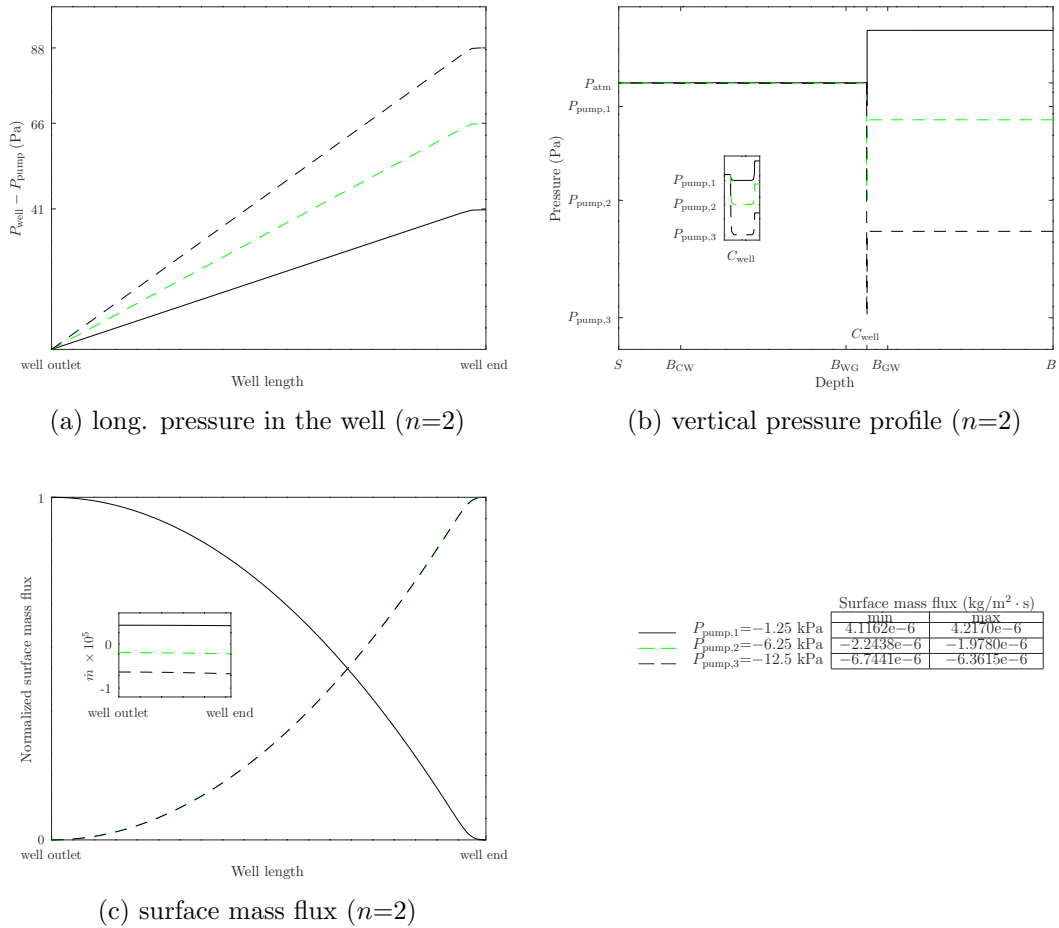
Figure 3.40: Effect of suction strength on pressure and surface flux for perforation shifting of 405 meters (n=2). Panel (a) shows the well pressure profile at the centerline. Panel (b) represents the pressure profile along a vertical line from top to bottom of landfill at x=405 m; inset represents the pressure values in the well and its slits. Panel (c) shows the normalized surface flux, $(\dot{m} - \dot{m}_{\min})/(\dot{m}_{\max} - \dot{m}_{\min})$, and the table contains scaling values for each plot. The inset demonstrates the actual surface flux profiles.

(a) long. pressure in the well ($n=2$)

(b) vertical pressure profile ($n=2$)

(c) surface mass flux ($n=2$)
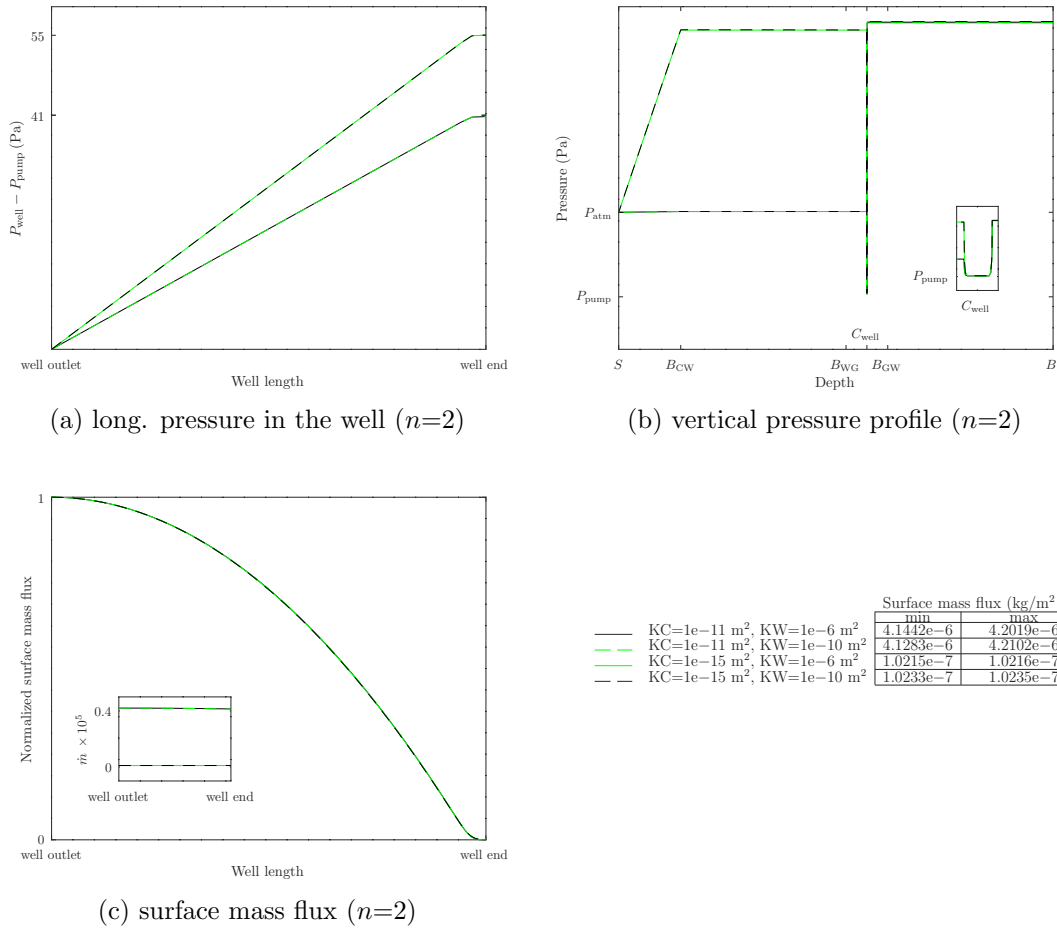
Figure 3.41: Effect of waste-cover permeability combinations on pressure and surface flux for perforation shifting of 405 meters ($n=2$). Panel (a) shows the well pressure profile at the centerline. Panel (b) represents the pressure profile along a vertical line from top to bottom of landfill at x=405 m; inset represents the pressure values in the well and its slits. Panel (c) shows the normalized surface flux, $(\dot{m} - \dot{m}_{\min})/(\dot{m}_{\max} - \dot{m}_{\min})$, and the table contains scaling values for each plot. The inset demonstrates the actual surface flux profiles.

According to figure 3.42 cover permeability and pump pressure significantly affect pressure drop and surface flux. As the lowest suction strength and highest cover permeability are applied minimum pressure drop within the well occurs (solid black line in panel (a)). On the other hand when maximum pump pressure and cover permeability are utilized, highest pressure drop within the well is obtained (solid green line in panel (a)). For other modifications well pressure drop lies between these two limits (dashed lines in panel (a)). Pressure in the landfill highly depends on pump pressure, so that in the case of lowest pump pressure and lowest or highest cover permeability, pressure in landfill is above atmospheric and at the surface there is gas escaping (solid black and dashed green lines in panel (b) and inset of panel (c)). The reason is that the well is not capable of collecting all generated gas. Once the highest suction strength is applied only air influx occurs at the surface, as shown by solid green and dashed black lines in the inset of panel (c). Locus of maximum surface flux relies on the fluid flow direction (inward or outward): for gas efflux it locates away from perforations and for air influx it lies above perforations (panel (c)).

Figure 3.43 demonstrates that suction strength significantly influences pressure drop and surface flux, as shown by solid black-dashed green and solid green-dashed black sets of lines in panels (a), (b) and inset of panel (c). Nevertheless waste permeability has an intangible impact on those parameters. Decreasing suction strength leads to a lower pressure drop within the well and vice versa (from top to bottom in panel (a)). In landfill a higher pump pressure results in collecting more generated gas (from top to bottom in the inset of panel (c)); gas escaping at surface reduces. In this case air influx is expected (solid green and dashed black lines in the inset of panel (c)). Locus of the maximum surface flux is above the single set of the well perforations (solid green and dashed black lines in panel (c)). Inversely once a lower pump pressure is applied well capability of collecting gas is reduced and due to pressure build-up as a result of gas generation, gas escaping increases, as shown by solid black and dashed green lines in panel (c). In such case maximum surface flux occurs above the well outlet.

The above analysis shows that extreme cases of perforation shifting can provide a substantial impact on surface flux. When the amount of shifting is adjusted with respect to the landfill properties, the well can effectively control the surface efflux and influx. This modification could be considered for controlling surface flux when changing pump pressure is not an option. The immediate impact of such a shift are a higher air intrusion near the outlet and gas escaping near the well end.

(a) long. pressure in the well (n=2)

(b) vertical pressure profile (n=2)

(c) surface mass flux (n=2)
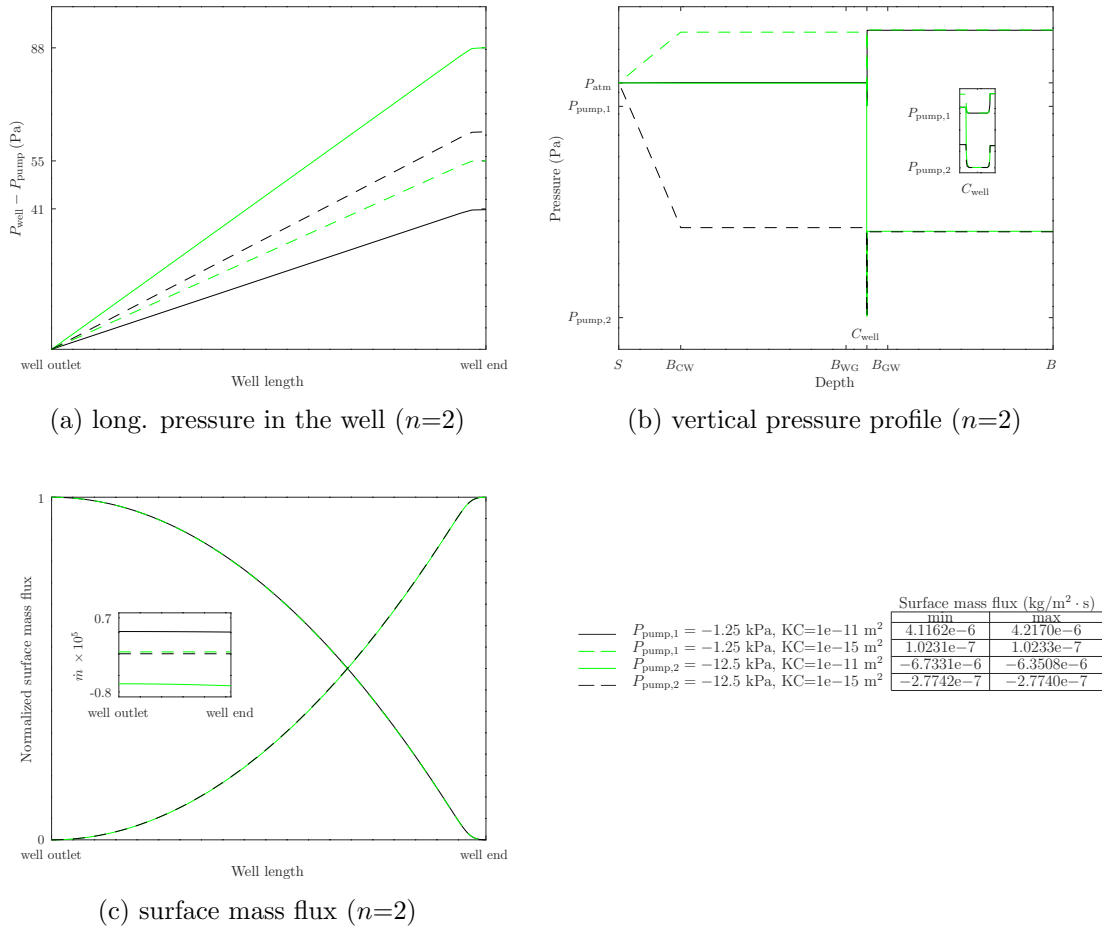
Figure 3.42: Effect of cover permeability-suction strength combinations on pressure and surface flux for perforation shifting of 405 meters (n=2). Panel (a) shows the well pressure profile at the centerline. Panel (b) represents the pressure profile along a vertical line from top to bottom of landfill at x=405 m; inset represents the pressure values in the well and its slits. Panel (c) shows the normalized surface flux, $(\dot{m} - \dot{m}_{\min})/(\dot{m}_{\max} - \dot{m}_{\min})$, and the table contains scaling values for each plot. The inset demonstrates the actual surface flux profiles.

(a) long. pressure in the well ($n=2$)

(b) vertical pressure profile ($n=2$)

(c) surface mass flux ($n=2$)
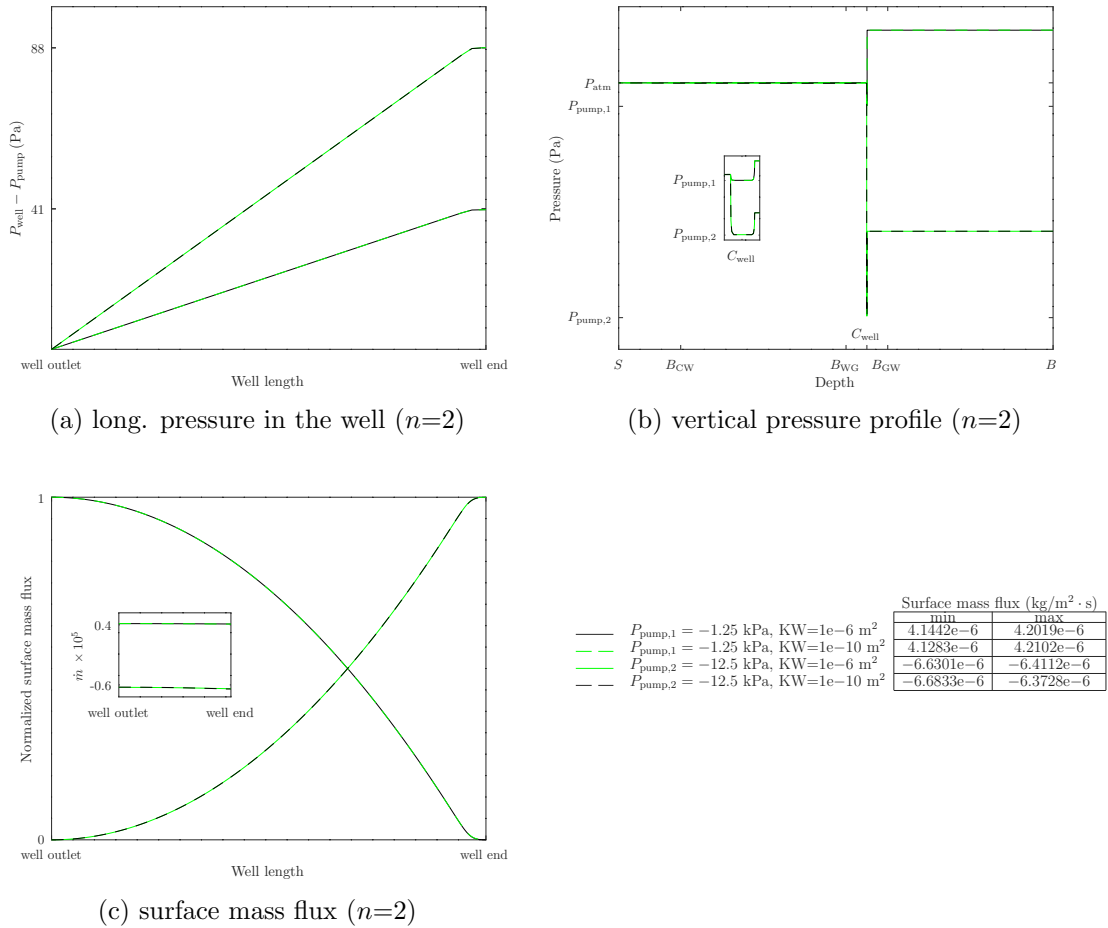
Figure 3.43: Effect of waste permeability-suction strength combinations on pressure and surface flux for perforation shifting of 405 meters ($n=2$). Panel (a) shows the well pressure profile at the centerline. Panel (b) represents the pressure profile along a vertical line from top to bottom of landfill at x=405 m; inset represents the pressure values in the well and its slits. Panel (c) shows the normalized surface flux, $(\dot{m} - \dot{m}_{\min})/(\dot{m}_{\max} - \dot{m}_{\min})$, and the table contains scaling values for each plot. The inset demonstrates the actual surface flux profiles.

3.8   Combination

This section assesses the influence of modification combinations on pressure drop and surface mass flux. According to the previous results it is comprehended that changing waste permeability does not affect pressure and surface flux. Moreover very tight cover permeabilities are hard to achieve in practice. Therefore in this evaluation only the feasible cover permeability in the order of 10^{-13} and medium waste permeability in the order of 10^{-9} are utilized. Suction strength is reduced as there is a tiny gas generation rate in the waste layer. The reason is that once the pump pressure is sufficient with respect to the gas generation rate, there might be both surface efflux and influx. This reduction makes the visualization possible for the comparison of different combinations in terms of shifting the point at which the surface flux sign changes. The base perforation size in this section is $1.5R_{\text{base}}$. As for the linear decrease and increase in perforation size variation are -0.3% and $+0.3\%$, respectively.

Figure 3.44 represents the effect of single modifications and their combinations on pressure drop and surface flux in a landfill-well open system. In panel (a) there are two groups of lines: the lower group corresponds to the linear decrease and linear increase in perforation size and the upper group is related to shifting perforations 225 m toward the blocked end and two combinations of mentioned modifications. Pressure drop relating to linear decrease and increase are visually indistinguishable. Although once perforation shifting modification is applied there is a significant variation in well pressure drop. Panel (b) shows the vertical pressure drop throughout the landfill at 225 m from the well end. Most of the pressure drop occurs in the landfill cover for linear perforation size changes. Nonetheless for the perforation shifting modification and two combinations the portion of pressure drop within the well is much higher than that of the cover layer. Surface flux profiles in panel (c) reveal the impact of modification combinations. Reverse S-shaped surface flux profiles for linear decrease and increase in perforation size fairly match. There is a V-shaped profile for simple perforation shifting 225 m toward the blocked end, which means that both surface efflux and influx happen. One part near the outlet undergoes gas escaping due to the absence of perforations and consequently lower suction strength. The other part away from the well outlet experiences air intrusion due to proximity to the perforations. When a linear decrease of perforation size in combination with the perforation shifting is used the point at which surface flux sign changes moves away from the well outlet since the portion of gas escaping increases. On the other hand once a linear increase of perforation size and perforation shifting are in use, the point is closer to the outlet as there is a higher air intrusion.

Combining the studied modifications adds more flexibility to landfill well design, leading to a more refined surface flux control.

(a) long. pressure in the well (n=2)

(b) vertical pressure profile (n=2)

(c) surface mass flux (n=2)
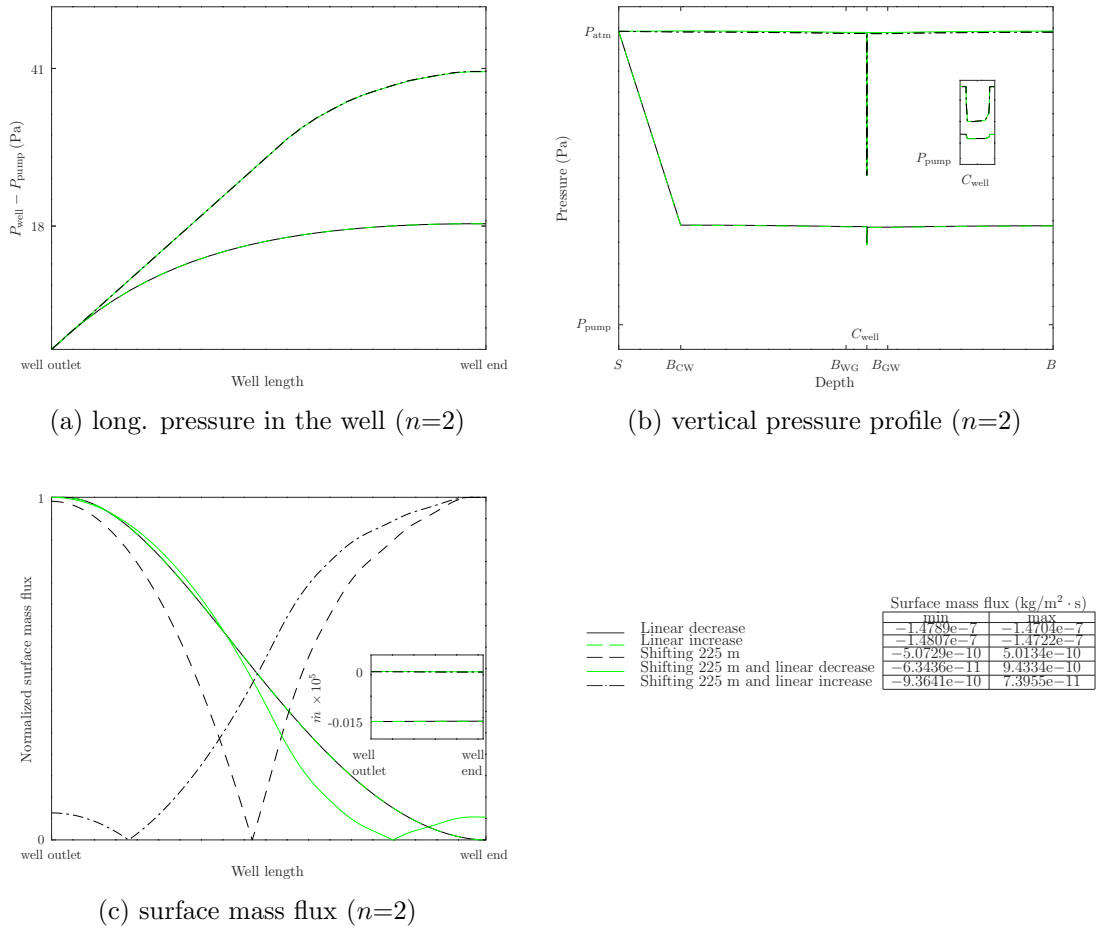
Figure 3.44: Effect of geometry combinations on pressure and surface flux for perforation shifting of 225 meters (n=2). Panel (a) shows the well pressure profile at the centerline. Panel (b) represents the pressure profile along a vertical line from top to bottom of landfill at x=225 m; inset represents the pressure values in the well and its slits. Panel (c) shows the normalized surface flux, $(\dot{m} - \dot{m}_{\min})/(\dot{m}_{\max} - \dot{m}_{\min})$, and the table contains scaling values for each plot. The inset demonstrates the actual surface flux profiles.

3.9 Gravity inclusion

In all previous sections gravity has been excluded from the simulations. In this section a comparison is made to assess the impact of gravity on the fluid flow through porous media and in the well. This investigation utilizes basic configuration and parameters (refer to figure 2.5 and table 2.3). In Figure 3.45 solid black and dashed green lines correspond to the simulations without and with gravity, respectively. In panel (a) there is a significant variation in well pressure drop values due to adding gravity, notwithstanding the profile trends are roughly the same. A higher well pressure drop in the case of gravity inclusion is due to the impact of gas weight. According to panel (b) for the waste layer when gravity is included there is a steep slope in the pressure profile which indicates that pressure at the bottom of the layer is higher than that of the top. This effect is evident in surface flux profiles (panel (c)). In the inset of panel (c) with gravity the amount of air intrusion from the surface (negative surface flux) is higher than that of without gravity case; despite the trend of the surface flux profile is fairly the same. From this argument it can be concluded that adding gravity to the landfill model strengthen fluid flow toward the suction source and might increase air intrusion. Therefore the influence of gravity on gas migration in a landfill should be considered in all scenarios and modifications.

Figure 3.46 shows the hydrostatic pressure created in the landfill as a result of adding gravity. Based on the figure the pressure gradient for the landfill is roughly 12 Pa/m. Adding gravity interferes with Darcy's law; the normal velocity is zero due to no flux boundary condition and based on equation (2.1b) pressure gradient equals gravity force: $\mathrm{d}P/\mathrm{d}y = \rho\mathrm{g}$. Consequently pressure at the bottom of the landfill is not constant, as represented by the dashed green line in figure 3.7. The maximum value of hydrostatic pressure In figure 3.46 corresponds to the bottom and equals approximately 249 Pa which matches the difference between pressure values at the bottom with and without gravity in figure 3.7. Furthermore to clarify the impact of gravity in terms of hydrostatic pressure from the upper and lower part of the landfill, pressure drops with and with out gravity are calculated and provided in table 3.3. Based on the table it is evident that for each part the difference between pressure drops with and without gravity equal corresponding hydrostatic pressure.

(a) long. pressure in the well (n=2)

(b) vertical pressure profile (n=2)

(c) surface mass flux (n=2)
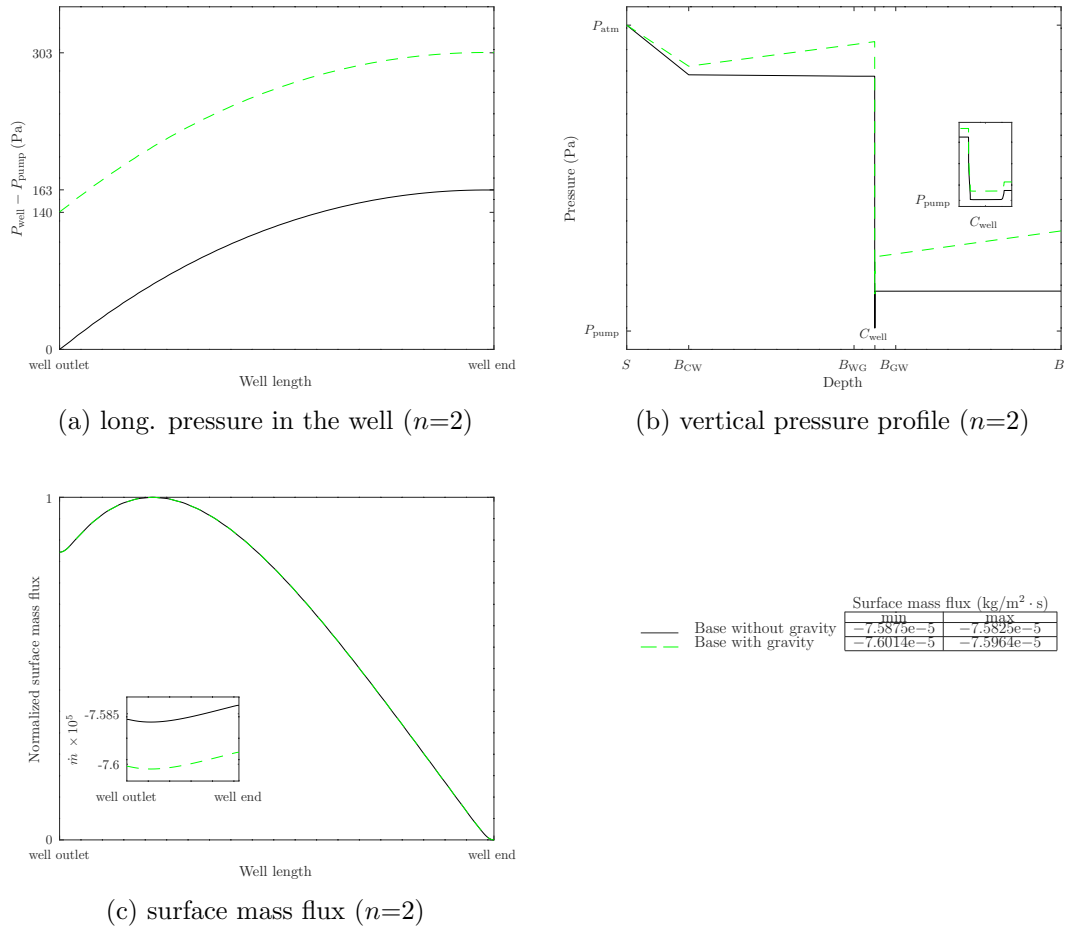
Figure 3.45: Effect of gravity on pressure and surface flux for basic configuration (n=2). Panel (a) shows the well pressure profile at the centerline. Panel (b) represents the pressure profile along a vertical line from top to bottom of landfill at x=15 m; inset represents the pressure values in the well and its slits. Panel (c) shows the normalized surface flux, $(\dot{m} - \dot{m}_{\min})/(\dot{m}_{\max} - \dot{m}_{\min})$, and the table contains scaling values for each plot. The inset demonstrates the actual surface flux profiles.
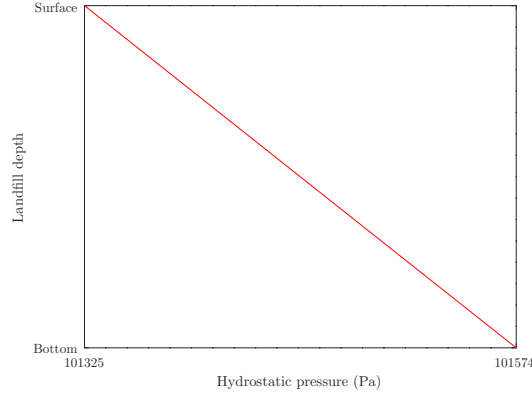
Figure 3.46: Hydrostatic pressure.

Table 3.3: Impact of gravity on the system.

	Domain	
Model type	Upper	
Model with gravity	$P_{\text{S}} = 101325$ Pa	$\Delta P_{\text{U},1} = 67.27$ Pa
	$P_{\text{U,ingress}} = 101257.72$ Pa	
Model without gravity	$P_{\text{S}} = 101325$ Pa	$\Delta P_{\text{U},2} = 208.65$ Pa
	$P_{\text{U,ingress}} = 101116.34$ Pa	
Hydrostatic model	$P_{\text{S}} = 101325$ Pa	$\Delta P_{\text{U},3} = 141.98$ Pa
	$P_{\text{U,ingress}} = 101466.98$ Pa	

	Domain	
Model type	Lower	
Model with gravity	$P_{\text{B}} = 100484.17$ Pa	$\Delta P_{\text{L},1} = 105.76$ Pa
	$P_{\text{L,ingress}} = 100378.41$ Pa	
Model without gravity	$P_{\text{B}} = 100238.17$ Pa	$\Delta P_{\text{L},2} = 0.28$ Pa
	$P_{\text{L,ingress}} = 100237.88$ Pa	
Hydrostatic model	$P_{\text{B}} = 101573.84$ Pa	$\Delta P_{\text{L},3} = 106.61$ Pa
	$P_{\text{L,ingress}} = 101467.22$ Pa	

Chapter 4

Conclusion

In this project the effect of well geometry on the pressure, velocity, and surface flux profiles in a coupled landfill-well open system are assessed qualitatively. It is observed that changing geometry can have tangible impact on pressure drop and surface flux. Five different well modifications were studied: (a) different number of perforations, (b) uniform perforation shifting to left or right, (c) non-uniform perforation distribution: linear increase or decrease in perforation intervals, (d) uniform changing of perforation radius with uniform distribution, and (e) non-uniform changing of perforation radius with uniform distribution. Studied modifications are prioritized based on their impact on surface flux, whereupon case (c) is excluded as its effect on the surface flux is insignificant, implying that it can be used interchangeably with the basic well geometry.

Conducting several sensitivity analyses, it is seen that for all simulations: there is no direct relationship between well and surface flux, and different landfill-well components can affect surface flux. Cover permeability and pump pressure, in contrast to waste permeability, have a substantial impact on the pressure and surface flux. As the permeability of any given porous layer decreases, the pressure drop over that layer increases. Furthermore it is observed that when cover permeability decreases, surface flux predictably decreases. It is shown that when the pressure drop in porous media increases, the well pressure drop decreases to keep the total pressure drop virtually constant. Therefore it can be concluded that reducing the cover permeability decreases the well pressure drop. These relationships between permeability, pressure drop and surface flux were observed in all simulations. A change in pump pressure significantly affects surface mass flux: in most cases, a higher suction strength leads to a greater surface flux. An interesting observation is that the well suction capability increases, the maximum surface flux locus is shifted toward the outlet.

By comparing the results of different well modifications, the landfill-well interactions and responses to different flow conditions are assessed. For a lower number of perforations, an incremental impact on well pressure drop is observed for a typical value of cover permeability, leading to lower pressure drop in porous media and mass flux at the surface. The same results ensue for the uniform perforation size changing along the well, since in terms of modeling it is equivalent to the variation of the number of perforations. When the perforation size is linearly increased, there

is a higher pressure drop in the well as the perforation size increases along the well toward the blocked end; this is due to the presence of larger perforations upstream. Comparing linear decrease and increase of perforation size, since the well pressure drop is higher for the latter modification, there is a lower flux at the surface.

An interesting result was obtained for the extreme cases of perforation shifting modification. There are three possibilities: pre-threshold, threshold, and post-threshold. Going from pre-threshold to post-threshold modifications, the surface flux will change from air intrusion to gas escaping. The reason is that by removing perforations along the well, well production capability reduces, leading to a reduction in well pressure drop. In the pre-threshold modification there is only air intrusion due to the sufficient well suction strength. In the threshold case there are two possibilities for surface flux: (1) when both gas efflux and air influx happen simultaneously and (2) when only gas efflux occurs across the landfill. The former case occurs for sufficiently high cover permeabilities. The surface is then divided into two parts: the first part near the outlet, but far from the perforations landfill gas flow into the atmosphere, whereas immediately above the perforations air is drawn into the landfill. A sufficiently tight cover layer can block air intrusion entirely and landfill gas will escape throughout due to a pressure build up within the porous media. A relatively low pump pressure is another scenario where surface efflux and influx co-occur. As the suction strength becomes higher, more mass is drawn into the well and therefore only air influx happens. For the post-threshold case well suction cannot counteract the pressure build up resulting from gas generation in the landfill, leading to gas escape.

When a linear decrease of perforation size is combined with the perforation shifting, the point at which the surface flux changes from efflux to influx moves away from the well outlet, since the portion of gas escaping increases. On the other hand, when a linear increase in perforation size and perforation shifting are combined, the point is closer to the outlet as there is a higher air intrusion. Therefore these combined modifications suggest surface flux control strategies: by carefully manipulating perforation size and longitudinal distribution the point of efflux/influx reversal can be shifted along the well.

Accounting for gravity leads to a significant variation in well pressure values. Comparing obtained surface flux values for models with gravity and without gravity, it is concluded that gravity force strengthens the downward gas flow, leading to more air intrusion. It is observed that the hydrostatic profile is fairly linear as in the landfill-well system the depth is not large and therefore the difference between the maximum hydrostatic pressure and reference pressure is small; in other words, a small part of the exponential plot seems like a linear graph.

In summary, finding a balance between surface efflux and influx depends on different factors such as layers permeability and pump pressure. Geometry change can be considered as a complementary approach to achieve a more refined surface flux control. Gravity should not be neglected when simulating surface flow, as it affects the fluid's absolute pressure as well as gradients.

Bibliography

Adler, M. J. (1994). International anthropogenic methane emissions: estimates for 1990. Report to Congress.

Alzaydi, A. A., Moore, C. A., and Rai, I. S. (1978). Combined pressure and diffusional transition region flow of gases in porous media. *AIChE Journal*, 24(1):35–43.

Arigala, S. G., Tsotsis, T. T., Webster, I. A., Yortsos, Y. C., and Kattapuram, J. J. (1995). Gas generation, transport, and extraction in landfills. *Journal of environmental engineering*, 121(1):33–44.

Bogner, J., Meadows, M., and Czepiel, P. (1997). Fluxes of methane between landfills and the atmosphere: natural and engineered controls. *Soil use and management*, 13:268–277.

Budka, A. (2003). Personal communication.

Chaudhuri, A. and Sekhar, M. (2005). Probabilistic analysis of pollutant migration from a landfill using stochastic finite element method. *Journal of geotechnical and geoenvironmental engineering*, 131(8):1042–1049.

Chen, Y.-C., Chen, K.-S., and Wu, C.-H. (2003). Numerical simulation of gas flow around a passive vent in a sanitary landfill. *Journal of Hazardous Materials*, 100(1-3):39–52.

Clayton, K. C. and Huie, J. M. (1900). Sanitary Landfill Cost. *Historical Documents of the Purdue Cooperative Extension Service*, (632).

COMSOL Multiphysics® (2021). v. 6.0 `https://www.comsol.com/`. Stockholm, Sweden.

Copty, N. K., Ergene, D., and Onay, T. T. (2004). Stochastic model for landfill gas transport and energy recovery. *Journal of environmental engineering*, 130(9):1042–1049.

Donovan, S., Bateson, T., Gronow, J., and Voulvoulis, N. (2010). Modelling the behaviour of mechanical biological treatment outputs in landfills using the GasSim model. *Science of the total environment*, 408(8):1979–1984.

Eggleston, S., Buendia, L., Miwa, K., Ngara, T., Tanabe, K., et al. (2006). IPCC guidelines for national greenhouse gas inventories.

El-Fadel, M., Findikakis, A., and Leckie, J. (1989). A numerical model for methane production in managed sanitary landfills. *Waste Management & Research*, 7(1):31–42.

El-Fadel, M., Findikakis, A. N., and Leckie, J. O. (1995). Migration and atmospheric emission of landfill gas. *Hazardous waste and hazardous materials*, 12(4):309–327.

Esmaili, H. (1975). Control of gas flow from sanitary landfills. *Journal of the Environmental Engineering Division*, 101(4):555–566.

Feng, S.-J., Zheng, Q.-T., and Xie, H.-J. (2015). A model for gas pressure in layered landfills with horizontal gas collection systems. *Computers and Geotechnics*, 68:117–127.

Feng, S.-J., Zhu, Z.-W., Chen, Z.-L., and Chen, H.-X. (2020). Analytical model for multicomponent landfill gas migration through four-layer landfill biocover with capillary barrier. *International Journal of Geomechanics*, 20(3):04020001.

Findikakis, A. N. and Leckie, J. O. (1979). Numerical simulation of gas flow in sanitary landfills. *Journal of the Environmental Engineering Division*, 105(5):927–945.

GNU Octave (2022). version 7.1.0 manual: a high-level interactive language for numerical computations `https://docs.octave.org/interpreter/index.html`.

Gregory, R. (2003). The validation and development of an integrated landfill gas risk assessment model: GasSim. In *Proceedings of Sardinia 2003, Ninth International Landfill Symposium*.

Halvorsen, D., Nec, Y., and Huculak, G. (2019). Horizontal landfill gas wells: Geometry, physics of flow and connection with the atmosphere. *Physics and Chemistry of the Earth, Parts A/B/C*, 113:50–62.

Hermann, T. (2005). Personal communication.

Ishii, K. and Furuichi, T. (2013). Estimation of methane emission rate changes using age-defined waste in a landfill site. *Waste management*, 33(9):1861–1869.

Jacobs, J. and Scharff, H. (2001). Comparison of methane emission models and methane emission measurements. *NV Afvalzorg, Netherlands*.

Jeong, S., Nam, A., Yi, S.-M., and Kim, J. Y. (2015). Field assessment of semi-aerobic condition and the methane correction factor for the semi-aerobic landfills provided by IPCC guidelines. *Waste Management*, 36:197–203.

Kamalan, H. (2016). A new empirical model to estimate landfill gas pollution. *Journal of Health Sciences & Surveillance System*, 4(3):142–148.

Kaza, S. and Bhada-Tata, P. (2018). Decision maker's guides for solid waste management technologies.

Kindlein, J., Dinkler, D., and Ahrens, H. (2006). Numerical modelling of multi-phase flow and transport processes in landfills. *Waste Management & Research*, 24(4):376–387.

Klusman, R. W. and Dick, C. J. (2000). Seasonal variability in CH4 emissions from a landfill in a cool, semiarid climate. *Journal of the Air & Waste Management Association*, 50(9):1632–1636.

Krause, M. J., Chickering, G. W., and Townsend, T. G. (2016). Translating landfill methane generation parameters among first-order decay models. *Journal of the Air & Waste Management Association*, 66(11):1084–1097.

Kumar, S., Nimchuk, N., Kumar, R., Zietsman, J., Ramani, T., Spiegelman, C., and Kenney, M. (2016). Specific model for the estimation of methane emission from municipal solid waste landfills in India. *Bioresource technology*, 216:981–987.

Lelieveld, J., Crutzen, P. J., and Dentener, F. J. (1998). Changing concentration, lifetime and climate forcing of atmospheric methane. *Tellus B*, 50(2):128–150.

Lu, S.-F. and Feng, S.-J. (2020). Comprehensive overview of numerical modeling of coupled landfill processes. *Waste Management*, 118:161–179.

Lu, S.-F., Xiong, J.-H., Feng, S.-J., Chen, H.-X., Bai, Z.-B., Fu, W.-D., and Lü, F. (2019). A finite-volume numerical model for bio-hydro-mechanical behaviors of municipal solid waste in landfills. *Computers and Geotechnics*, 109:204–219.

Metcalfe, D. E. and Farquhar, G. J. (1987). Modeling gas migration through unsaturated soils from waste disposal sites. *Water, Air, and Soil Pollution*, 32(1):247–259.

Mohsen, M., Farquhar, G., and Kouwen, N. (1978). Modelling methane migration in soil. *Applied Mathematical Modelling*, 2(4):294–301.

Mohsen, M., Farquhar, G., and Kouwen, N. (1980). Gas migration and vent design at landfill sites. *Water, Air, and Soil Pollution*, 13(1):79–97.

Moore, C. A., Alzaydi, A. A., and Rai, I. S. (1979). Methane migration around sanitary landfills. *Journal of the Geotechnical Engineering Division*, 105(2):131–144.

Nastev, M., Therrien, R., Lefebvre, R., and Gelinas, P. (2001). Gas production and migration in landfills and geological materials. *Journal of contaminant hydrology*, 52(1-4):187–211.

Nec, Y. and Huculak, G. (2017). Solution of weakly compressible isothermal flow in landfill gas collection networks. *Fluid Dynamics Research*, 49(6):065505.

Nec, Y. and Huculak, G. (2019). Landfill gas flow: Collection by horizontal wells. *Transport in Porous Media*, 130(3):769–797.

Oonk, H. (2010). Literature review: methane from landfills. *Final report for Sustainable landfill foundation.*

Oonk, J. and Boom, A. (1995). Landfill gas formation, recovery and emissions. *TNO Inst. of Environmetal and Energy Technology, The Hague*, pages 95–203.

Ozkaya, B., Demir, A., and Bilgili, M. S. (2007). Neural network prediction model for the methane fraction in biogas from field-scale landfill bioreactors. *Environmental Modelling & Software*, 22(6):815–822.

Perera, L., Achari, G., and Hettiaratchi, J. (2002a). Determination of source strength of landfill gas: a numerical modeling approach. *Journal of Environmental Engineering*, 128(5):461–471.

Perera, L. A. K. (2001). *Gas migration model for sanitary landfill cover systems.* Graduate Studies, University of Calgary.

Perera, M. D., Hettiaratchi, J. P., and Achari, G. (2002b). A mathematical modeling approach to improve the point estimation of landfill gas surface emissions using the flux chamber technique. *Journal of Environmental Engineering and Science*, 1(6):451–463.

Poulsen, T. G., Christophersen, M., Moldrup, P., and Kjeldsen, P. (2001). Modeling lateral gas transport in soil adjacent to old landfill. *Journal of Environmental Engineering*, 127(2):145–153.

Poulsen, T. G., Christophersen, M., Moldrup, P., and Kjeldsen, P. (2003). Relating landfill gas emissions to atmospheric pressure using numerical modelling and state-space analysis. *Waste management & research*, 21(4):356–366.

Pruess, K. (1987). TOUGH user's guide, Nuclear Regulatory Commission. *Report NUREG/CR-4645 (also Lawrence Berkeley Laboratory Report LBL-20700.*

Pruess, K. (1991). TOUGH2-A general-purpose numerical simulator for multiphase fluid and heat flow.

Pruess, K., Oldenburg, C. M., and Moridis, G. (1999). TOUGH2 user's guide version 2. Technical report, Lawrence Berkeley National Lab.(LBNL), Berkeley, CA (United States).

Ptak, T., Piepenbrink, M., and Martac, E. (2004). Tracer tests for the investigation of heterogeneous porous media and stochastic modelling of flow and transport—a review of some recent developments. *Journal of hydrology*, 294(1-3):122–163.

Sabour, M. R., Mohamedifard, A., and Kamalan, H. (2007). A mathematical model to predict the composition and generation of hospital wastes in Iran. *Waste Management*, 27(4):584–587.

Scharff, H. and Jacobs, J. (2006). Applying guidance for methane emission estimation for landfills. *Waste management*, 26(4):417–429.

Shariatmadari, N., Sabour, M. R., Kamalan, H., Mansouri, A., and Abolfazlzadeh, M. (2007). Applying simple numerical model to predict methane emission from landfill. *Journal of Applied Sciences*, 7(11):1511–1515.

Spokas, K. and Bogner, J. (1996). Field system for continuous measurement of landfill gas pressures and temperatures. *Waste management & research*, 14(3):233–242.

Sudicky, E., Illman, W., Goltz, I., Adams, J., and McLaren, R. (2010). Heterogeneity in hydraulic conductivity and its role on the macroscale transport of a solute plume: From measurements to a practical application of stochastic flow and transport theory. *Water Resources Research*, 46(1).

Townsend, T. G., Wise, W. R., and Jain, P. (2005). One-dimensional gas flow model for horizontal gas collection systems at municipal solid waste landfills. *Journal of environmental engineering*, 131(12):1716–1723.

US-EPA (2001). *Landfill*, volume 3: chapter 15. U.S. Environmental Protection Agency. Availabe at: `https://www.epa.gov/sites/default/files/2015-08/documents/iii15_apr2001.pdf`.

Vigneault, H., Lefebvre, R., and Nastev, M. (2004). Numerical simulation of the radius of influence for landfill gas wells. *Vadose Zone Journal*, 3(3):909–916.

Xi, Y. and Xiong, H. (2013). Numerical simulation of landfill gas pressure distribution in landfills. *Waste management & research*, 31(11):1140–1147.

Xie, H., Wang, Q., Bouazza, A., and Feng, S. (2018). Analytical model for vapour-phase VOCs transport in four-layered landfill composite cover systems. *Computers and Geotechnics*, 101:80–94.

Xie, H., Wang, Q., Wu, J., and Chen, Y. (2019). Analytical model for methane migration through fractured unsaturated landfill cover soil. *Engineering Geology*, 255:69–79.

Xie, J. and Chen, J. (2014). Numerical simulation of landfill gas migration around a vertical extraction well in Xiangshan landfill. *Energy Sources, Part A: Recovery, Utilization, and Environmental Effects*, 36(16):1764–1773.

Young, A. (1989). Mathematical modeling of landfill gas extraction. *Journal of Environmental Engineering*, 115(6):1073–1087.

Yu, L., Batlle, F., Carrera, J., and Lloret, A. (2009). Gas flow to a vertical gas extraction well in deformable MSW landfills. *Journal of Hazardous Materials*, 168(2-3):1404–1416.

Zacharof, A. and Butler, A. (2004). Stochastic modelling of landfill leachate and biogas production incorporating waste heterogeneity. Model formulation and uncertainty analysis. *Waste management*, 24(5):453–462.

Zeng, G. (2020). Study on landfill gas migration in landfilled municipal solid waste based on gas–solid coupling model. *Environmental Progress & Sustainable Energy*, 39(2):e13352.

Zheng, Q.-T., Rowe, R. K., and Feng, S.-J. (2019). Design of horizontal landfill gas collection wells in non-homogeneous landfills. *Waste Management*, 98:102–112.

Appendix

A   COMSOL code

The following Java code was used in Application Builder module of COMSOL software to change well perforation size and position automatically.

```java
//START ---> Removing existing nodes in the Geometry
int counter = 1;
String[] tags = model.geom("geom1").feature().tags(); // Tags of the
  existing nodes in the Geometry
while (contains(tags, "part"+counter)) {
model.geom("geom1").feature().remove("part"+counter);
model.geom().remove("part"+counter);
counter++;
}
if (contains(tags, "uni1")) // check
{
model.geom("geom1").feature().remove("uni1");
}
//STOP ---> Removing existing nodes in the Geometry

//START ---> Creating parts
double[] hpp = {0.00016016, 0.00016007, 0.00015998, 0.00015989,
  0.0001598, 0.00015971, 0.00015962, 0.00015953, 0.00015945,
  0.00015936, 0.00015927, 0.00015918, 0.00015909};
double tww = 0.001;
double Heew = 0.009121;
int numslits = 13; // number of slits
double holeradius[] = hpp;
for (int i = 0; i < numslits; i++) {
String tag = "part"+(i+1);
//model.geom().remove(tag);
model.geom().create(tag, "Part", 2);
model.geom(tag).create("r1", "Rectangle");
model.geom(tag).feature("r1").set("size", new double[]{holeradius[i],
  tww});
```

```
27  model.geom(tag).feature("r1").set("pos", new double[]{0-(hpp[i]/2),
    ↪  -Heew-tww});
28  model.geom(tag).create("r2", "Rectangle");
29  model.geom(tag).feature("r2").set("size", new double[]{holeradius[i],
    ↪  tww});
30  model.geom(tag).feature("r2").set("pos", new double[]{0-(hpp[i]/2),
    ↪  Heew});
31  model.geom(tag).run("r1");
32  model.geom(tag).run("r2");
33  }
34
35  //END ---> creating parts
36
37  //START ---> Defining new nodes in the Geometry
38
39  //----------Defining slits----------
40  double slitPositions[] = {225, 240, 255, 270, 285, 300, 315, 330,
    ↪  345, 360, 375, 390, 405}; // slits positions
41  for (int i = 0; i < numslits; i++) {
42  String tag = "part"+(i+1); // Create a unique tag for each part
43  model.geom("geom1").create(tag, "PartInstance");
44  with(model.geom("geom1").feature(tag));
45  set("part", tag);
46  setIndex("displ", slitPositions[i], 0); // Place the part instance
    ↪  at the correct position
47  endwith();
48  }
49  //------------------------------
50  //double extraPositions[] = {15, 30, 45, 60, 75, 90, 105, 120, 135,
    ↪  150, 165, 180, 195, 210, 225, 240, 255, 270, 285, 300, 315,
    ↪  330, 345, 360, 375, 390}; // slits positions
51  //model.component("comp1").geom("geom1").feature("copy3").set("displx",
    ↪  extraPositions);
52  //model.component("comp1").geom("geom1").feature("copy4").set("displx",
    ↪  extraPositions);
53
54  //----------Unifying slits and well----------method1();
55
56  String item = null;
57  String[] allslits = new String[numslits];
58  for (int i = 0; i < numslits; i++) {
59  item = "part"+(i+1);
60  allslits[i] = item;
61  }
62  String[] wellandslits = new String[allslits.length+1];
63  for (int i = 0; i < allslits.length; i++) {
```

```
64  wellandslits[i] = allslits[i];
65  }
66  wellandslits[wellandslits.length-1] = "r1";
67  model.geom("geom1").create("uni1", "Union");
68  model.geom("geom1").feature("uni1").selection("input").set(wellandslits);
69  model.geom("geom1").feature("uni1").set("intbnd", true);
70  model.geom("geom1").run("fin");
71  //-------------------------------
72  //STOP ---> Defining new nodes in the Geometry
```

B   Octave code

The following Octave code implements the window sliding method in order to smooth
raw COMSOL data.

```
1   clear all
2   clc
3   format long e
4   pkg load signal
5   %--------------------------------%
6   z=5;
7   x=(0:0.04:z)';
8   y=100*cos(pi/10*x)+15*sawtooth(100*cos(100*x));
9   %y=sawtooth(10*x)+0.01*(x.^2);
10  %y = awgn(y,10,'measured');
11  xb=x(2:end-1);
12  yb=y(2:end-1);
13  [m,n]=size(yb);
14  wl=13;%length of the window%
15  ws=7; %window sliding%
16  if rem(m,ws)==0
17    t=floor((m)/ws);
18  else
19    t=floor((m)/ws)+1;
20  endif
21  for i=1:t
22    if m>=wl
23      xavg(i)=mean(xb(1:wl));
24      xb(1:ws)=[];
25      yavg(i)=mean(yb(1:wl));
26      yb(1:ws)=[];
27    else
28      xavg(i)=mean(xb(1:end));
29      xb(1:end)=[];
30      yavg(i)=mean(yb(1:end));
```

```matlab
31        yb(1:end)=[];
32      endif
33      [m,n]=size(yb);
34      if m==0
35        break
36      endif
37    end
38    xs=[x(1),xavg,x(end)];
39    ys=[y(1),yavg,y(end)];
40    plot(x,y,'k',xs,ys,'r')
41    %hold on
42    %plot(xs,ys,'r')
43    %legend('noisy curve','W_L=3 and W_S=1','W_L=7 and W_S=1')
```